

**Selected Pyrotechnic Publications of  
K.L. and B.J. Kosanke,  
Part 2 (1990 through 1992)**

**Table of Contents — Part 2**

Report of Aerial Shell Burst Height Measurements .....	1
Introduction to the Physics and Chemistry of Low Explosives (Parts 1-3) .....	3
Shimizu Aerial Shell Ballistic Predictions, Parts 1 & 2 .....	13
Hazard Data for Chemicals Used in Pyrotechnics .....	25
Burn Characteristics of "Visco" Fuse .....	29
Saran Resin – Its Properties and Uses .....	34
Pyrotechnic Fuse Burn Rates .....	35
A Collection of Star Formulations .....	37
Production of Benzoate Color Agents .....	39
Parallel and Propagative Burning .....	42
Dautriche - Shock Tube Measurement of High Propagation Rates in Pyrotechnic Materials .....	49
Repeat Firing from HDPE Mortars .....	55
Aerial Shell Drift Effects .....	67
Computer Modeling of Aerial Shell Ballistics .....	80
Pyrotechnic Accelerants .....	93

## Biographical Information on Ken and Bonnie Kosanke

Ken has a Ph.D. in physical chemistry and post-doctoral training in physics. He has directed numerous research projects and served as the Quality Assurance Manager for a government subcontractor. Bonnie has a M.S. in Biology and Computer Science. She has extensive experience conducting and directing research and as a computer scientist. Today they operate a pyrotechnic research facility located on 80 acres in Western Colorado. In addition to test ranges and an explosion chamber, there are chemistry, electronics, and video labs, fabrication shops, and assembly buildings.

In the past they have commercially manufactured fireworks and operated a fireworks display company. They have both served as officers and on numerous committees of the Pyrotechnics Guild International. Currently they serve on Technical committees of the National Fire Protection Association. They also lecture and consult in pyrotechnics.

Together they have published more than 130 articles on fireworks, pyrotechnics and explosives. They recently finished their first book, *The Illustrated Dictionary of Pyrotechnics*. Bonnie is also the publisher of the *Journal of Pyrotechnics*. Ken served for many years as a senior technical editor for *Pyrotechnica* and for the *Pyrotechnics Guild International Bulletin*.

### CAUTION

The experimentation with, and the use of, pyrotechnic materials can be dangerous; it is felt to be important for the reader to be duly cautioned. Anyone without the required training and experience should never experiment with nor use pyrotechnic materials. Also, the amount of information presented in these articles is not a substitute for the necessary training and experience.

A major effort has been undertaken to review this text for correctness. However, it is possible that errors remain. Further, it must be acknowledged that there are many areas of pyrotechnics, fireworks in particular, for which there is much “common knowledge”, but for which there has been little or no documented research. Some articles herein certainly contain some of this unproven common knowledge. It is the responsibility of the reader to verify any information herein before applying that information in situations where death, injury, or property damage could result.

## Report of Aerial Shell Burst Height Measurements

K.L. Kosanke, L.A. Schwertley and B.J. Kosanke

Aerial shell burst height data is perhaps one of the more interesting and important pieces of information that an artistically minded display designer needs. Unfortunately, this information has generally not been available and has essentially never been reported in the technical fireworks literature. One of the authors recently published an article suggesting a simple design for an instrument to collect burst height data.<sup>1</sup> Another author fabricated an instrument based on that design, and now offers similar instruments (Pyro-Meter II) for sale to the industry.<sup>2</sup> This article reports on the first use of the instrument to collect burst height data for commercial aerial shells.

The Pyro-Meter II is capable of automatically measuring the times between shell firing and shell burst. However, this was not done for most of these test firings.

Air density has an effect on the height to which shells will be propelled. These data were collected at approximately 1000 feet above sea level.

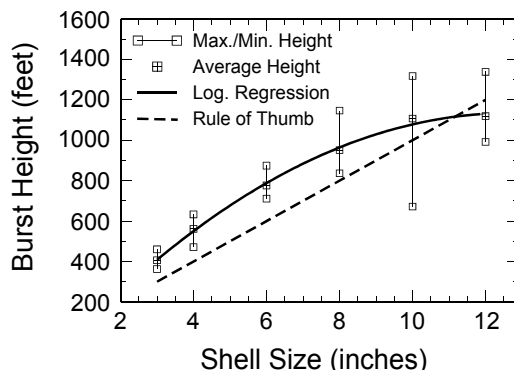


Figure 1. Spherical aerial shell burst height data.

Author Schwertley recently attended a test shoot of commercial aerial shells conducted by Jack Harvey of Harvey Productions, Inc. The purpose of his attending was to measure burst heights of the spherical shells as they were being test fired. Prior to these measurements, the instrument was calibrated using small test salutes fired at known distances. Table 1 summa-

Table 1. Spherical Aerial Shell Burst Height Measurement Results.<sup>a,b</sup>

Shell Size (inches)	Number of Trials	Highest Burst Height (feet)	Lowest Burst Height (feet)	Average Burst Height (feet)	Logarithmic Regression Height (feet)
3	3	460	362	406 (50)	400
4	5	633	471	561 (66)	560
5	0	—	—	—	680
6	9	874	711	776 (52)	785
8	9	1146	836	949 (88)	950
10	8	1371	671	1092 (193)	1070
12	6	1338	992	1164 (134)	1175

(a) The Pyro-Meter II is capable of automatically measuring the times between shell firing and shell burst. However, this was not done for most of these test firings.

(b) Air density has an effect on the height to which shells will be propelled. These data were collected at approximately 1000 feet above sea level.

rizes the results of the measurements. Also included in Table 1 are standard deviations using the  $n-1$  method (listed parenthetically after average burst heights) and the burst heights determined from a logarithmic regression fit to the average burst heights.

Figure 1 is a graphic presentation of highest, lowest and average burst heights. The solid line is the logarithmic regression fit to the average burst heights. Also included is a dashed line corresponding to the traditional rule-of-thumb that burst heights are 100 feet per shell inch. For shells less than 12 inches, the rule-of-thumb under-estimates true burst heights by about 150 feet.

The authors gratefully wish to acknowledge Jack Harvey for granting permission to publish these data. The authors hope that other persons in the industry will volunteer to allow the collection and publication of similar data during their testing of aerial shells.

## References

K.L. Kosanke, "Determination of Aerial Shell Burst Altitudes," *PGI Bulletin*, No. 64, 1989.

For a specification brochure on the **Pyro-Meter II**, contact L. Alan Schwertley, RR 1 Box 5, Modale, IA 51556, (712) 645-2077.

## Introduction to the Physics and Chemistry of Low Explosives (Part 1)

by K.L. and B.J. Kosanke

This article is a slight modification of an article originally prepared for the International Association of Bomb Technicians and Investigators. Because much of this same material is of interest to the fireworks community, this article was offered to the PGI Bulletin. However, in order to enhance its usefulness, some additional material was included and other sections were re-written. Because of the length of this paper, it will appear in three parts.

In part, this paper is intended to stand alone as an introduction to the basic physics and chemistry of low explosives (i.e., pyrotechnics). However, this paper is also intended to present information needed in preparation for other papers to follow.

Following the presentation of a few definitions, this paper addresses the basic physics of explosions, chemical combustion, requirements for initiation and propagation, effects of form and confinement, effects of particle size and shape, and sensitivity to accidental ignition.

Occasionally this article includes some tidbits of practical information for the pyrotechnician. These items are indented and in italic-typeface for emphasis.

### Initial Definitions

The word "explosion" is widely understood by laypersons and professionals alike, and it would seem that its definition should be almost trivial. However, it is not that simple. A fairly good definition<sup>1</sup> for an explosion is that the necessary and sufficient conditions are:

- 1) That gas is released.
- 2) That energy is released.
- 3) That 1 and 2 occur very rapidly.

By this definition, all three conditions must be met for there to be an explosion. For example, in the case of burning wood, gas is released (carbon dioxide and water vapor) and energy is released, but there certainly is no explosion. Of course, the reason is that the third condition is not met, the gas and energy are not released "very rapidly."

"Explosive" can be defined by adding one further condition to the three above:

- 1) It must be capable of producing a gas.
- 2) It must be capable of producing energy.
- 3) That 1 and 2 must be produced very rapidly.
- 4) That once initiated, 1, 2, and 3 must be self-sustaining, continuing throughout the mass of material.

Something similar to the above definitions are the ones most often used. However, these are not perfect definitions, and when using these definitions, some degree of caution is necessary. Some limitations of these definitions are discussed later in this paper.

The term "pyrotechnics" is also somewhat difficult to define. In some instances, it is defined as the study of explosives that burn rather than detonate. In other cases, it is defined as the study of materials capable of undergoing a self-sustained chemical reaction producing heat and often gases, but generally at rates less than sufficient to produce an explosion without confinement. For the purposes of this paper, it is the latter definition that will be used.

As one example of the difficulties with the definition of explosives given above, consider pyrotechnic materials. For the most part, these materials react too slowly when unconfined to cause an explosion. Take for example the chemical composition used in making safety matches.

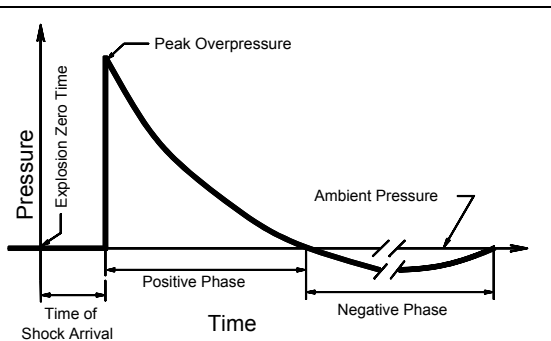


Figure 1. Explosive overpressure versus time.

When a match is struck, there certainly is no explosion. It is only when such materials are confined that they can be made to function explosively. Further, many of these materials must be highly confined or must be present in very large quantity before they can be made to react explosively. Nonetheless, the US Department of Transportation classifies most of these materials as explosives, whether confined or not, when highly combustible might be a better description. It is important to recognize that in many instances the legal definition of explosives may not be consistent with the technical definition.

### Basic Physics of Explosions

Although very high temperatures (usually exceeding 3000 °C) are produced by explosives, much of the damage is usually the result of pressure. The reason for this can be seen in the defining relationship for pressure (P),

$$P = F/A, \quad (\text{Eq. 1})$$

where F is the force exerted and A is the area on which the force is acting.

By rearranging Equation 1, it is seen that

$$F = P \cdot A, \quad (\text{Eq. 2})$$

which states that the force applied to an object is equal to the pressure acting on the object times the area of the object (i.e., the force experienced is directly proportional to pressure).

All objects are held together by internal cohesive forces. When the external force (pressure) exerted on an object is greater than the cohesive forces holding it together, the object

will break apart producing fragments. This is true for all objects, containment vessels, walls, windows, people, etc.

From Newton's Second Law of Motion, it is known that a force applied to an object results in an acceleration (a) of that object. Expressed as an equation,

$$a = F/m, \quad (\text{Eq. 3})$$

where m is the mass of the object.

By substituting equation 2 for F in equation 3

$$a = P \cdot A/m, \quad (\text{Eq. 4})$$

which states that the acceleration of an object is also directly proportional to the pressure applied to it.

Thus the high pressures produced during an explosion have two direct effects, fragmentation and acceleration of those fragments. When fragments, which have been accelerated to high velocity, impact other objects, those objects too, will be damaged and may become secondary projectiles. In all cases the seriousness of the damage at any point and the range over which the damage extends, is a function of the pressure generated during the explosion. Figure 1 is a sketch of overpressure versus time for a shock (pressure) wave produced by a typical explosion. (Overpressure is that pressure in excess of atmospheric or ambient pressure.)

In part, the pressure generated by an explosion is the result of the gas produced by the explosive chemical reaction. However, this can only begin to explain the very high pressures generated. The other factor responsible for pressure generation is the release of large amounts of thermal energy (i.e., temperatures over 3000 °C are produced). The way in which gas generation and temperature are related to pressure can be seen in the Ideal Gas Law, which can be expressed as:

$$P = n \cdot T (R/V), \quad (\text{Eq. 5})$$

where n is the amount of gas, T is temperature, R is a constant, and V is volume.

Equation 5 states that pressure is proportional to the amount of gas and also to temperature. Thus if the explosive produces both a large quantity of gas and high temperatures, the pressures generated will be very high.

Equation 5 also points out another reason to be cautious using the definitions given for explosion and explosive. It is not absolutely necessary for an explosion to generate both gas and energy (high temperatures), either one may suffice to generate explosive pressures. To illustrate this, consider the example of copper(III) acetylide,  $\text{Cu}_2\text{C}_2$ . When this material decomposes, the products are copper metal and carbon, neither of which are gases. Nonetheless, its decomposition is surely an explosion.<sup>2</sup> The reason it acts explosively is that, upon its decomposition, a great amount of energy is produced, which manifests itself by raising all nearby materials to high temperature. These nearby materials include atmospheric air, which, as a result

of being raised to high temperature, produces high pressure causing the explosive effect. Contrary to the standard definitions, this is one of a number of explosives that produce no gaseous products.

### References for Part 1

- 1) H.J. Yallop and S.S. Kind, *Explosion Investigation*, The Forensic Science Society and Scottish Academic Press, 1980.
- 2) T.L. Davis, *The Chemistry of Powder and Explosives*, Angrif Press, Reprint of 1943 edition.

---

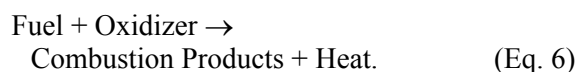
## Introduction to the Physics and Chemistry of Low Explosives (Part 2)

by K.L. and B.J. Kosanke

---

### Chemical Combustion

The chemical reactions responsible for the explosive production of gas and energy, fall into the broad category called combustion. The general chemical equation for combustion is:



Fuels are generally chemical elements, or molecules primarily composed of those elements, that can form very strong chemical bonds with oxygen. Some good fuels are hydrogen (H), carbon (C), phosphorous (P), sulfur (S), and many metals such as, magnesium (Mg), aluminum (Al), titanium (Ti) and zinc (Zn). Many of the most common molecular fuels are organic materials, which consist primarily of two excellent fuels, carbon and hydrogen.

The feature that differentiates between pyrotechnic reactions and most other combustion

reactions is the nature of the oxidizer. For most combustion reactions, the oxidizer is oxygen in the air. However, for pyrotechnic reactions, the oxidizer is usually present in solid form as a chemical ingredient. This is a very important difference. If pyrotechnic reactions can proceed without the benefit of airborne oxygen, they can proceed even when tightly confined inside containers, thus allowing the possibility of producing explosive results.

Pyrotechnic oxidizers are generally salts that contain an abundance of easily released oxygen (O). Some good oxidizing salts are potassium nitrate ( $\text{KNO}_3$ ), ammonium perchlorate ( $\text{NH}_4\text{ClO}_4$ ), potassium chlorate ( $\text{KClO}_3$ ), and potassium perchlorate ( $\text{KClO}_4$ ).

Combustion products include various materials, many of which are gases, but some of which may be solids. Table 1 lists the major combustion products and reaction energies for some combustion reactions.

**Table 1. Major Combustion Products and Reaction Energies for Typical Combustion Reactions.**

Reaction Type	Reactants	Combustion Products	Energy Output	Reference
Wood Burning	Wood Air Oxygen	H <sub>2</sub> O <sub>(g)</sub> CO <sub>2(g)</sub> Ash <sub>(s)</sub>	1.9 kcal/g	Authors
Black Powder	KNO <sub>3</sub> S C	CO <sub>2(g)</sub> N <sub>2(g)</sub> K <sub>2</sub> SO <sub>4(s)</sub> K <sub>2</sub> CO <sub>3(s)</sub>	0.7 kcal/g	3
Flash Powder	KClO <sub>4</sub> Al	KCl <sub>(s)</sub> Al <sub>2</sub> O <sub>3(s)</sub>	1.8 kcal/g	3
Nitroglycerin	C <sub>3</sub> H <sub>5</sub> N <sub>3</sub> O <sub>9</sub>	CO <sub>2(g)</sub> H <sub>2</sub> O <sub>(g)</sub> N <sub>2(g)</sub> O <sub>2(g)</sub>	1.5 kcal/g	4

(g) = gas (s) = solid

In terms of gas producing ability, nitroglycerin is the best, followed very closely by wood burning. In terms of energy production, wood burning is best, followed closely by flash powder. The fact that wood burning has the best combined performance in terms of gas and energy production, and yet obviously does not represent a state of explosion, serves to emphasize the importance of the requirement (see Part

I) that the gas and energy must be produced very rapidly for an explosion.

Combustion reactions may be divided into one of three classifications depending on the rate (speed) of the chemical reaction. Table 2 identifies the approximate burn rates associated with each of the three classifications and gives some examples.

There are a number of things about Table 2 that should be discussed further. First, the chemical reactions of all the examples are of the same general nature, combustion. The principal difference is only the speed of the reaction. Second, under the proper conditions any of the listed examples can be made to produce an explosion. Third, explosive mixtures are physical mixtures of different materials (individual particles of fuel and oxidizer), neither of which is normally explosive by itself. Fourth, explosive molecules are chemicals that contain both fuel

**Table 2. Classes of Combustion Reactions.**

Combustion Class	Usual Burn Rate Units	Examples
Burning	Inches/Minute	Wood Burning Safety Matches Most Fireworks Unconfined Black Powder Rocket Propellants
Deflagration	Feet/Second	Confined Black Powder Explosive Fireworks Comp. Explosive Mixtures
Detonation	Miles/Second	Dynamite Primary Explosives Explosive Molecules



and oxidizer within the same molecule, which partly explains their very high burn rates. Since the fuel and oxidizer atoms are in very close proximity, it is relatively easy for them to react with explosive speed. In contrast, consider explosive mixtures. In this case even very fine powders, those only about 0.001 inch in diameter, consist of nearly a million billion atoms. Of these, less than one in ten thousand is on the surface of the particles; all the rest are buried inside. For the most part, it is only the atoms on the surface that are available to react. Those atoms inside have to wait until the ones on the surface have reacted and left, thus exposing the ones further inside. This is the principle reason why explosive mixtures are not capable of the very high reaction rates of most explosive molecules.

Perhaps at this point it is appropriate to discuss the often-used terms, low and high explosives, and also primary explosives. Low explosives, better termed deflagrating explosives, can be considered those that, under optimum conditions, have burn rates less than 6000 feet/second. The choice of 6000 feet/second in the definition is somewhat arbitrary but is alleged to be based on the speed of sound in a more or less typical explosive under standard temperature and pressure conditions. By that definition, all pyrotechnic mixtures would be considered low explosives. However, it must be acknowledged that there are at least three other common definitions of low explosives. According to two of these definitions, some pyrotechnic flash powders have burn characteristics that class them beyond the range of low explosives. (A more complete discussion of this subject is beyond the scope of this paper and will form the basis of a future article by the authors.) High explosives, better termed detonating explosives, can be considered those that have burn rates greater than 6000 feet/second.

Most commercial high explosives are difficult to initiate, which tends to make them safe to handle under ordinary circumstances. Many explosives can be burned or struck with a bullet without detonating. However, there is a subclass of high explosives, called primary explosives, which are very sensitive to heat and impact, which tends to make them difficult to handle safely even under the best of conditions.

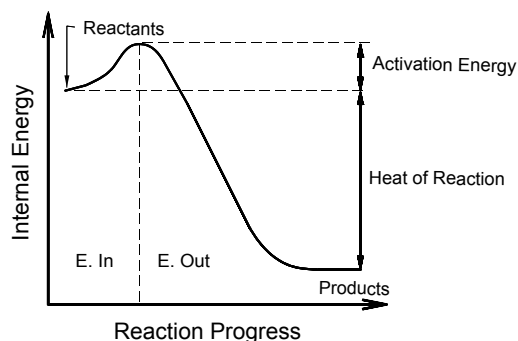


Figure 2. Chemical reaction energy relationships.

Primary explosives are often used in detonators (caps) for other high explosives.

## Ignition and Propagation

Pyrotechnic compositions generally will not initiate (begin to burn) without the input of some external energy. For example, at room temperature, matches and Black Powder are stable and will not spontaneously begin to burn. However, when the mechanical energy of striking is supplied to the match, it will begin to burn. Similarly, when thermal energy from the match is supplied to the Black Powder, it too will burn. This initiating energy is called activation energy. Following the input of the necessary activation energy the chemical reaction will proceed, normally producing an excess of energy, called heat of reaction. Figure 2 illustrates these energy relationships for a typical combustion reaction.

It is possible to think of the chemical reaction as proceeding in two distinct steps. First, when energy input is required, the existing weak chemical bonds within the fuel and oxidizer particles are being broken (in preparation for their inter-reaction). Second, when energy production occurs, new stronger chemical bonds are forming between individual fuel and oxidizer atoms as they combine to form the reaction products.

The amount of activation energy needed depends on how strong the chemical bonds are in the fuel and oxidizer. When the bonds are rather weak, only a small amount of energy is neces-

sary. For example, a mixture of potassium chlorate and red phosphorous has an activation energy barrier so very low that the mechanical action of gentle mixing may be sufficient to initiate a very violent reaction. On the other hand, when the fuel and oxidizer chemical bonds are relatively strong, greater amounts of energy must be supplied to initiate the reaction. For example, a mixture of calcium sulfate (Plaster of Paris) and aluminum has an activation energy barrier so high that a temperature of about a thousand degrees Celsius is required before it will begin to react.

Similarly, the amount of energy produced by the pyrotechnic reaction, the heat of reaction, also depends on the strength of chemical bonds. However, this time it is the strength of chemical bonds formed in the reaction products. The stronger these bonds are, the more energy the reaction produces.

It follows directly that the values for both activation energy and heat of reaction depend on the formulation of the pyrotechnic mixture. With every change in formulation, whether changing the type of ingredients or only changing the percentages of the ingredients, there will be changes in the amount of energy required to initiate the reaction and in the amount of the energy produced by the reaction. This is because in each case the reaction will occur differently; different numbers and/or types of bonds will be broken in the oxidizer and fuel, and different numbers and/or types of bonds will be formed in the reaction products.

It should be noted that there is no simple relationship between the activation energy required and the heat of reaction produced. Some reactions are very easy to start and produce large amounts of energy, while others that are easy to initiate produce very little energy and vice versa.

Once a pyrotechnic reaction starts, it will propagate, providing the reacting material supplies the unreacted composition with the necessary activation energy. This requirement for propagation can be made more clear using Figure 3, which is a model of a rod of reacting pyrotechnic composition. Toward the left in the drawing, the pyrotechnic composition remains in an unreacted state and is at room tempera-

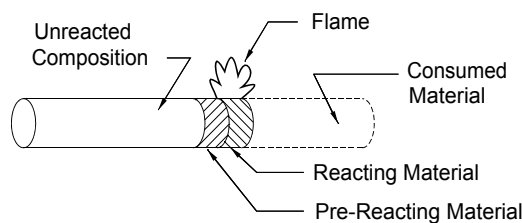


Figure 3. Model of propagating pyrotechnic reaction.

ture. Toward the right, the pyrotechnic composition has already reacted and been transformed into combustion products. In between are the two thin disks of material that are of interest. The one labeled "reacting material" has already received its activation energy, is reacting and producing heat energy. The reacting material is heating the next disk of material, labeled "pre-reacting material." However, much of the heat energy produced by the reacting disk is lost to the surroundings and thus is not available to heat the pre-reacting disk. It is only after the necessary activation energy has been acquired by the pre-reacting material, that it too will begin to react. If this occurs, then it too reacts, producing heat energy, some of which is available to be passed on as the activation energy needed by the next disk of material. In this manner, the reaction will propagate along the rod of pyrotechnic composition. However, if for any reason, the reaction of one disk of material does not provide the needed activation energy for the adjacent disk, the reaction will terminate, leaving all the remaining material completely unreacted.

There are many reasons why the propagation of the chemical reaction through a pyrotechnic material may be interrupted; often it is not because the unreacted material is incapable of reacting. Thus, after burning pyrotechnic materials, it should never be assumed that any remaining unreacted material is safe; it is quite possible it has the same reactive properties as the material that was consumed.

**Table 3. Mechanisms for Energy Transfer from Reacting to Pre-Reacting Material.**

Energy Type	Transfer Mechanism	Efficient Conditions
Thermal	Convection	Many "fire paths" for hot combustion gases to follow.
	Conduction	Use of metal fuels or other materials with high thermal conductivities.
	Radiation	Use of materials that are dark or black in color.
Kinetic	Shock Wave	Compact materials in intimate contact.

There are three factors that make it more likely that a pyrotechnic reaction will propagate, consuming the total composition. First is if the pyrotechnic composition has a low activation energy barrier, such that the feedback of only a small amount of energy is required. Second is if the heat of reaction is large; obviously the more heat produced by the composition the more likely that each succeeding layer of mate-

rial will receive its necessary activation energy. Third is if the mechanism of energy transfer within the pyrotechnic composition is highly effective, making the feedback of energy more efficient. Table 3 lists the mechanisms for energy transfer and the conditions that make the transfer more efficient.

### References for Part 2

- 3) J.A. Conkling, *The Chemistry of Pyrotechnics*, Marcel Dekker, 1985.
- 4) R. Meyer, *Explosives*, 3ed., VCH Verlagsgesellschaft, 1987.

## Introduction to the Physics and Chemistry of Low Explosives (Part 3)

K.L. and B.J. Kosanke

### Effects of Particle Size and Shape

The burn rate of a pyrotechnic mixture is strongly influenced by size and shape of fuel and oxidizer particles (grains) making up the mixture. To better understand why this is the case, consider again some information presented in Part 2 of this article. In large measure, it is only those atoms on the surface of a fuel or oxidizer grain that are ready to participate in a chemical reaction. Atoms buried inside the grain, generally must wait until those on the surface have reacted or have been vaporized before they too can participate in the reaction. Accordingly, the rate of a pyrotechnic reaction depends on the fraction of atoms ready to par-

ticipate in a reaction, which is the fraction located on the surface of the grains in the mixture, i.e. the surface area to mass ratio of individual particles.

The surface area to mass ratio for a particle depends mostly on the particle's size and to a lesser extent on the particle's shape. Particles that are small and those that are flakes or highly angular have the greatest surface area to mass ratios. Accordingly, pyrotechnic mixtures consisting of particles with those characteristics will tend to have the highest burn rates. The data in Table 4 demonstrates the effect of increasing rate of reaction as a result of decreasing particle size.

There is a second reason why pyrotechnic mixtures consisting of small and angular parti-

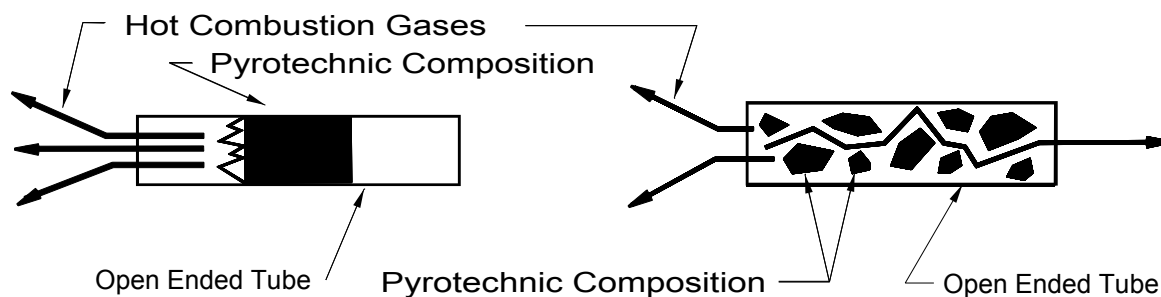


Figure 4. Effect of form on pyrotechnic burning.

cles tend to have higher burn rates. When such particles are exposed to high temperatures, the individual atoms, particularly those in any pointed or thin extremities, quickly gain thermal energy, and thus rapidly acquire the activation energy necessary to allow the reaction to proceed.

Even if one has extensive experience with a type of pyrotechnic composition, when the materials used in compounding it come from different production lots, or if there is uncertainty about particle size and shape, it cannot be assumed that the composition will perform with previously experienced burn rates.

### Effects of Form and Confinement

Any reasonably well-formulated pyrotechnic composition can be made to cause an explosion, even if under normal conditions the material only burns slowly. The main factors affecting the potential for explosive output are the form of the material and, to a much greater extent, the degree of confinement of the material.

To illustrate the effect of form on the rate of a pyrotechnic reaction, consider Figure 4. On the left, an amount of pyrotechnic composition has been compressed very tightly into a tube, forming a plug of material. If that material is ignited on one side, it will begin to burn, and that burning will occur relatively slowly. This is because

the reaction only takes place on the surface of the plug of composition and the hot combustion gases easily vent through the open end of the tube. As was discussed in Part 2, the material just behind the burning surface will not begin to react until it receives the necessary activation energy from the burning surface. Similarly, the material just behind that will not begin to react until the material in front of it burns. Thus the burning is in an orderly fashion, one layer at a time, until finally all the pyrotechnic material has been consumed. Now consider the other case shown in Figure 4, in which granules of pyrotechnic composition are packed rather loosely into a tube. Here each granule is a proper mixture of fuel and oxidizer such as might be produced if the plug in the first case was crushed into several smaller pieces. When burning starts, most of the hot gases generated still vent through the open end of the tube.

Table 4. Effect of Particle Size on Performance of a Flare Composition.<sup>3</sup>

Composition: Component	Percent by Weight	Average Particle Size
Magnesium metal	48	See Table Below
Sodium nitrate	42	34 micrometers
Laminac binder	8	—
Polyvinyl chloride	2	27 micrometers

Magnesium Average Particle Size, Micrometers	Flare Candlepower (1,000 candles)	Flare Burning Rate, inches/minute
437	130	2.62
322	154	3.01
168	293	5.66
110	285	5.84

However, some also pass between the small spaces between the granules (sometimes called fire paths). When this occurs, some of the granules farther into the tube are immediately heated, receiving the activation energy necessary for them to begin to burn. As these additional granules burn, more hot gases are produced, some of which pass farther into the tube heating more granules, which also begin to burn. In this manner, very rapidly all the granules of pyrotechnic composition in the tube are consumed. Of these two cases, it is the second that has a far greater potential for explosion. As a specific example, consider two long, narrow paper tubes filled with equal amounts of Black Powder. However, in one tube the powder has been tightly compacted into a solid plug, while the other tube has been filled with granules. In the first case the device probably will perform somewhat like a weak rocket burning at a rate of about 1/4-inch per second. In the second case the device will burst the tube explosively because of a burn rate of about 30 feet per second.

Even if one has vast experience with a pyrotechnic composition in one form, that cannot be used as a predictor for how the same material will act in another form.

The degree of physical confinement is a very important factor in determining the potentially explosive output of pyrotechnic compositions. One reason is that in most instances unconfined pyrotechnic material burns relatively slow; so slow that in moderately small quantities it usually only represents a flammability hazard. When such material is confined within a vessel of some sort and then ignited, the material will burn producing hot gases. If the gases are produced at a rate greater than they can escape, such as through a fuse hole, then the pressure inside the vessel will rise. If the pressure rises beyond the strength limits of the vessel, it will burst. If the vessel is strong, such that the pressure before rupturing is high, then the bursting will be seen as an explosion. In this case the violence of the explosion directly relates to the strength of the containment vessel and not so much to the pyrotechnic material within it.

Another reason that the degree of confinement is an important consideration is that the rate of the combustion reaction is usually a

function of pressure. Equation 7 shows this general relationship.

$$(Eq. 7) \quad R = A \cdot P^b,$$

where R is the burn rate for a pyrotechnic composition (in cm/sec), P is the gas pressure on the composition (in atmospheres), and A and b are constants dependent on the pyrotechnic composition.

As an example of the effect of pressure on burn rate, consider the case of sporting grade Black Powder. For Black Powder,<sup>5</sup> A = 1.21 and b = 0.24. Using these constants, and converting to inch/second, Black Powder would have the pressure dependent burn rate as indicated in Table 5.

One result of burn rate being pressure dependent is that pressures inside a containment vessel rise faster than might be expected, and this can have an effect on explosive output. It was stated above that the burst strength of a containment vessel largely determines the explosive potential for a device. While this is true, the burst strength of the vessel depends, to some extent on the rate of pressure rise within it. When the rate of pressure rise is very great, the "effective" burst strength of the vessel is greater because of inertial-like effects. Even though the vessel may be in the process of bursting, the tendency for objects at rest to remain at rest, acts to hold the vessel together slightly longer. This allows the pressure within the vessel to continue to rise to higher values and increases the explosive output beyond what might have been predicted.

Even if one has much experience with a pyrotechnic composition in one degree of con-

**Table 5. Predicted Pressure Dependence of the Burn Rate for Black Powder.<sup>3</sup>**

Pressure (atm)	Pressure (psia)	Linear Burn Rate (in/sec)
1	14.7	0.48
2	29.4	0.56
5	73.5	0.70
10	147	0.83
20	294	0.98
30	441	1.07

finement, that cannot be used as a predictor for how the same material will act if the level of confinement changes.

The inertial effect discussed above is also the reason that many pyrotechnic compositions, when present in large amounts, can cause an explosion even when unconfined. When there is a large mass of pyrotechnic material, the material itself and its reaction products tend to act as a containment vessel because of their inertial resistance. In these situations the minimum weight of material necessary for an unconfined explosion is sometimes called the critical mass for the pyrotechnic composition.

When disposing of pyrotechnic materials it is appropriate to test materials in small quantities before disposing of larger quantities. However, one cannot use the performance of a small amount of a pyrotechnic composition as an absolute predictor for how the same material will react in larger quantities.

As a final note, such unconfined explosions are often incorrectly called a detonation or described as "going off high order." By the definitions adopted in this article they are actually inertially confined deflagrations.

### **Sensitivity to Accidental Ignition Stimulus**

It was discussed above that there is an activation energy barrier that must be surmounted before a combustion reaction will be initiated. It is fortunate that this barrier exists. If it did not, the forests would spontaneously burst into flame, all pyrotechnic materials would spontaneously burn, all high explosives would spontaneously explode, and biologic life could not exist. All chemical reactions that are energetically favored would occur immediately and then nothing else would happen forever more. It is the activation energy barrier that allows chemical energy to be stored for future release, and it is the height of that barrier which determines how easy it is to stimulate the release of

that energy. A major problem in dealing with pyrotechnic (low explosive) compositions is that they generally have rather low activation energy barriers.

Great care must be exercised when handling pyrotechnic compositions because often only a modestly energetic stimulus is necessary to start the pyrotechnic reaction. (This is in contrast with most commercial high explosives for which a greater ignition stimulus is required.)

There are three basic types of stimuli that can supply the energy needed to initiate pyrotechnic reactions:

- 1) Thermal — Elevated Temperatures,
- 2) Mechanical — Impact or Friction, and
- 3) Electrical — Electrostatic Discharge.

The height of the activation energy barrier is an accurate measure of the amount of energy needed to initiate a reaction. However, the mechanisms through which each of the above stimuli operate are significantly different. As a result, the effectiveness of the energy transfer for each of the stimuli depends heavily on the characteristics of the pyrotechnic composition involved. Thus, even if one knows the relative height of the activation energy barrier, it is often not possible to predict accurately how easily the material will be initiated by the different stimuli. For this reason, the sensitivity of pyrotechnic compositions is generally reported separately, as auto-ignition temperature, impact sensitivity, friction sensitivity, and electrostatic sensitivity.

Unless all four of these sensitivities are known to be low (hard to initiate a reaction) for a particular pyrotechnic material, great caution is appropriate when handling the material.

### **References**

- (3) J.A. Conkling, *The Chemistry of Pyrotechnics*, Marcel Dekker, 1985.
- (5) A.A. Shidlovskiy, *Principles of Pyrotechnics*, Mashinostroyeniye Press, 1964.

## Shimizu Aerial Shell Ballistic Predictions (Part 1)

by K.L. and B.J. Kosanke

### Introduction

The effect of varying aerial shell and mortar parameters is a frequent topic of discussion in the display fireworks industry. Dr. Takeo Shimizu has published equations describing both internal (within the mortar) and external (after leaving the mortar) aerial shell ballistics<sup>1</sup>. These equations can be used to make general predictions of the effects of aerial shell and mortar characteristics on shell and mortar performance. Shimizu's work only addressed spherical shells; however, his equations can be used for cylindrical shells providing an appropriate drag coefficient is used. (For the purposes of this article, the drag coefficient of air resistance for cylindrical shells was assumed to be twice the value used by Shimizu for spherical shells.)

In this article, the authors have used the Shimizu equations in order to determine the relative effects of varying aerial shell and mortar characteristics. In the belief that the results generally speak for themselves, the reader is usually left to draw their own conclusions and supply their own rationales. Occasionally, however, this article presents some conclusions or discusses the reasons for the results.

Before presenting the results of this study, two subjects must be presented. The first is a general discussion of the reliability of predictions based on mathematical models (equations). The second is an enumeration of nominal aerial shell and mortar input values used in this study.

### Reliability of Predictions Using Mathematical Models

The reliability of predictions made using mathematical models (equations) is almost always limited because simplifications and assumptions usually have been made in their derivation. In some cases, simplifications are made in order to make it possible to perform the calculations; in other cases the simplifications just make it easier or faster to perform the calculations.

As an example of one type of simplification that is required in the case of aerial shell ballistics, consider the following. The microscopic airflow around an aerial shell first being propelled within a mortar and then moving through the air, is so very complex that even the best aerodynamic engineers, using the most sophisticated computers, cannot perform the necessary calculations. In this case, there is no choice except to simplify the calculations by only considering average (macroscopic) effects of airflow. When this is done, it is appropriate to ask whether this limits the accuracy of the calculated results. Of course, the answer is yes; but the errors are not great, and remember, the choice was to simplify the problem or to not perform the calculations at all.

Simplifying assumptions always introduce some error, at least under some circumstances. Thus it is important to consider when such simplifications are appropriate. One such case is when there are uncertainties in input parameters, such as the exact weight, diameter, or amount of lift for a typical shell. Those uncertainties in input parameters cause uncertainties in the results. When those uncertainties in the results are significantly greater than the errors introduced by the simplifying assumptions, the simplifications are appropriate. Another case

**Table 1. Nominal Shell and Mortar Parameters.**

Shell Type	Shell Size	Shell		Lift		Dead Volume (cubic in.)	Mortar Length (inches)
		Diameter (inches) <sup>(a)</sup>	Weight (pounds) <sup>(a)</sup>	Powder Type <sup>(c)</sup>	Weight (ounces) <sup>(a)</sup>		
<b>Spherical</b>	3	2.75	0.3	2-3Fg	0.5	12	24
	4	3.70	0.8	2-3Fg	1.0	24	24
	5	4.60	1.5	2-3Fg	1.7	46	30
	6	5.55	2.5	2-3Fg	2.7	72	36
	8	7.50 <sup>(b)</sup>	5.5	2-3Fg	5.5	150	42
	10	9.50 <sup>(b)</sup>	11.	2-3Fg	10	290	48
	12	11.50 <sup>(b)</sup>	18.	2-3Fg	17	520	48
<b>Cylindrical</b>	3	2.75	0.4	2FA	1.0	9	24
	4	3.7	1.0	2FA	1.9	20	24
	5	4.7	2.0	2FA	3.0	35	30
	6	5.7	4.0	2FA	4.5	57	36
	8	7.6	10.	2FA	9.0	121	42
	10	9.5	20.	2FA	16	234	48
	12	11.5	36.	2FA	26	394	48

Notes:

- a) Values for spherical shells were derived by interpolating values reported by Shimizu1 p.183.
- b) Values derived from Shimizu were 0.05 to 0.1 inches smaller, but it was decided to follow the NFPA guideline that the gap between shell and mortar not exceed 0.5 inches.
- c) See Table 3, this suggests that 2Fg powder is the US grade most nearly like the Type 0 lift powder used by Shimizu.

when simplifications are appropriate, is when it is only desired to draw general conclusions from the results, and the accuracy of each individual calculated result is of lesser importance. In the present study of aerial shell ballistics, both cases are applicable, and Shimizu's simplifying assumptions are appropriate.

When considering errors introduced by simplifications, there is one more thing that must be addressed. The magnitude of those errors generally depends on how greatly conditions differ between those being calculated and those assumed by the simplification. In effect this introduces limits on when these errors can be safely ignored. As an example of this consider the following. One result predicted by the Shimizu equations is the location of an aerial shell inside a mortar when it will be subjected to the greatest lift pressure. Generally an aerial shell will be 7 to 11 inches above the bottom of the mortar when maximum pressure is reached. As an example of the limits that are imposed by simplifying assumptions, consider the very ex-

treme case of a mortar that is only five-inches tall. In this case, the Shimizu equations still predict that the maximum pressure will occur when the shell has risen 7 to 11 inches in the mortar. Obviously this is impossible! The lesson here is that, while the Shimizu equations may work quite well when using values only a little different from normal, as more and more extreme values are used, one must be more and more cautious in accepting the results.

Within the purpose of this paper, which is only to draw some very general conclusions about internal and external aerial shell ballistics, the authors feel that the errors introduced because of simplifying assumptions are within acceptable limits. However, the reader must be cautioned that no experimental data was collected by the authors for the purpose of verifying the results using the Shimizu equations. Thus, it is not possible to quantify the magnitude of the errors in the results reported here.



**Table 2. Comparison between Japanese and American Black Powder Mesh Sizes.**

Japanese Powder type <sup>(a)</sup>	Mesh Range (inches) <sup>(b)</sup>	American Powder type	Mesh Range (inches) <sup>(c)</sup>
0	0.016–0.047	4Fg	0.006–0.016
1	0.008–0.016	3Fg	0.012–0.033
2	0.016–0.047	2Fg	0.023–0.047
3	0.047–0.067	4FA	0.033–0.066
4	0.094–0.134	Fg	0.047–0.066
		3FA	0.047–0.079
		2FA	0.066–0.187

Notes:

- a) As defined by Shimizu<sup>1</sup>, Table 33, p. 170.
- b) Values were converted to sieve openings in inches. See Shimizu<sup>1</sup>, Table 33, p. 170 for percent passing and retained on sieves.
- c) Values derived from information contained in *Engineering Design Handbook* (AMCP 106-175) - Explosives Series - Solid Propellants Part One - The percent passing fine mesh sieve is 3%, and the retained on coarse mesh sieve is 12%.

### Nominal Shell and Mortar Input Values

Table 1 lists the nominal values for input parameters used in this paper. For spherical shells, many of the values were taken from Shimizu<sup>1</sup> by interpolation to US shell sizes. Other values were derived using a combination of measurements of actual shells and mortars, and recom-

mendations of various fireworks experts. Unless otherwise specified, the results reported in this paper use those nominal values as input parameters for the calculations.

The Black Powder granulations used in Japan differ from those used in the United States. Table 2 compares Japanese and US granulations. Shimizu reports "characteristic values" for Japanese Black Powder granulations, and these are used as input parameters in his equa-

**Table 3. Characteristic Values for Lift Powders**

Japanese Powder type	Corresponding American Powder type <sup>(b)</sup>	Characteristic Values <sup>(a)</sup>		
		Af (dm <sup>3</sup> /kg·sec)	AG (dm <sup>2</sup> /kg·sec)	f/G (dm)
0	2-3Fg	17200	0.256	67100
1	4Fg	17500	0.356	49100
2	2Fg	16000	0.213	75100
3	Fg or 3-4FA	13200	0.182	72500
4	2FA	10900	0.128	85200

Notes:

- a) Characteristic values were taken from Shimizu (1), Table 33, p. 170, where A is Charbonnier's "vivacity" of the lift powder in dm<sup>2</sup>/kg·sec, f is the explosive force of the lift powder in kg·dm/kg, and G is the grain shape functions of the lift powder which is dimensionless. (Note dm is decimeter = 10 cm, and kg is kilogram = 1000 grams.)
- b) From Table 2, these are the American powder types with mesh range most nearly duplicating those reported by Shimizu.

**Table 4. Shell Performance for Nominal Input Parameters.**

Shell Type	Shell Size (in.)	Muzzle Velocity (ft/sec)	Maximum Pressure (psi)	Distance to Max. Pres. (inches)	Max. Shell Height (feet)	Time to Max. Ht. (sec.)	Velocity on impact (ft/sec)	Time on Impact (sec)
<b>Spherical</b>	3	358	70	7.5	470	4.4	82	6.5
	4	360	114	7.4	596	5.1	98	7.2
	5	370	127	8.3	680	5.5	107	7.6
	6	389	158	8.4	765	5.9	114	8.0
	8	389	202	9.0	847	6.2	123	8.4
	10	365	248	10.0	893	6.6	133	8.4
	12	278	278	11.4	898	6.7	137	8.3
<b>Cylindrical</b>	3	508	222	5.8	452	4.0	70	6.9
	4	485	271	6.6	551	4.5	81	7.4
	5	479	304	7.1	633	4.9	90	7.8
	6	457	382	7.4	751	5.5	103	8.3
	8	432	515	7.8	878	6.2	119	8.7
	10	400	610	8.7	939	6.6	131	8.8
	12	358	721	9.5	929	6.8	139	8.5

tions. In order to make this paper of greater value to users of US Black Powder granulations, it was necessary to designate which US granulations correspond to Shimizu's characteristic values. These assignments are shown in Table 3.

**Nominal Aerial Shell Performance Values**

Table 4 lists the shell performance values predicted by the Shimizu equations, when using the nominal input values given in Table 1. Figures 1 through 3 present maximum mortar pressure, maximum shell height, and time to maximum shell height as functions of shell size for both spherical and cylindrical shells. It is of interest to note that maximum mortar pressures for cylindrical shells are approximately 2.5 times greater than those for spherical shells. Of course, the importance of this result is that cylindrical shells place considerably more stress on a mortar than do spherical shells, a fact well known to experienced pyrotechnicians.

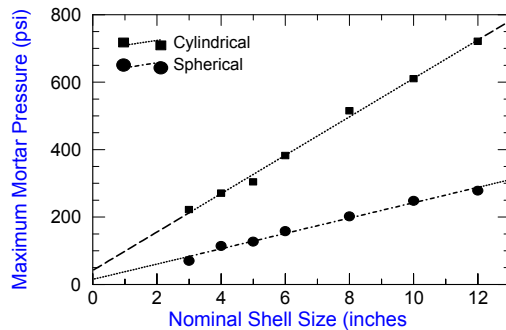


Figure 1. Maximum mortar pressure as a function of shell size for nominal input parameters.

Figure 2 also includes empirically determined burst heights for spherical shells<sup>2</sup>. This curve represents a rather limited amount of data; however, it is in general agreement with some data published by Shimizu<sup>1</sup>. This experimentally determined data was included because it was felt it must be acknowledged that the data for large shells deviate from the maximum shell heights predicted using the Shimizu equations. (At the time of this writing, the reason for this difference has not been established.)

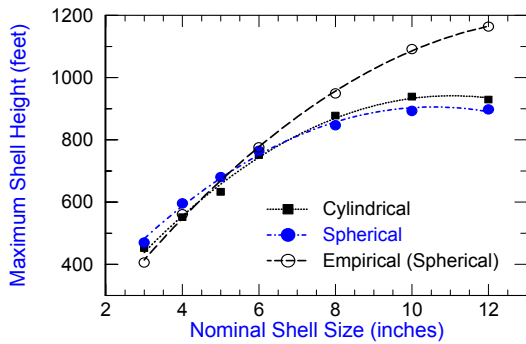


Figure 2. Maximum shell height as a function of shell size for nominal input parameters.

In addition, it may be of interest to note that:

- Muzzle velocities are largely independent of shell size.
- Maximum mortar pressures are reached before the shells rise very far above the bottom of the mortar.
- Rise times for shells are shorter than fall times.

Readers are again cautioned to consider these shell performance values only within the context of this paper. These values are calculated results based on numerous assumptions and only for the nominal input values assumed. These performance values are not the results of actual measurements and they may be only approximately correct.

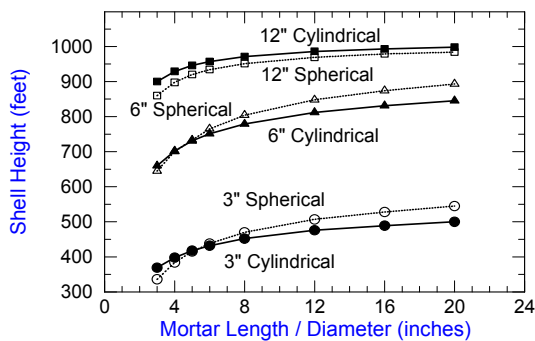


Figure 4. Maximum shell height as a function of mortar length.

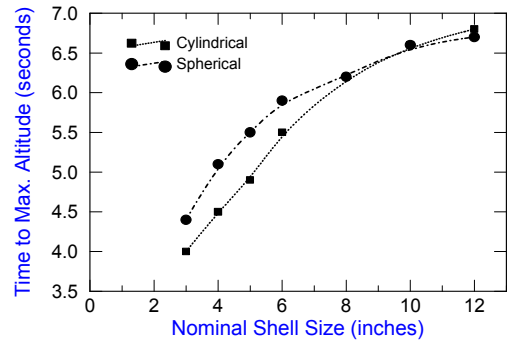


Figure 3. Time taken to reach maximum shell height as a function of shell size for nominal input parameters.

### Effects of Mortar Length

Over the years, there has probably been more speculation regarding the effect of mortar length on the flight of aerial shells than any other single factor. The results of calculations of maximum shell height for 3, 6, and 12-inch shells as a function of mortar length are listed in Table 5. Maximum shell heights are listed both in absolute terms and as a percent of the heights achieved when using mortar lengths 20 times the diameter. These same data are presented in Figure 4. For convenience in plotting, mortar lengths are expressed as multiples of mortar internal diameters.

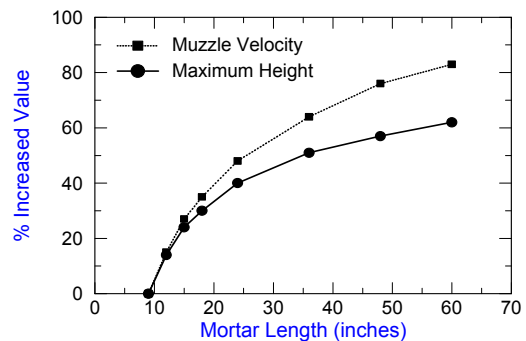


Figure 5. Comparison of increases in maximum shell height and muzzle velocity as a function of mortar length for three-inch spherical shells.

**Table 5. Effect of Mortar Length on Maximum Shell Height.**

	Mortar Length Divided by Diameter	3" Shell		6" Shell		12" Shell	
		Height (feet)	Percent (a)	Height (feet)	Percent (a)	Height (feet)	Percent (a)
<b>Spherical</b>	3	336	62	645	72	860	87
	4	384	70	701	78	898	91
	5	415	76	733	82	920	93
	6	438	80	765	86	934	95
	8	470	86	804	90	951	97
	12	507	93	848	95	969	98
	16	528	97	874	98	979	99
	20	545	100	893	100	984	100
<b>Cylindrical</b>	3	369	74	660	78	900	90
	4	398	80	702	83	929	93
	5	418	84	731	87	946	95
	6	432	86	751	89	957	96
	8	452	90	779	92	971	97
	12	476	95	812	96	986	99
	16	489	98	831	98	993	99
	20	500	100	845	100	998	100

(a) Height expressed as the percent of the height reached when mortar length is 20 times the mortar diameter.

It may be of interest to examine the data in order to evaluate the appropriateness of the rule-of-thumb recommending use of mortars 5-times their ID for shells less than 8-inches and 4-times their ID for shells 8-inches or more. For small shells, it seems there might be an advantage in using mortars that were somewhat longer. However, given the burst radii of hard breaking shells<sup>3</sup>, it does not seem that the 5-

times diameter rule represents a safety concern.

It might also be of interest to comment on the relationship between a shell's muzzle velocity and the maximum height it attains. In order to do this, consider the muzzle velocity and maximum height data for three-inch spherical shells, listed in Table 6 and shown in Figure 5. With increasing mortar length, muzzle velocity

**Table 6. Effect of Mortar Length on Maximum Shell Height and Muzzle Velocity for Three-Inch Spherical Shells.**

Mortar Length (inches)	Muzzle Velocity (ft/sec)	Percent In- creased Velocity (a)	Maximum Height (feet)	Percent In- creased Shell Height (a)
9	242	0	336	0
12	279	15	383	14
15	307	27	415	24
18	327	35	438	30
24	358	48	470	40
36	398	64	507	51
48	425	76	529	57
60	444	83	545	62

(a) Muzzle velocity and height as the percent increase to that for a nine-inch long mortar.

and maximum height both increase; however, the increase in maximum height is not as great as the increase in muzzle velocity. The reason for this difference is that aerodynamic drag is a function of a shell's velocity<sup>1,4</sup>. The faster a shell is moving, the greater are the losses due to drag forces. Thus increases in muzzle velocity cause greater drag forces, which in turn allow less than proportional increases in shell height.

**End of Part 1:** (The remainder of this article will continue to address the effects of altering input values; for example varying mortar to shell clearance, shell weights, and loading spaces.)

### References for Part 1

- 1) Shimizu, T., 1985. *Fireworks from a Physical Standpoint Part III*, Pyrotechnica Publications, Austin, TX.
- 2) Kosanke, K.L., Schwertly, L.A., and Kosanke, B.J., "Report of Aerial Shell Burst Height Measurements", *PGI Bulletin*, No. 68 (1990).
- 3) Kosanke, K.L. and B.J., "Japanese Shell Break Radii", *PGI Bulletin*, No. 59 (1988).
- 4) Kosanke, K.L. and B.J., "Computer Modeling of Aerial Shell Ballistics," *Pyrotechnica XIV* (1992).

---

Originally appeared in *Pyrotechnics Guild International Bulletin*, No. 73 (1990).

## Shimizu Aerial Shell Ballistic Predictions (Part 2)

by K.L. and B.J. Kosanke

(Continuation of Part 1, which appeared in *Pyrotechnics Guild International Bulletin* No. 72 (1990).)

---

### Effects of Shell Clearance in Mortar

Another area of frequent speculation is the effect of various shell clearances within mortars. However, Shimizu warns that his Black Powder characteristic values are only correct for shells with diameters about 11 percent smaller than the mortar. (In effect, this is one of the simplifying assumptions he has made.) It is not possible to run calculations of the effect of varying shell clearance, without having the appropriate Black Powder characteristic values. Unfortunately, the derivation of the needed values is beyond the present limits of the authors' expertise, and thus the desired clearance calculations cannot be performed and reported here.

### Effects of Shell Lift Weight

The results of calculations of maximum shell height and maximum mortar pressure as functions of the amount of lift charge are listed

in Table 7 and shown in Figures 6 and 7. For these calculations, the range of values used for lift charge weights was limited to 80 percent through 140 percent of the nominal amounts listed in Table 1 (Part 1). Even though results for more extreme values would certainly be of interest, these are not reported here. This is because there was evidence that the characteristic values for Black Powder were not appropriate for use in more extreme cases. Rather than include highly suspicious results, the authors chose the conservative approach of limiting the range of reported results.

As can be seen when comparing Figures 6 and 7, the effect of lift charge amount on maximum shell height, is predicted to be much less than its effect on maximum mortar pressure. For example, varying lift charge weight for 6-inch spherical shells produced an increase in maximum shell height of 34 percent, it simultaneously produced an increase in maximum mortar pressure of 164 percent!

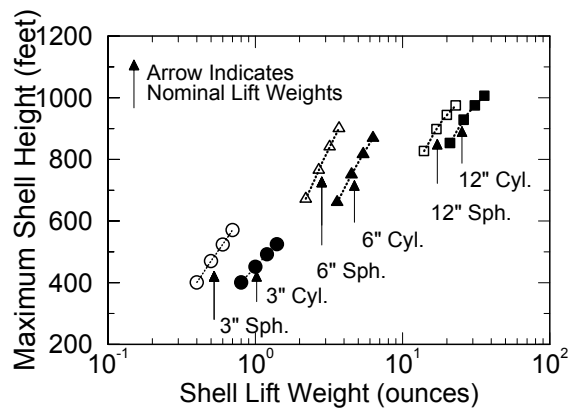


Figure 6. Maximum shell height as a function of lift weight.

### Effects of Lift Charge Type

The results of calculations of maximum shell height, maximum mortar pressure, and distance to maximum pressure as functions of lift charge type are listed in Table 8. The authors have some concern as to whether the results are totally believable (e.g. maximum mortar pressures for 4Fg lift powder are consistently less than expected when compared to reported values for other granulations). In part, this may be a result of the authors' assigning US Black Powder granulations to characteristic

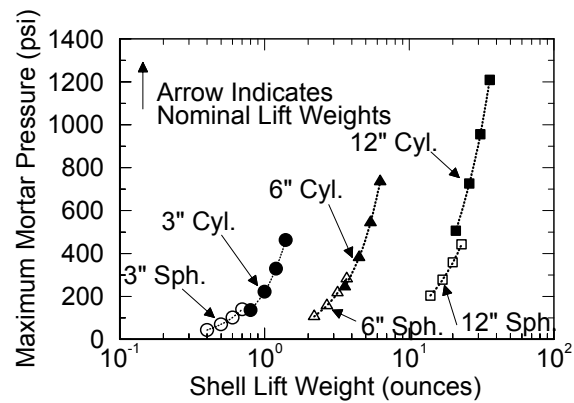


Figure 7. Maximum mortar pressure as a function of shell lift weight.

values for Japanese lift powder. Nonetheless, several things seem clear:

- For small and medium spherical shells, the use of finer grained powders is predicted to be useful in propelling the shells to their proper heights.
- For large spherical shells and all cylindrical shells, the use of coarser grained powders is preferred because the use of finer grained powders produces little if any gain in maximum shell height, while at the same time producing much higher mortar pres-

Table 7. Effect of Shell Lift Weight on Maximum Shell Height and Maximum Mortar Pressure.

3" Spherical			3" Cylindrical			6" Spherical		
Lift Weight	Max. Height	Max. Pressure	Lift Weight	Max. Height	Max. Pressure	Lift Weight	Max. Height	Max. Pressure
(ounces)	(feet)	(psi)	(ounces)	(feet)	(psi)	(ounces)	(feet)	(psi)
0.4	401	44	0.8	401	137	2.2	672	107
0.5	470	70	1.0	452	222	2.7	765	158
0.6	524	102	1.2	492	330	3.2	841	217
0.7	571	140	1.4	525	463	3.7	901	283
6" Cylindrical			12" Spherical			12" Cylindrical		
Lift Weight	Max. Height	Max. Pressure	Lift Weight	Max. Height	Max. Pressure	Lift Weight	Max. Height	Max. Pressure
(ounces)	(feet)	(psi)	(ounces)	(feet)	(psi)	(ounces)	(feet)	(psi)
3.6	661	246	14	827	204	21	853	506
4.5	751	382	17	898	278	26	929	726
5.4	817	545	20	944	358	31	975	956
6.3	869	735	23	975	443	36	1006	1209

**Table 8. Effect of Shell Lift Type on Maximum Shell Height, Maximum Mortar Pressure and Distance of Shell Travel within Mortar at the Moment of Maximum Pressure.**

	3" Spherical			3" Cylindrical		
Lift Type	Max. Height (feet)	Max. Pressure (psi)	Dist. to Max. press. (inches)	Max. Height (feet)	Max. Pressure (psi)	Dist. to Max. Press. (inches)
2FA	346	29	9.5	452	222	5.8
3-4FA	399	42	8.7	477	317	5.0
2Fg	455	61	8.0	503	449	4.4
2-3Fg	470	70	7.5	501	500	4.0
4Fg	457	71	6.75	468	479	3.6
	6" Spherical			6" Cylindrical		
Lift Type	Max. Height (feet)	Max. Pressure (psi)	Dist. to Max. press. (inches)	Max. Height (feet)	Max. Pressure (psi)	Dist. to Max. Press. (inches)
2FA	625	70	12.1	751	382	7.4
3-4FA	694	100	10.4	737	500	6.2
2Fg	768	142	9.2	736	657	5.6
2-3Fg	765	158	8.4	681	683	5.2
4Fg	687	151	7.4	546	594	4.8
	12" Spherical			12" Cylindrical		
Lift Type	Max. Height (feet)	Max. Pressure (psi)	Dist. to Max. press. (inches)	Max. Height (feet)	Max. Pressure (psi)	Dist. to Max. Press. (inches)
2FA	964	158	16.5	929	721	9.5
3-4FA	964	206	13.7	706	790	8.5
2Fg	982	269	12.3	600	923	8.1
2-3Fg	898	278	11.4	475	886	7.9
4Fg	681	241	10.5	292	698	7.6

sures.

- The use of progressively finer lift powders has the expected effect of decreasing the distance traveled by the shell in the mortar before maximum mortar pressure is reached.

The results of calculations of maximum shell height and maximum mortar pressure as functions of shell weight are listed in Table 9 and shown in Figures 8 and 9. The results for maximum shell height, at first seem somewhat surprising. The calculations suggest that small spherical shells will travel to greater heights when they are made heavier. The reason is that for each shell size and lift charge weight, there is an optimum shell weight that results in the greatest height for the shell. At lesser weights the situation becomes increasingly like a person trying to throw a feather; it is almost impossible

to throw a feather farther than a few feet no matter how hard it is thrown. At weights greater than the optimum, the situation becomes increasingly like a person trying to throw a cement block; again, it is almost impossible to throw a cement block more than a short distance. However, for objects near the optimum size and weight (e.g. a baseball), it is relatively easy for a person to throw the object a hundred feet or more. Following this analogy, small shells fall more nearly into the category of feathers rather than cement blocks, and an increase in their weight actually causes them to be propelled to greater heights. It may be of interest to note that nominal 8 and 10-inch spherical shells, and 12-inch cylindrical shells are very nearly at their optimum projection weights.

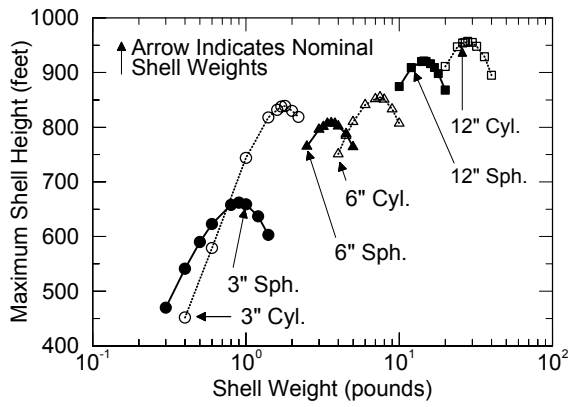


Figure 8. Maximum shell height as a function of shell weight.

As would be expected, maximum mortar pressure universally increases as shell weights increase. This is primarily the result of the shell's increasing inertia. Heavier shells accelerate more slowly in response to a given lift gas pressure. Accordingly, heavier shells spend a longer time traveling any given distance within the mortar. In turn, this means that during the early stages of the shell's travel within the mortar, greater percentages of the lift power will have been consumed, generating more gas in the same space, which manifests itself as greater mortar pressure.

It may be of interest to note that, independent of shell size, all shells of approximately the optimum shell weight, result in nearly constant

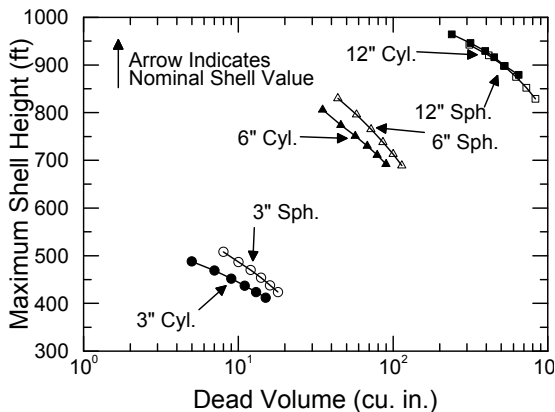


Figure 10. Maximum shell height as a function of shell dead volume.

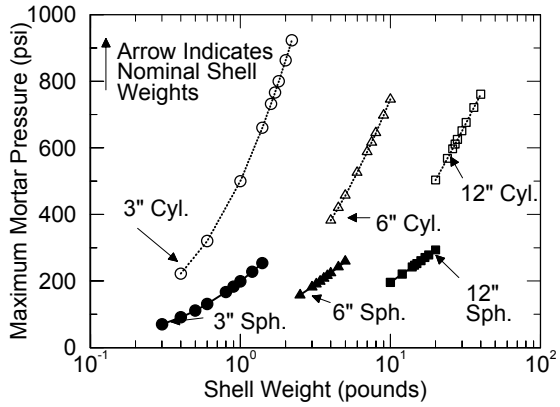


Figure 9. Maximum mortar pressure as a function of shell weight.

maximum mortar pressures. For spherical shells this is roughly 200 psi, and for cylindrical shells this is roughly 700 psi.

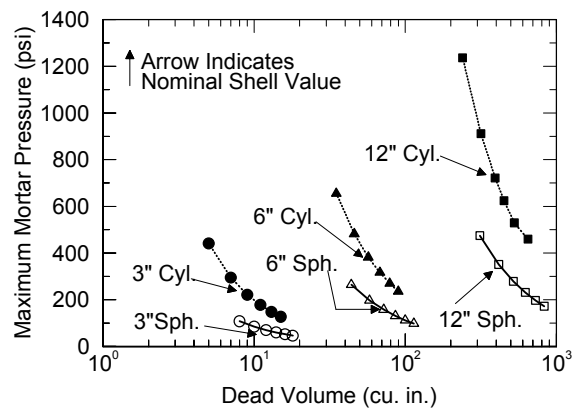


Figure 11. Maximum mortar pressure as a function of dead volume.



**Table 9. Effect of Shell Weight on Maximum Shell Height and Maximum Mortar Pressure.**

3" Cylindrical			3" Spherical			6" Cylindrical		
Shell Weight (lbs.)	Max. Height (feet)	Max. Pressure (psi)	Shell Weight (lbs.)	Max. Height (feet)	Max. Pressure (psi)	Shell Weight (lbs.)	Max. Height (feet)	Max. Pressure (psi)
0.3	470	70	0.4	452	222	2.5	765	158
0.4	541	91	0.6	579	320	3.0	796	182
0.5	590	111	1.0	744	500	3.2	801	191
0.6	623	131	1.4	818	660	3.4	807	199
0.8	658	167	1.6	832	732	3.6	808	208
0.9	662	183	1.7	838	766	3.8	807	216
1.0	659	199	1.8	839	800	4.0	802	224
1.2	637	228	2.0	830	863	4.5	788	242
1.4	603	254	2.2	819	923	5.0	764	259
6" Cylindrical			12" Spherical			12" Cylindrical		
Shell Weight (lbs.)	Max. Height (feet)	Max. Pressure (psi)	Shell Weight (lbs.)	Max. Height (feet)	Max. Pressure (psi)	Shell Weight (lbs.)	Max. Height (feet)	Max. Pressure (psi)
4.0	751	382	10.	874	196	20.	911	503
4.5	785	420	12.	909	221	24.	947	568
5.0	810	457	14.	920	242	26.	954	597
6.0	841	526	14.5	921	247	27.	955	611
7.0	852	588	15.	920	252	28.	957	625
7.5	855	617	16.	916	261	30.	955	651
8.0	851	645	17.	909	270	32.	948	676
9.0	833	698	18.	898	278	36.	929	721
10.0	807	746	20.	868	293	40.	895	761

### Effects of Dead Volume

Dead volume (also called loading space) is defined as the unoccupied volume below a shell in a mortar. Results of calculations of maximum shell heights and maximum mortar pressures as functions of dead volume are listed in Table 10 and shown in Figures 10 and 11. It should be noted that while dead volume is predicted to have an effect on maximum shell height, the effect is not particularly great. For example, a 60% increase in dead volume for a 6-inch cylindrical shell results in only a 7% decrease in maximum shell height. (Note that a 60% increase in dead volume is equivalent to raising the shell an extra 1¼-inch off the bottom of the mortar.) One could conclude from this observation that small amounts of debris, remaining in mortars between firings, and thereby increasing dead volume, will not result in an

unsafe decrease in maximum shell height. This is one reason (combined with personnel safety considerations) why it is no longer recommended that mortars be cleaned after each use during a manually fired display. The effect of dead volume on maximum mortar pressure, shown in Figure 11, is of much greater consequence. For example a 40% decrease in dead volume for a 6-inch cylindrical shell results in a 71% increase in maximum mortar pressure (Note that a 40% reduction in dead volume is equivalent to pushing the shell ¼-inch further into the mortar.). Thus, when attempting to fire a massive shell and have both the shell and mortar survive the process, one should employ ample dead volume. In many cases, the modest loss in shell height that results can be eliminated by using a slightly longer mortar. As an alternative, even if slightly more lift is used to fully restore the shell's height, maximum mortar

**Table 10. Effect of Dead Volume on Maximum Shell Height and Maximum Mortar Pressure.**

3" Spherical			3" Spherical			6" Spherical		
Dead Volume (cu. in.)	Max. Height (feet)	Max. Pressure (psi)	Dead Volume (cu. in.)	Max. Height (feet)	Max. Pressure (psi)	Dead Volume (cu. in.)	Max. Height (feet)	Max. Pressure (psi)
8	508	108	5	488	441	44	830	264
10	487	85	7	469	295	58	796	197
12	470	70	9	452	221	72	765	158
14	454	60	11	437	178	86	738	131
16	438	52	13	424	148	100	713	112
18	424	46	15	412	127	114	689	98
6" Spherical			12" Spherical			12" Spherical		
Dead Volume (cu. in.)	Max. Height (feet)	Max. Pressure (psi)	Dead Volume (cu. in.)	Max. Height (feet)	Max. Pressure (psi)	Dead Volume (cu. in.)	Max. Height (feet)	Max. Pressure (psi)
35	806	655	312	942	474	240	964	1236
46	774	482	416	920	351	317	946	911
57	751	382	520	898	278	394	929	721
68	730	316	624	875	231	451	916	624
79	711	269	728	852	197	528	898	529
90	692	235	832	829	172	650	879	459

pressures will still be lower than was the case when there was less dead volume.

Dead volume is also one reason why spherical shells, even heavy ones, can be lifted using rather fine-grained powders. The shape of spherical shells automatically provides ample dead volume, which tends to reduce the maximum mortar pressures below that which would normally result from the use of fine grained (faster burning) lift powder.

### Conclusion

The information presented in this article is only intended to illustrate the general effects of varying shell and mortar parameters. It is not intended to imply that any of the results can be

taken as precisely accurate. In spite of the limitations implicit in these data, they should prove to be of interest to both manufacturers and display companies.

### Acknowledgments

The authors wish to gratefully acknowledge T. Shimizu for his original efforts in developing the formulas used in these calculations and for reviewing an earlier draft of this article. The authors wish to acknowledge D. Rowe for assistance with defining nominal input parameters for large cylindrical shells. Finally, the authors wish to acknowledge R. Winokur and J. Bergman for their assistance in editing this article.

## Hazard Data for Chemicals Used in Pyrotechnics

K.L. and B.J. Kosanke

In recent months, the authors have received a surprising number of requests for sources of chemical hazard information. Perhaps this is a consequence of the industry's increasing concern for health and safety. Whatever the reason for the requests for information, the authors have prepared this article to assist those needing to locate reliable and practical hazardous chemical information.

Perhaps the most commonly used reference text on chemical hazards is the *Hazardous Chemicals Desk Reference (HCDR)* by Sax and Lewis; published by Van Nostrand Reinhold. If this is the only reference consulted in evaluating potential chemical hazards, a very strong word of caution is warranted. The *HCDR* assigns a "Hazard Rating" to each of the approximately 5000 chemicals listed. However, these ratings are based exclusively on chemical toxicity. Often included in the discussion about each chemical is some information on reactivity and flammability. Unfortunately, that information is quite general in terms of hazard level (e.g., "moderate fire hazard" or "slight explosion hazard") and it is not considered at all in assigning the overall hazard rating to the chemical. Thus, the first word of caution is that users of the *HCDR* must not assume that its hazard ratings apply to anything more than chemical toxicity.

In the *HCDR*, toxicities are addressed in terms of  $LD_{50}$ 's. (For a chemical, its  $LD_{50}$  is the weight of that chemical, in milligrams per kilogram of body weight, which will constitute a lethal dose to 50% of those persons exposed, within a specified period of time.) The hazard ratings are divided into three categories:

HR3,  $LD_{50} < 400$  mg/kg;

HR2,  $LD_{50} > 400$  mg/kg, but  $< 4,000$  mg/kg; and

HR1,  $LD_{50} > 4,000$  mg/kg, but  $< 40,000$  mg/kg.

One might assume that there is a fourth (implicit) hazard-rating category, HR0, for chemicals with essentially no toxic hazard. Further, one might assume that this was the hazard rating assigned to all common chemicals not included among the 5000 listed. The latter assumption certainly is not true. Thus, the second word of caution is that it could be a serious mistake for a reader to assume that any chemical not listed in the *HCDR* is relatively non-toxic.

This article has addressed two areas in which the *HCDR* may understate the hazards associated with some chemicals. While these are of concern, it is not the area of greatest concern regarding the use of the *HCDR*. As a result of stopping with HR3 as the greatest toxicity hazard, instead of having at least a HR4 and HR5, the *HCDR* equates chemicals of vastly differing toxic hazards, listing them all as HR3. The problem is that one is often left without the appropriate guidance as to how to handle many toxic chemicals. An illustration of this problem for chemicals with the highest reported toxic hazard (HR3), one might think it would be totally inappropriate to ever eat them, cook in them, breathe them, wear them as clothing and jewelry, or spread billions of pounds of them around in our cities. One might think that but it would not be true. Consider the following list of chemicals all rated as having the highest toxicity, HR3: Fruit Sugar (Fructose), Milk Sugar (Lactose), Vitamins (A, B<sub>3</sub>, B<sub>6</sub>, B<sub>12</sub>, C), Grain Alcohol (Ethanol), Caffeine, Aluminum, Teflon, Oxygen, Silk, Nylon, Gold, Silver, Platinum, and (Road) Asphalt. The list of materials with HR3 is incredible, and also includes, Penicillin, Human Sperm, Cellophane, Rust (Iron Oxide), and Gasoline. Most, if not all, of these things are not what comes to mind when one thinks of "extremely toxic" chemicals for which special care is required. Your dilemma when using the *HCDR*, and finding a chemical listed as HR3, is

how should it be handled; take along a spoon (in case you get hungry and want a snack) or don disposable coveralls and a respirator. In large measure the problem would be eliminated if higher hazard ratings (HR4 and HR5) were used for those chemicals that deserve those higher ratings. The authors of the *HCDR* chose not to do this; thus the final word of caution is to definitely seek further chemical hazard information than can be found in the *Hazardous Chemicals Desk Reference*.

Another commonly used reference for hazard information, is the National Fire Protection Association's document, NFPA 49-1975 *Hazardous Chemicals Data (HCD)*. The authors suggest this is a better source of information, but that it still falls significantly short of meeting a person's need for hazardous chemical information. (This NFPA document will be replaced by a new version later this year, but it will contain the same basic deficiency discussed in this article.)

The major strength of the *HCD* listing is that it provides safety information in three areas: Health, Flammability, and Reactivity. The listed chemicals are assigned a rating from 0 to 4 in each category, with 0 corresponding to "no special hazard" and 4 corresponding to an "extreme hazard." Another strength of the *HCD* listing is that it provides other useful information such as a description of the material, extensive information on fire hazards including explosive hazards in fire situations, and proper storage practices.

Unfortunately, the *HCD* listing's of health hazard ratings are based only on acute health hazards. (Note that acute health hazards are those associated with exposures for limited time periods, e.g., hours, whereas chronic hazards are those associated with exposures over very much longer periods, e.g., years.) Fireworks plant personnel's exposure to hazardous chemicals will normally only be for extended time periods; thus it is both acute and chronic health hazards that are of interest. Another, and probably the most serious weakness of the *HCD* listing is that all its hazard ratings are in the strict context of fire fighting situations. Quite simply, this is a hazard rating system designed to be of use to fire service personnel when fighting chemical fires. Occasionally the *HCD* listing also includes haz-

ard ratings for "non-fire" situations. However, even then, the ratings are in the context of the unique needs of fire service personnel. The *HCD* listing's hazard ratings are often applicable to the needs of others, but not always. As obvious examples of when the NFPA system breaks down for use by non-fire service personnel, consider the following *HCD* hazard ratings:

- Nitric and hydrochloric acids are rated as 0 Reactivity Hazard (i.e., non-reactive). This is because, in a fire situation, they are stable and unreactive with water (and other fire extinguishing agents). However, anyone that has physical contact with concentrated nitric or hydrochloric acid will be quick to attest that they are indeed dangerously reactive.
- Potassium chlorate and many of the most common pyrotechnic oxidizers are rated as 0 Reactivity Hazard, regardless of their potential to react explosively with powdered fuels.
- Lead nitrate and barium nitrate, in non-fire situations, are rated as 0 Health Hazard, regardless of the fact that they are water soluble, which makes them heavy metal poisons. (Note that the *HCDR* assigns these their highest toxic hazard rating, 3.)

The *Hazardous Chemicals Data* listing (NFPA 49) may be invaluable to fire service personnel. However, fireworks plant operators needing chemical hazard information should be very cautious in using these hazard ratings, even those listed as applicable to non-fire situations.

In terms of completeness, the best sources of chemical hazard information are Material Safety Data (MSD) sheets. These are the documents required by OSHA's Hazard Communication standard (29 CFR 1910.1200) for all hazardous materials and must be on the premises of any commercial site where those materials are being used or stored. MSD sheets generally are two to four pages in length and, when properly completed, contain a wealth of information. Among the facts documented on MSD sheets are: general chemical data, a list of hazardous ingredients, physical data, fire and explosion data, health hazard data, reactivity data, spill or leak procedures, special protection information, and special precautions.

As good as MSD sheets are, it must be acknowledged, that their exclusive use may also present some practical problems. In part this is because of all the highly technical information they contain; they are somewhat difficult for plant personnel to interpret and understand.

Considering the ease of use, the authors feel the J.T. Baker SAF-T-DATA system should be considered as a practical adjunct to the use of MSD sheets. The SAF-T-DATA system assigns a hazard rating from 0 (no known hazard) to 4 (extreme hazard) in each of four areas. The hazard areas are Health, Flammability, Reactivity, and Contact, where:

- Health hazard is the danger or toxic effect of a substance if inhaled, ingested, or absorbed;
- Flammable hazard is the tendency of the substance to burn in air;
- Reactivity hazard is the potential of a substance to explode or react violently with air, water, or other substances (e.g., substances with a flammability hazard); and
- Contact hazard is the danger a substance presents when exposed to skin, eyes, and mucous membranes.

A listing of SAF-T-DATA ratings is included in J.T. Baker's chemical catalog for those materials that they sell. However, as a convenience, the authors have prepared a listing of those chemicals one is likely to encounter in pyrotechnics and their hazard ratings.

#### SAFETY RATING SYSTEM FOR PYRO-CHEMICALS

- 0 = None,
- 1 = Slight,
- 2 = Moderate,
- 3 = Severe, and
- 4 = Extreme.

The safety ratings are given for four areas of hazard concern:

H = Health is danger or toxic effect a substance presents if inhaled, ingested, or absorbed,

F = Flammability is the tendency of the substance to burn,

R = Reactivity is the potential of a substance to explode or react violently with air, water or other substances, and

C = Contact is the danger a substance presents when exposed to skin, eyes, and mucous membranes.

Description	<u>H</u>	<u>F</u>	<u>R</u>	<u>C</u>
Accroides resin (red gum)	1	2	0	1
Acetone (nitrocellulose solvent)	1	3	2	1
Aluminum (400 mesh flake)	1	4	2	1
Aluminum (325 mesh, granular)	1	3	2	1
Ammonium dichromate	4	1	3	3
Ammonium nitrate	1	0	3	2
Ammonium perchlorate	1	0	3	2
Anthracene	1	1	0	1
Antimony trisulfide (325 mesh)	3	3	2	1
Barium carbonate	1	0	0	1
Barium chlorate	3	0	3	1
Barium nitrate	3	0	3	1
Barium sulfate	1	0	0	0
Benzene	4	3	2	1
Boric acid	2	0	0	2
Cab-o-sil (colloidal silica)	2	0	0	1
Calcium Carbonate	0	0	0	1
Calcium Sulfate	1	0	0	1
Charcoal (80 mesh)	0	1	0	1
Charcoal (air float)	0	2	0	1
Chlorowax	2	1	1	1
Clay (bentonite)	1	0	0	0
CMC (sodium carboxymethylcellulose)	1	1	1	1
Copper(II) carbonate (basic)	2	0	0	1
Copper(II) oxide (black)	2	0	0	1
Copper oxychloride	2	0	0	1
Copper(II) sulfate	2	0	0	2
Cryolite	1	0	0	1
Dechlorane	2	1	1	2
Dextrin (yellow)	0	1	0	0
Gallic acid, monohydrate	1	1	0	1
Graphite (325 mesh)	1	2	0	0
Hexachlorobenzene (HCB)	2	1	1	1
Hexachloroethane (HCE)	2	1	1	1
Hexamine (hexamethylene-tetramine)	1	1	1	1
Hydrochloric acid (conc.)	3	0	2	3
Iodine, sublimed	3	0	2	3
Iron(II) oxide (black)	1	0	1	1
Iron(III) oxide (red)	1	0	1	1
Isopropanol (isopropyl alcohol)	1	3	1	1

Description	H	F	R	C
Lactose	0	1	1	0
Lampblack (oil free)	1	2	0	1
Lead, granular	3	0	0	1
Lead dioxide	3	0	3	1
Lead nitrate	3	0	3	1
Lead oxide (red, minium)	3	0	1	1
Magnesium (200 mesh)	1	3	2	0
Magnesium (325 mesh)	1	4	2	0
Magnesium alum. 50/50 (gran., 100–200 m.)	1	3	2	1
Magnesium alum. 50/50 (gran., 200–400 m.)	1	4	2	1
Magnesium carbonate	1	0	1	0
Manganese dioxide	1	0	1	1
Methanol (methyl alcohol)	3	3	1	1
Methylene chloride	3	1	1	2
Mineral oil	1	1	0	1
Nitric Acid (Concentrated)	3	0	3	4
Nitrocellulose (lacquer 10% solution)	1	3	2	1
Paraffin oil	1	1	0	1
Parlon (chlorinated natural rubber)	2	1	1	1
Phosphorous, red	0	2	2	2
Picric acid, crystal	2	2	2	2
Polyvinyl chloride (PVC)	2	1	1	1
Potassium, lump	3	3	3	4
Potassium bicarbonate	1	0	1	0
Potassium chlorate	1	0	3	2
Potassium dichromate (fine granular)	4	0	3	3
Potassium hydroxide, pellets	3	0	2	4
Potassium nitrate	1	0	3	2
Potassium perchlorate	1	0	3	2
Potassium permanganate	2	0	3	2
Potassium sulfate	1	0	0	0
PVC (polyvinyl chloride)	2	1	1	1
Red gum (accroides resin)	1	2	0	1
Shellac (–120 mesh, orange)	1	2	0	1
Silica (fumed-colloidal, Cab- o-sil)	2	0	0	1
Silica gel (60–200 mesh)	2	0	0	1
Silicon metal powder (325 mesh)	2	3	1	1
Silver nitrate, crystal	3	0	3	3
Smoke dye	1	1	1	2
Sodium, lump	3	3	3	4

Description	H	F	R	C
Sodium azide	3	2	3	2
Sodium benzoate	1	1	0	1
Sodium bicarbonate	0	0	1	1
Sodium carboxymethyl- cellulose (CMC)	1	1	1	1
Sodium chlorate, crystal	1	0	3	1
Sodium cyanide, granular	3	0	2	3
Sodium hydroxide, pellets	3	0	2	4
Sodium nitrate	1	0	3	1
Sodium oxalate	3	0	1	2
Sodium salicylate	1	1	0	1
Sodium silicate (water glass, liquid)	1	0	0	2
Sodium sulfate	0	0	0	1
Starch, soluble potato	0	1	0	1
Stearic acid	1	1	1	1
Strontium carbonate	1	0	0	1
Strontium nitrate	1	0	3	1
Strontium sulfate	1	0	0	1
Sulfur (flour)	1	1	0	1
Sulfuric acid (Conc.)	3	0	3	4
Talc, powder	1	0	0	1
Tetrachloroethane	3	0	1	2
Tin, granular (20 mesh)	0	0	0	1
Titanium metal powder (100 mesh)	1	3	2	1
Titanium metal powder (300 mesh)	1	4	2	1
Titanium tetrachloride	3	0	2	3
Trichloroethylene (stabilized)	3	1	2	2
Water	0	0	1	0
Zinc metal powder (dust)	1	3	2	1
Zinc oxide	4	0	3	3

## Burn Characteristics of Visco Fuse

by K.L. and B.J. Kosanke

From time to time there is speculation regarding the performance characteristics of visco fuse under various conditions. This article presents the results of a brief study of this topic.

The fuse for this study was purchased from American Visco Fuse<sup>1</sup> in 1989. While it is likely that visco fuse from other manufacturers will perform similarly, that has not been verified.

### Typical Fuse Burning Statistics

Before attempts were undertaken to establish the effects of temperature, coverings and abuse on the burn rate of visco fuse, it was felt that first a check should be made to determine to what extent the burn rate varies along sequential pieces of fuse. To accomplish this, 204 pieces of fuse were cut from a new roll of visco fuse. Each piece of fuse was five inches long, with an uncertainty of approximately  $\pm 0.2$  inch. The pieces of fuse were kept in their original sequence for testing. The test of each piece of fuse consisted of igniting it and measuring the

time from ignition until the fire spit from the opposite end. All tests were performed at a constant temperature of about 50 °F, and the fuse had been maintained at that temperature for more than a day.

Figure 1 is a graph of burn times for the sequential fuse segments. Much of the data appears, as might be expected, relatively small, mostly random, fluctuations in burn times occurring from segment to segment. These fluctuations could be the result of actual small changes in burn rate along the length of fuse. However, they could be, and to at least some extent must be, the result of small experimental errors in timing the burning fuse. The average burn time was calculated and found to be 12.8 seconds per 5 inches; this corresponds to a burn rate of 0.39 inches/second (2.6 seconds/inch). The coefficient of variation of burn time was found to be 6.9 percent.<sup>(a)</sup>

The above notwithstanding, there are features in Figure 1 that must result from actual changes in fuse burn rate. One occurs in the range of segments 70 to 90. Initially the segments burn increasingly slower, then progressively faster, and finally return to normal. The chance that this cycle of burn rate changes was a normal statistical fluctuation is approximately one in a hundred billion. Thus one must conclude that it represents a systematic change in burn rate, resulting from a change in some characteristic of the fuse. A second feature seen from segments 90 to 204, is even less likely to be merely a statistical fluctuation. Here the first 70 segments all tend to burn about one-half standard deviation fast, then the next 45 all tend to burn about one standard deviation slow. As before, this must result from an actual change affecting the burn rate of the fuse.

Because the data contains features that definitely are not typical random fluctuations, the

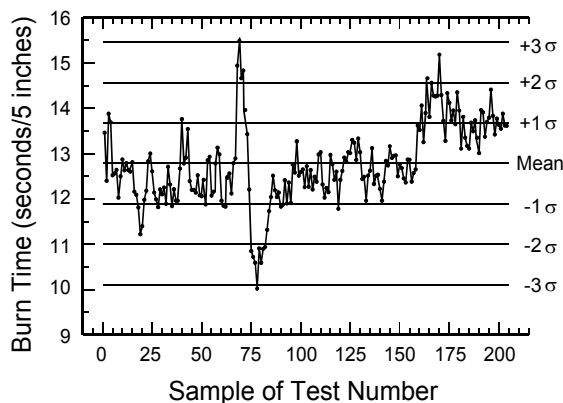


Figure 1. Burn times of sequential five-inch segments of visco fuse.

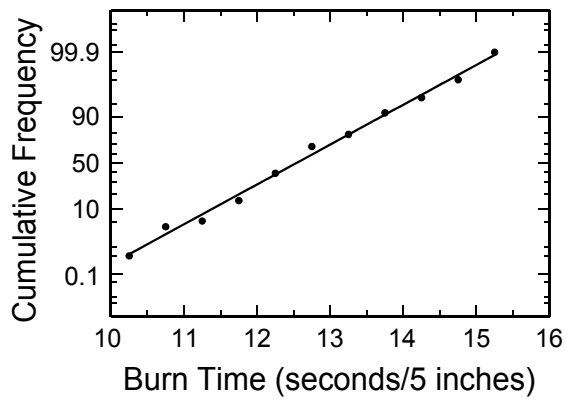


Figure 2. Cumulative frequency graph of burn times reported in Figure 1.

data was tested to determine the extent to which it deviated from a statistically “normal distribution.” This was done by plotting cumulative frequency on probability paper, shown in Figure 2. When a distribution is normal, its cumulative frequency graph will be a straight line<sup>2</sup>. As can be seen, there is very little departure from normality. Accordingly, the coefficient of variation reported above can be viewed as a fairly accurate predictor of the probability of observing various burn rates, providing the sample set is large enough.

Because relatively few measurements were made for each condition investigated in this study, a procedure was required in order to limit the adverse effect of any small systematic changes in burn rate. The method used was to distribute sequential fuse segments among the groups of fuse pieces for each series of tests. For example, suppose one test series consists of sets of ten measurements under each of three different conditions. In this case, three groups of ten fuse segments would be assembled as follows. The first segment would be placed into the first group, the second sequential segment into the second group, and the third segment into the third group. Similarly, fuse segments 4, 5 and 6 would be placed into groups 1, 2 and 3, respectively. This process would continue until each group had 10 segments. In this manner, by distributing sequential fuse segments between the groups, any effect caused by systematic changes in fuse performance along the roll would be minimized. This general procedure

was followed for each of the tests reported in this article.

### Effect of Temperature

Changes in ambient temperature alter the burning characteristics of pyrotechnic materials. One effect is that, as the temperature is increased the burn rate also increases<sup>3</sup>. This is because less thermal energy is needed to raise unburned composition to its ignition temperature. This means that less time is required to raise unburned material to its ignition temperature, and that manifests itself as an increase in burn rate.

The effect of ambient temperature on visco fuse burn rate was investigated. In preparation for these measurements, five groups of ten fuse segments (each five inches long) were assembled as described above. Each group was placed in a separate container and the temperature of the container and fuse segments was raised or lowered to one of the values desired for testing. Once certain that the container and fuse had reached the desired temperature, the burn rate for each fuse segment was measured. To minimize changes in fuse temperature during measurements, the tests were conducted under ambient temperature conditions approximately equal to that of the fuse. Further, only one piece of fuse at a time was removed from its container and its burn time measured immediately. Without delay, the next piece of fuse was measured, and so on, until all ten fuse segments in that temperature group had been measured. The re-

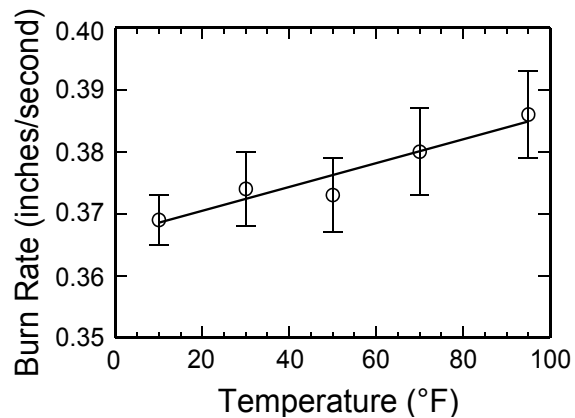


Figure 3. Temperature dependence of visco fuse burn rate.



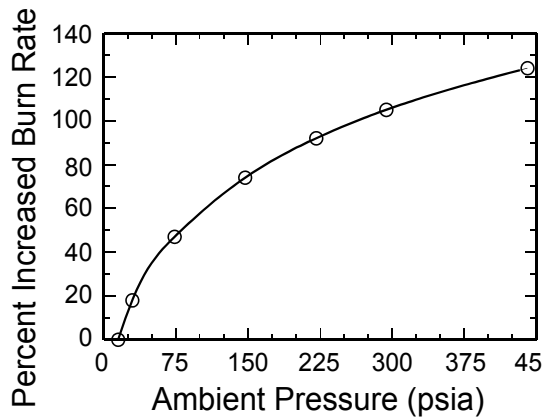


Figure 4. Functional relationship between pressure and black powder burn rate.

sults of the temperature dependence tests are shown in Figure 3. The error bars shown are  $1\sigma$  standard errors.<sup>(b)</sup> The slope of the line fit to the data is the change in burn rate as a function of temperature, which is  $1.92 \times 10^{-4}$  inches per second per degree Fahrenheit. As a result of this determination, two things seem obvious. First, burn rate has only a slight temperature dependence (i.e., extrapolating to an increase of 100 °F only results in about a 5% increase in burn rate). Second, the technique of distributing fuse segments, in order to minimize the sequence dependent changes in burn rate described in the section above, seems to have worked well.

### Effect of Fuse Coverings (Pressure)

When visco fuse burns, the pressure at the burning surface of its powder core, will be somewhat greater than atmospheric pressure. This results from the temporary confinement of the gaseous combustion products by the thread and lacquer coating of the fuse. Anything that alters the degree of confinement, such as gluing or taping the fuse, must then be expected to alter the pressure at the burning surface. It is known that changes in pressure alter the burning characteristics of pyrotechnic materials.<sup>3,4</sup> This is because, as pressure increases, the thermal density of the flame increases. The flame becomes smaller, hotter, and is held closer to the burning surface. The effect is to increase the efficiency of the feedback mechanism for ther-

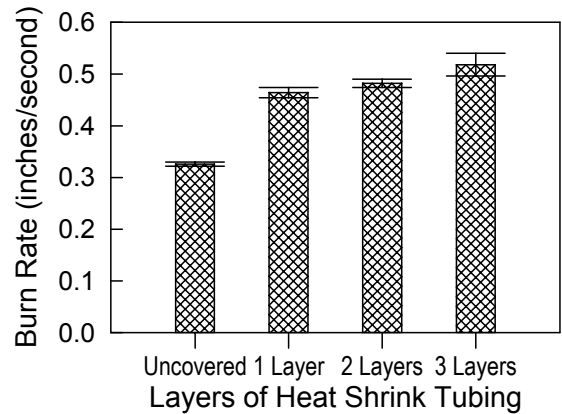


Figure 5. Burn rate variation as a result of tightly covering visco fuse.

mal energy, and this increases the rate of burning.

Figure 4 illustrates the effect of pressure on the burn rate of Black Powder (derived from information in Reference 4). Typical of most pyrotechnic materials, black powder burn rate obeys the general relationship:

$$R = A \cdot P^b \quad \text{Eq. 1}$$

where R is linear burn rate, P is pressure, and A and b are constants.<sup>3</sup> For black powder, when R is in centimeters per second and P is in atmospheres, the constants A and b are 1.21 and 0.24, respectively.<sup>3,4</sup>

The effect of coverings on the burn rate of visco fuse was investigated. In preparation for these tests, four groups of ten fuse segments (each five inches long) were prepared as described above. The method chosen to cover the fuse segments was to apply layers of heat shrink tubing, using as high a temperature as possible without injuring the tubing or igniting the fuse. This method was selected because it was felt to be reproducible and similar to the effects produced by taping or gluing. In addition to one group of fuse segments with no added covering, groups were prepared with one, two and three layers of heat shrink tubing. After all the fuse was allowed to come to about 50 °F, each of the four groups was burned and their burn times recorded. The results of these tests are shown in Figure 5. Covering the fuse with 1, 2 and 3 layers of heat shrink tubing produced increases of 42%, 48%, and 59% in burn rate,

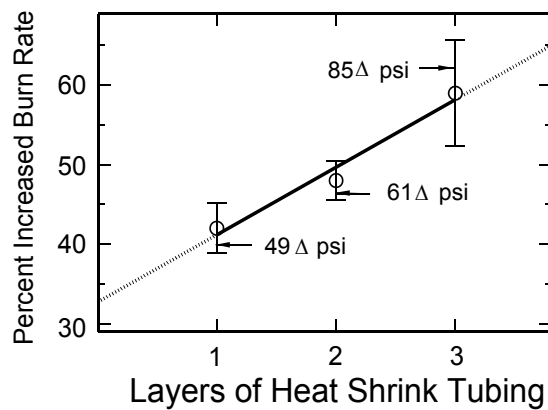


Figure 6. Burn rate variation and corresponding effective pressures as a result of tightly covering visco fuse.

respectively. The error bars are  $1\sigma$  standard errors.<sup>(b)</sup>

It might be of interest to estimate what increase in pressure at the burning surface must have been produced by the layers of heat shrink tubing. For the purpose of this discussion, assume that the pressure acting on the burning surface is one atmosphere (14.7 psi) when there is no added covering on the fuse. With this assumption Figure 4 can be used to determine the pressure that corresponds to the increased burn rates for the covered fuse. The percent increase in burn rate and the effective increases in pressure for 1, 2 and 3 layers of heat shrink tubing is shown in Figure 6. Note that the reported pressures seem reasonable; this is important because it tends to confirm that the mechanism producing the increased burn rate is the same one described in Equation 1.<sup>(c)</sup>

### Effect of Fuse Abuse

It is possible that mild to moderate damage to the fuse could produce significant changes in its burn rate. To examine this, a brief series of tests were undertaken. In preparation for this study, three groups of ten fuse segments (each five inches long) were prepared as described above. The fuse segments in the first group were left in their original condition. The second group received light abuse by repeatedly drawing each segment back and forth over an 11/16-inch radius edge, flexing it about 180° each

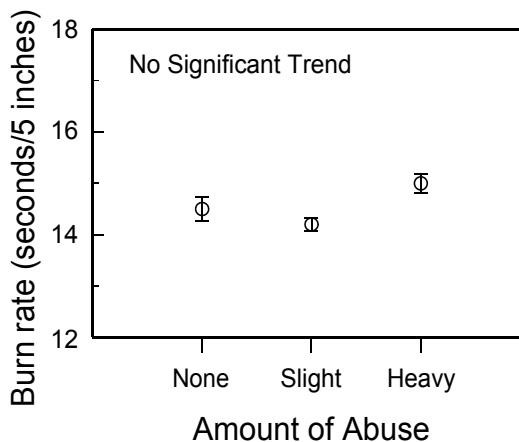


Figure 7. Effect of physical abuse on the burn rate of visco fuse.

time. After each pair of passes, the fuse was rotated slightly so as to bend the fuse in a new direction each time. The process was continued for a total of 20 passes. Some of the lacquer coating flaked off, but there was no significant damage to the outer thread covering. It is felt that this amount of damage was as much as would ever occur during normal use of the fuse. The third group received heavy abuse by following the same procedure used for group two; however, the edge used had a radius of less than  $\frac{1}{8}$  inch. This time, at the completion of the abuse, all the lacquer had been worn away and the outer threads were becoming significantly frayed. It is felt that this amount of damage greatly exceeded that which would ever occur during normal use. Once the fuse segments were allowed to come to about 50 °F, each segment was burned, and its time recorded. Figure 7 presents the average results of these trials. The error bars are  $1\sigma$  standard errors.<sup>(b)</sup> As can be seen, there was no effect of abuse on burn rate. In addition, it is interesting to note there was a high degree of consistency among the individual fuse segments. None demonstrated any significant difference in their performance. Thus it seems reasonable to conclude that no amount of normal abuse to visco fuse will affect its burn rate.

## Conclusion

The results reported in this article are for one series of tests of one manufacturer's visco fuse. While it is likely that other manufacturers' products behave similarly, that has not been verified.

Regarding visco fuse, there appears to be:

- a small amount of variation in burn rate along a length of fuse (approximately  $\pm 7\%$ ).
- a very small amount of variation in burn rate as a function of temperature (approximately  $\pm 5\%$  extrapolating over the range 0 to 100 °F).
- a moderate amount of variation as a function of fuse covering or gluing (perhaps an increase of approximately 50% for the portion tightly covered or glued).
- no burn rate effect from normal abuse.

## Acknowledgments

The authors gratefully acknowledge the background information supplied by Quentin Robinson of American Visco Fuse and the review and comments of Clive Jennings-White and Charles Hill.

## References

- 1) American Visco Fuse, 11984 N. Telegraph Road, Carleton, MI 48117.
- 2) F.P. Agterberg, *Geomathematics*, Elsevier, The Netherlands, 1974.

- 3) A.A. Shidlovskiy, *Principles of Pyrotechnics*, Mashinostroyeniye Press, 1964, Reprinted by American Fireworks News.
- 4) J. Conkling, *Chemistry of Pyrotechnics*, Marcel Dekker, Inc., New York, 1985.

## Notes

- (a) Coefficient of Variation is a statistical measure of the degree of randomness in a series of repeated measurements. The coefficient of variation equals the standard deviation, expressed as a percent of the mean (average).
- (b) Standard Error is a statistical measure of the uncertainty in the average value determined from a series of repeated measurements. The standard error equals the standard deviation divided by the square root of the number of measurements. One  $\sigma$  (sigma) is an indication that the true value has a 67% chance of falling within the limit of the error bars.
- (c) There is another mechanism that could have been operating to significantly increase the burn rate of visco fuse when covered. Had there been an indication that this was the source of the increases observed in this study, there could have been important safety ramifications. However, a proper discussion of this subject is beyond the scope of this paper and must be delayed for a future article, which is already in preparation.

## Saran Resin — Its Properties and Uses

by Ken Kosanke

---

Saran™ resin in its most common form is Saran Wrap,™ the original plastic food wrap manufactured by Dow Chemical. Technically, Saran resin is polyvinylidene chloride, which has the chemical formula of:



Polyvinyl chloride (PVC), has the empirical formula of:



Thus Saran resin is essentially PVC with a second chlorine atom per formula unit. Where PVC is only 57% chlorine, Saran resin is 73% chlorine. (Note that Parlon,™ which is 68% chlorine, also falls short of Saran resin.)

Saran resin is highly resistant to attack by chemicals and solvents as it is quite inert at temperatures below about 150 °C (≈300 °F.)

Saran resin, Parlon and PVC are all chlorinated hydrocarbons, and are used in pyrotechnics

as so-called chlorine donors or color enhancers. The mechanism of chlorine color enhancement is beyond the scope of this short article, but is discussed at length in the author's "Physics, Chemistry and Perception of Colored Light (Part 2)," which appeared in *Pyrotechnica IX*, 1984.

Besides acting as a source of chlorine in a colored flame, chlorinated hydrocarbons also function as a fuel. However, all fuels are not equal in their burn characteristics. Thus a brief study was undertaken using Saran resin, with potassium perchlorate as the oxidizer. With properly adjusted formulations, Saran resin was found to equal or surpass PVC and Parlon with respect to ease of ignition, size of flame envelope, and resistance to being extinguished (blown blind).

\* Note that this may be a copolymer made with up to 20% of other unsaturated compounds.

## Pyrotechnic Fuse Burn Rates

K.L. and B.J. Kosanke

Over the years, we have had occasion to work with a fairly large number of different fuse products. One of the more important characteristics of a pyrotechnic fuse is its burn rate, but often that is not specified by the supplier. Thus, when we have had a large enough supply of a type of fuse to make an accurate determination, we measured its burn rate. To do this, three pieces of fuse, 36 inches in length were prepared. Then, using a stopwatch, the time taken to burn each piece of fuse was measured, and the average determined. For future reference, these values were recorded, along with burn times (in seconds per inch) and burn rates (in inches per second). We had not given the matter much further thought, until, following a lecture on the "Identification of Pyrotechnic Devices," we received a number of requests for that information. Unfortunately, the data was scattered throughout several notebooks, and not in a form ready for distribution. In order to fulfill our promise for the data, we compiled the table following. With the thought that there might be others wishing the same data, this brief article was prepared.

Most pyrotechnic materials have a pressure dependent burn rate, and burn rates in the table were determined in Whitewater Colorado at about 4600 feet above sea level. Thus, it is likely that somewhat different values would have resulted had they been determined at another elevation. It is possible that this is the reason we observed burn times for Ensign-

Bickford's Orange Sword and Explo Industrias Quimicas Explosivos' safety fuse that were 22% and 14% (respectively) longer than specified for them.

Most fuse products experience end-effects when burned, wherein the first and last small portion of fuse burns at a different rate than that in between. Thus the length of fuse segment used makes a difference in the average burn rate measured. For example, the fireworks time fuse distributed by Fire Art, displayed a burn rate of 0.33 inch per second when burned in 36-inch lengths, and only 0.27 inch per second when burned in  $\frac{3}{4}$ -inch lengths. The burn rates reported here were generally for 36-inch lengths. However, because of its high rate of burn, that for the fireworks quick match was determined using lengths ranging from 35 to 50-feet. Further, the burn rate for Chinese (firecracker) fuse was determined using many lengths of fuse, each only about 2-inches long. This was because that was the longest length available for measurement.

From time to time, whether intentional or not, manufacturing methods or fuse powder formulations can vary for a specific fuse product. Thus, even under identical conditions, it is not possible to be certain that all fuse of a specific type will exhibit the same burn rate as reported here. One example of this can be seen for the CXA slow Thermalite, where two values differing by 16% are reported.

**Table of Pyrotechnic Fuse Burn Rates.**

Description	36" Burn Time (sec.)	Burn Time (sec./in.)	Burn Rate (in./sec.)
<b>Visco (Cannon) Fuse:</b>			
American Safety Fuse (≡" Green)	102	2.8	0.36
American Visco Fuse (≡" Green)	92	2.6	0.39
Ensign-Bickford (≡" Red)	94	2.6	0.38
Dist. by Fire Art (1/8" Green)	84	2.3	0.43
<b>Hobby Fuse:</b>			
Dist. by Midwest Fwks. (≡" Pink & White Braid)	77	2.1	0.47
<b>Fireworks Time Fuse:</b>			
Japanese Time Fuse (Paper, 2-White & 2-Red Threads)	106	2.9	0.34
Dist. by Fire Art, China (Paper, 10-White Threads)	109	3.0	0.33
Dist. by Advanced Imp., China (Paper, 9-White & 1-Pink Threads)	72	2.0	0.50
Rozzi ≡", United States (White Gauze over Asphalt)	112	3.1	0.32
Ruggieri, France (Paint, White Crossed Threads)	84	2.3	0.43
Ruggieri, France (Black Plastic)	126	3.5	0.29
<b>Blasting Safety Fuse:</b>			
Ensign-Bickford (Orange Sword, Waxed Threads)	147	4.1	0.24
Explo Ind. Qui., Brazil (White Plastic)	146	4.1	0.25
<b>Igniter Cord:</b>			
<b>CXA (Canadian Safety Fuse) Thermalite</b>			
(Fast, White)	16	0.44	2.2
(Medium, Green)	30	0.83	1.2
(Slow, Red, Non-Std.)	54	1.5	0.67
(Slow, Red, Std. Prod.)	64	1.8	0.56
<b>Imperial Chemical Ind., Scotland</b>			
(Fast, Brown)	2.9	0.08	12.
(Slow, Green)	42	1.2	0.86
Explo Indus. Qui., Brazil (Silver)	45	1.2	0.80
<b>Fireworks Match:</b>			
Black Match (Average of Various Mfg.)	30	0.83	1.2
Quick Match (Average of Various Mfg.)	--	0.008	120
<b>Chinese (Firecracker) Fuse:</b>			
Average of Various Mfg.	--	1.9	0.53

## A Collection of Star Formulations

by K.L. and B.J. Kosanke

At one time, we were engaged in the commercial manufacture of stars. During that time we assembled (developed, borrowed or modified) a series of star formulations. It was felt that the formulations were reasonably safe and cost effective, while at the same time, performed well (relatively easy ignition and fairly good color or comet effects). Over the years, when asked for advice concerning useful star formulations, we frequently supplied copies of these formulations. In the thought that there are

others that might wish to have access to them, this short article has been assembled.

Following are the formulations, given in parts by weight. Unless otherwise noted, water was the solvent used to activate the binder. Normally round stars were manufactured in a star-rolling machine. However, the formulations should work equally well to make cut or pressed stars. Where needed, notes have been included for clarity.

**Table 1. Color Star Formulations.**

Chemical	Red	Blue	Purple	Green	Red Strobe	White Strobe	Green Strobe
Potassium perchlorate	68	61	61	—	—	—	—
Ammonium perchlorate	—	—	—	—	34	—	—
Barium nitrate	—	—	—	56	—	53	49
Copper carbonate	—	12	5	—	—	—	—
Strontium carbonate	13	—	8	—	15	—	—
Sulfur	—	—	—	9	24	23	18
Parlon	—	13	12	14	—	—	—
Hexachlorobenzene	—	—	—	—	5	—	6
Red gum	14	9	9	3	—	—	—
Mg/Al (60 mesh)	—	—	—	—	12	12	11
Mg/Al (200 mesh)	—	—	—	4	—	6	9
Aluminum (12 mic., atom.)	—	—	—	9	—	—	—
Dextrin	5	5	5	4	5	5	5
Boric acid	—	—	—	1	—	0.5	0.5
Potassium dichromate	0.5	—	—	—	5	2	2
Notes:					(A)	(B & C)	(B & C)
References:		(1)	(1)			(2)	(2)

Notes:

- (A) Do not prime with meal prime, use only red strobe prime.
- (B) Adjust strobe rate by using greater or lesser amounts of Mg/Al (200 mesh).
- (C) Priming consisted of a very heavy application of meal prime (30-50% of total star weight).

**Table 2. Prime and Comet Formulations.**

Chemical	Meal Prime	Red Strobe Prime	Willow	Gold Glitter	Soft Silver	Bright Silver	Pearl
Potassium perchlorate	—	68	—	—	—	—	—
Potassium nitrate	75	—	64	55	50	64	35
Barium nitrate	—	—	—	—	10	—	—
Charcoal (air float)	15	18	13	11	10	13	15
Charcoal (80 mesh)	—	—	9	—	—	—	—
Zinc dust	—	—	—	—	—	—	40
Aluminum (12 mic.,atom.)	—	—	—	5	—	—	—
Aluminum (50-120 mesh)	—	—	—	—	10	—	—
Titanium (20-40 mesh)	—	—	—	—	—	9	—
Red gum	—	9	—	—	—	—	—
Sulfur	10	—	9	17	15	9	5
Dextrin	5	4	5	5	5	5	5
Potassium dichromate	—	1	—	—	—	—	—
Sodium bicarbonate	—	—	—	7	—	—	—
Notes:	(D)	(D)					
References:				(3)	(4)		

Notes:

(D) Can also be mixed with nitrocellulose lacquer for use as a quick drying slurry prime.

At one time, we were engaged in the commercial manufacture of stars. During that time we assembled (developed, borrowed or modified) a series of star formulations. It was felt that the formulations were reasonably safe and cost effective, while at the same time, performed well (relatively easy ignition and fairly good color or comet effects). Over the years, when asked for advice concerning useful star formulations, we frequently supplied copies of these formulations. In the thought that there are others that might wish to have access to them, this short article has been assembled.

Following are the formulations, given in parts by weight. Unless otherwise noted, water was the solvent used to activate the binder. Normally round stars were manufactured in a star-rolling

machine. However, the formulations should work equally well to make cut or pressed stars. Where needed, notes have been included for clarity.

### References

- 1) T. Shimizu, "Studies on Blue and Purple Flame Compositions Made with Potassium Perchlorate," *Pyrotechnica VI*, 1980.
- 2) R. Winokur, Private communication.
- 3) T. Fish, "Glitter Stars without Antimony," *PGI Bulletin*, No. 24, 1981.
- 4) R. Sheard and others, Private communication.



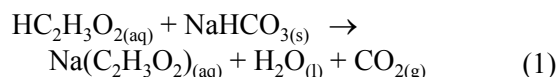
## Production of Benzoate Color Agents

by K.L. and B.J. Kosanke

The use of copper(II) benzoate as a blue color agent was discussed by Bleser.<sup>1</sup> In large part, the endorsement for its use is based on its ability to serve as both color agent (copper) and fuel (benzoate). There is something to be said for this approach. For example, consider a color agent such as copper(II) carbonate ( $\text{CuCO}_3$ ); it is only the copper that is useful in producing color. (See Reference 2 for a more complete description of colored flame production.) What is more, energy is required to free copper from its carbonate ion. Consequently, the flame temperature is lowered, which in turn results in less colored light output. It would be preferred if the copper could be made available without having to pay the full energy cost of freeing it from the carbonate ion. One way to do this is to chemically combine copper with a fuel such as the benzoate ion. Then, when the fuel is consumed, copper will be left over and ready to make the blue color-generating molecule, copper monochloride ( $\text{CuCl}$ ). Because copper benzoate is not commonly available, Bleser described one way to produce it. There is, however, another way to produce copper benzoate. This process is a little more complicated, but the same basic process can also be used to make many other interesting pyro-chemicals, only one class of which are benzoates.

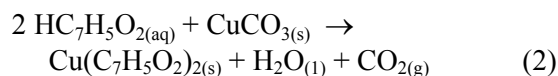
When an acid is mixed with a carbonate or bicarbonate in the presence of water, the resulting chemical reaction produces carbon dioxide [soda water gas,  $\text{CO}_2$ ] and water [ $\text{H}_2\text{O}$ ], plus the metal salt of the acid. One familiar example of the process is that observed when vinegar [a dilute solution of acetic acid,  $\text{HC}_2\text{H}_3\text{O}_2$ ] is added to baking soda [sodium bicarbonate,  $\text{NaHCO}_3$ ] producing the sodium salt of acetic acid [sodium acetate,  $\text{Na}(\text{C}_2\text{H}_3\text{O}_2)$ ] with much froth-

ing and fizzing as gaseous carbon dioxide escapes. The reaction is described in the following chemical equation:



The physical states of the substances are indicated by (s) for solid, (l) for liquid, (g) for gas, and (aq) for aqueous or dissolved in water.

In a manner similar to Equation 1, the reaction of a benzoic acid solution [ $\text{HC}_7\text{H}_5\text{O}_2$ ] with copper(II) carbonate [ $\text{CuCO}_3$ ] yields the color agent and fuel, copper(II) benzoate [ $\text{Cu}(\text{C}_7\text{H}_5\text{O}_2)_2$ ]. This is shown in Equation 2.



Since benzoic acid comes as a solid (much like boric acid or stearic acid, which are more familiar to pyrotechnists), it must be dissolved before it will react in this way. In addition, because benzoic acid is not very soluble, the water must be heated to encourage more of the benzoic acid to go into solution and thus allow the reaction to proceed. After the reaction is completed, recovery of the benzoate is easy; the carbon dioxide by-product is lost to the atmosphere, and the water by-product is removed by drying.

In Equation 2, if the copper(II) carbonate is replaced with strontium carbonate, strontium benzoate can be produced. Similarly, the use of barium carbonate produces barium benzoate, and calcium carbonate produces calcium benzoate.

Following is a simple procedure to produce these unusual, but potentially effective color agents. See Table 1.

**Table 1. Production or Benzoate Color Agents.**

Reactant	Parts by Weight <sup>(a)</sup>	Product	Parts by Weight <sup>(b)</sup>
Benzoic acid	12		
Metal Carbonates:		Metal Benzoates:	
Barium carbonate	11	Barium benzoate	19
Calcium carbonate	5.5	Calcium benzoate	14
Copper(II) carbonate <sup>(c)</sup>	6	Copper(II) benzoate	15
Strontium carbonate	8	Strontium benzoate	17

Notes:

- (a) These amounts include a slight excess of carbonate to assure the complete reaction of the benzoic acid.
- (b) These are the theoretical amounts that can be produced. In actual practice, the amount produced depends on the exact procedure followed. However, generally only about 80% of these amounts will be recovered for use.
- (c) Note that copper(II) carbonate as used in fireworks is more accurately basic copper(II) carbonate, which is  $\text{CuCO}_3 \cdot \text{Cu(OH)}_2$ . The weight shown in the table correctly reflects this fact.

### Procedure

- A) Place no more than about 50 parts by weight of water into a glass container. (It is desirable to use a minimum amount of water. With experience, it will often be found that less water can be used.) The container should be generously oversized so that when the reaction proceeds with the evolution of carbon dioxide, and the mixture froths-up, none will be spilled.
- B) Using the information in Table 1, weigh the ingredients to make the desired metal benzoate; for example, to make barium benzoate, weigh out 12 parts benzoic acid and 11 parts barium carbonate.
- C) Add all of the benzoic acid and about  $\frac{1}{4}$  of the metal carbonate to the water and stir. The mixture may be a fairly thick slurry.
- D) Begin warming the mixture until bubbles of carbon dioxide are observed. Stir the mixture to help break-up the froth of gas bubbles being produced.
- E) When the production of  $\text{CO}_2$  is essentially complete, add another increment of the carbonate. Repeat until all the remaining carbonate has been added.
- F) Once all of the carbonate has been added and no more bubbling is observed, heat a little further and continue to stir to insure that the reaction is complete.
- G) Before proceeding to the next step it is useful (and sometimes, important, depending on the solubility of the product benzoate) to boil off most of the excess water. Heat the mixture slowly until no significant amount of water remains visible. (This will assure a good yield of product even for benzoates that are highly soluble in water.)
- H) Allow the mixture to cool and then dump the product material (the metal benzoate) on a mat of paper towels to absorb most of the remaining water.
- I) Allow the material to air dry for several days or place in an oven, at 225 °F, with air circulation until dry.
- J) Pass the dried material through a screen to break up any lumps.

## Cautions

Essentially all copper, strontium and barium salts are somewhat toxic. For example, the J.T. Baker Saf-T-Data health and contact ratings for these metal carbonates range from 1 (slight) to 2 (moderate). Because of the increased solubility of benzoates, their ratings will probably all be at least 2 (moderate). [As a point of reference, note that barium nitrate has a health rating of 3 (severe).] Accordingly, some degree of caution is appropriate when working with these materials. Certainly any glassware used to make these benzoates, and any oven used to dry them, should not be used to prepare food.

The authors have produced metal benzoates using this method, but have not developed for-

mulations for them, nor have they tested the sensitivity of any formulation using them.

## Acknowledgments

The authors gratefully acknowledge the technical and editorial assistance of Wes Smith and Clive Jennings-White in the preparation of this article.

## References

- 1) D. Bleser, "New Electric Purple," *American Fireworks News*, No. 89, 1989.
- 2) K.L. Kosanke, "The Physics, Chemistry and Perception of Colored Flame, Part II," *Pyrotechnica IX*, 1989.

## Parallel and Propagative Pyrotechnic Burning

by K.L. and B.J. Kosanke

### Introduction

In effect, there are two basic mechanisms for pyrotechnic burning. One, which is primarily burning inward, perpendicular to the burning surface, and one in which accelerated burning along surfaces is most important. These can be termed “parallel” and “propagative” burning, and the same pyrotechnic material can manifest radically different burn rates depending on which type of burning predominates. A theoretical discussion of burn rates and the many factors effecting burn rate is beyond the scope of this article; however, a working knowledge of these two types of burning is useful in understanding the way in which a number of fireworks items function and, on occasion, malfunction. Also, should the need arise to dispose of pyrotechnic materials by burning, a knowledge of these two types of burning, and the potentially dangerous transition that might occur between the two, could be of critical importance.

It must be acknowledged that in the literature there is conflicting usage of the terms describing burn types and that the propellant powder industry uses similar terms in a somewhat different manner. In an attempt to avoid confusion, an appendix has been included to explain the powder industry’s use of the terms degressive, neutral, and progressive burning. Also, erosive burning is briefly discussed.

### Background

To prepare for the discussion of burn types, it is useful to review a few points from basic pyrotechnic chemistry (for further background, also see Reference 1):

- Pyrotechnic compositions are mixtures of a fuel with an oxidizer; thus burning is possible without the necessity of drawing oxygen from the air.
- Pyrotechnic compositions are called “metastable” because, although they may burn rapidly once ignited, they generally will not spontaneously combust.
- In simple terms, the process of ignition requires the raising of a pyrotechnic composition to its ignition temperature.
- Burning of solidly compacted pyrotechnic composition generally proceeds in an orderly fashion, layer by layer, as shown in Figure 1. The “reacting” layer produces heat, some of which acts to raise the temperature of the “pre-reacting” layer. Once the ignition temperature of the pre-reacting layer is reached, it too begins to burn and passes some of the heat it generates along to the next layer. In that manner, the entire stick of pyrotechnic composition is consumed.

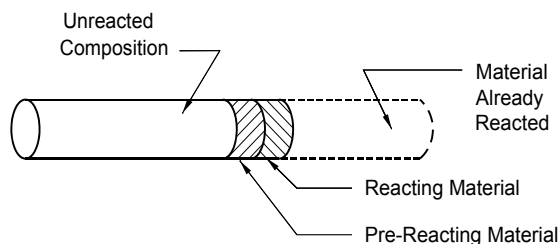


Figure 1. Model of pyrotechnic burning.

Figure 1 illustrates parallel burning (sometimes also called progressive burning), in which burning occurs, layer by “parallel” layer, in an orderly fashion.

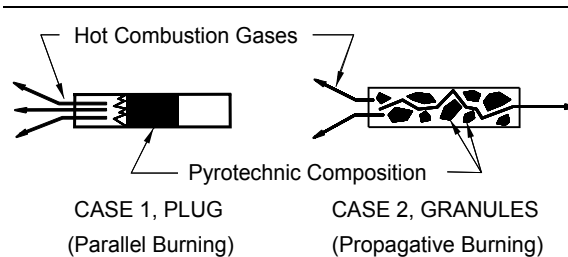


Figure 2. Examples of "parallel" and "propagative" burning.

A comparison between the conditions leading to parallel burning and propagative burning is shown in Figure 2. In Case One, parallel burning, some pyrotechnic composition has been compressed very tightly inside a tube, forming a solid cylinder of material. When that material is ignited at one end, it will burn layer by parallel layer as described above. The burn rate will be relatively slow, because the reaction only takes place on the exposed surface of the plug, and hot combustion gases vent easily through the open end of the tube.

Now consider Case Two, propagative burning, in which granules of pyrotechnic composition are packed rather loosely in a tube. In this instance each granule is a proper mixture of fuel and oxidizer such as might be produced if the cylinder from Case One were crushed into small pieces. During the first instant of burning the first grain, it will be parallel burning, and the hot gases generated will vent through the open end of the tube. However, very soon some of the hot combustion gas will begin to pass into the tube through the small spaces between granules (called "fire paths"). When this occurs, some of the granules farther into the tube receive the energy necessary to ignite. As these additional granules burn, more hot gases are produced, some of which pass still farther into the tube igniting even more granules. In this manner, all the granules of pyrotechnic composition are soon ignited. This type of rapid burning is called propagative, and quickly "propagates" throughout the entire amount of pyrotechnic composition.

In parallel burning, linear burn rates generally range from about 0.01 inch per second [0.025 cm/sec] to about 1 inch per second [2.5 cm/sec]. In propagative burning, the linear burn

rate of each individual granule is the same as it would be in parallel burning. However, the linear burn rate along a collection of granules can range to more than 1000 times that for the same material burning in a parallel fashion. For example, a single grain of Black Powder or a solid plug burns progressively at about 0.4 cm/sec; however, a long line of individual grains of the same Black Powder, burns propagatively at about 60 cm/sec, or about 150 times faster.<sup>2</sup> In tests performed by the authors, when Black Powder was compacted tightly into a 3/8-inch internal diameter plastic tube, and ignited on one end, the burn rate was measured to be about 0.5 cm/sec. When an identical tube was filled with the same weight of loose 4FA granular Black Powder and ignited on one end, the burn rate was measured to be about 1000 cm/sec, or about 2000 times faster than when tightly compacted.

### Black Match / Quick Match

Black match is generally made by applying a coating of rough powder (hand-mixed meal powder ingredients) bound with dextrin over a collection of thin cotton strings. In the absence of wind, black match burns at a rate<sup>3</sup> of about 1.2 in/sec [3.0 cm/sec]. The burning progresses in a more or less orderly manner along the length of fuse. Except for occasional sparks being propelled ahead, and igniting material farther along, black match can be considered to be an example of primarily parallel burning.

When black match is encased in a thin, loose-fitting layer of paper (match pipe), it becomes quick match, which burns at a rate<sup>3</sup> of about 10 ft/sec [3 m/sec], about 100 times faster than without the paper sheath. Based on what has already been said about burn types, one might expect that the burning of quick match is an example of propagative burning, and this is correct. The mechanism is made more clear in Figure 3, which is based on a description by Shimizu.<sup>4</sup> On the left of the figure it is suggested that the burning of black match produces a flame similar to that of a candle burning without obstruction. On the right, when a barrier is imposed above the candle, obstructing the flame, the flame spreads out along the barrier. Shimizu suggests that, in much the same way,

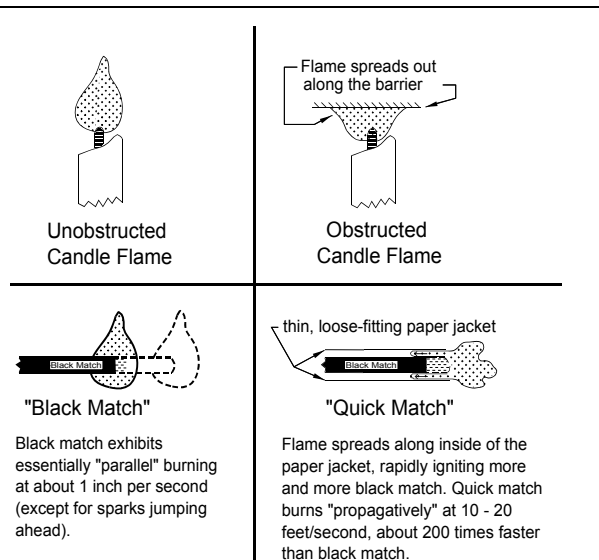


Figure 3. The quick match phenomenon.

the loose paper sheath of quick match acts as a temporary barrier for its flame. When the flame spreads out along the barrier, some passes freely out the open end, but some also passes inside toward unignited composition. When that composition is ignited by the flame, it produces more flame, some of which passes out and some passes still farther inward along the fire path provided by the loose paper wrap, igniting even more composition. In this fashion the linear burn rate of the quick match rapidly accelerates to its high value.

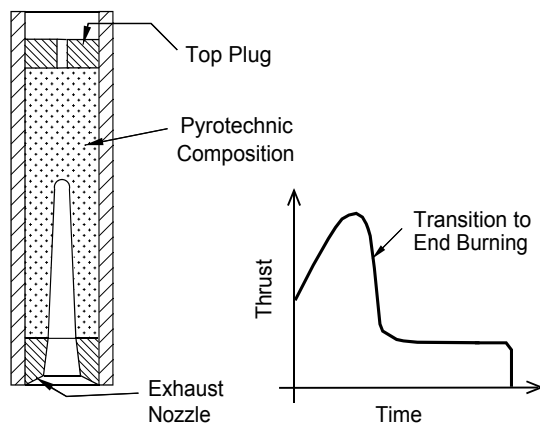


Figure 4. Core burning rocket motor.

## Rockets

The quick match example is an instance when propagative burning is desired to achieve the intended pyrotechnic result. An example of undesired propagative burning can occasionally be found in rockets. Figure 4 is a sketch of a core burn rocket. Once ignited, the thrust and internal pressure of the rocket is roughly proportional to the area of the burning surface. Because of the large open core, produced by a spindle during manufacture, the area of burning surface and thrust starts out at a large value. As parallel burning proceeds the area of burning surface and thrust increases as the diameter of the open core increases further. For a normally performing rocket, burning proceeds until all the composition in the lower portion of the rocket motor has been consumed, but some composition still remains in the upper portion of the motor. At this point, the area of burning surface and thrust fall to a low value, which remains constant until finally the rocket burns out, having consumed all its propellant. However, if during the time its thrust and internal pressure are increasing, the yield strength of the rocket casing is exceeded, the casing will begin to bulge. When this happens, as illustrated in Figure 5, cracks develop in the rocket composition and between the composition and the casing. The parallel burning will now become propagative along the fire paths provided by the cracks. In this manner, the area of burning surface increases, and along with it, internal rocket pressure. The rise in pressure causes further bulging, more cracking, increased area of burning and still higher internal pressure. In this manner, the burst strength of the rocket casing

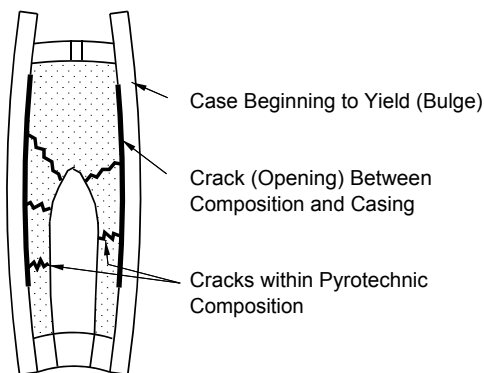


Figure 5. Rocket case failure mechanism.

is quickly exceeded and the rocket motor explodes. (This example is just one way in which cracks can develop in rocket propellants. Other ways are gas production as a result of chemical reactions during storage and shrinkage upon drying when overly moist composition is used.)

### Disposal by Burning

On those occasions when it becomes necessary to dispose of pyrotechnic materials by burning, a knowledge of burn types can have important safety ramifications. In parallel burning, linear burn rates are mostly independent of the amount of material present. Thus, a test burn of a small amount of parallel burning material, will usually be a good indicator of how a larger amount of the same material will behave. In propagative burning, linear burn rates can be very dependent on the amount of material present. Thus, a test burn of a small amount of material, capable of burning propagatively, may offer little indication of how a larger amount of that material will behave.

Obviously, then, in planning for disposal by burning, it is important to know which type of burning will predominate and whether a transition from parallel to propagative burning is possible or likely. Unfortunately, that is not absolutely predictable; however, for the following two classes of materials, some generalizations can be stated.

1) A Single Solid Mass of Composition (not often found in fireworks manufacturing, e.g., a large solid rocket fuel casting):

- The burning will begin as parallel burning and will continue as such.

- The duration of burn will be approximately proportional to physical size (i.e., an item twice as large in all physical dimensions will burn about twice as long).
- The fire output from the burn will be approximately proportional to surface area, the square of physical size (i.e., an item twice as large in all physical dimensions will produce roughly four times the volume of fire throughout the burn).
- With most materials, it is unlikely that there will be a transition to propagative burning or that the burning will somehow accelerate to an explosion. (Some materials, capable of detonation, may do so when burned in large quantity due to local over-heating, e.g. dynamite.)

2) A Collection (Pile) of Many Granules of Composition (e.g., granulated Black Powder or fireworks stars):

- There may be a very brief period of parallel burning, but almost immediately, a transition to propagative burning will occur.
- The duration of the burn will be nearly independent of the amount of material and will be roughly the same length of time as is required to burn a single granule.<sup>5</sup>
- The fire output from the burn will be approximately proportional to the total mass of material, which equals the cube of the physical size of the pile of material (i.e., a pile twice as large will produce roughly eight times the volume of fire).
- It is possible that the parallel burning

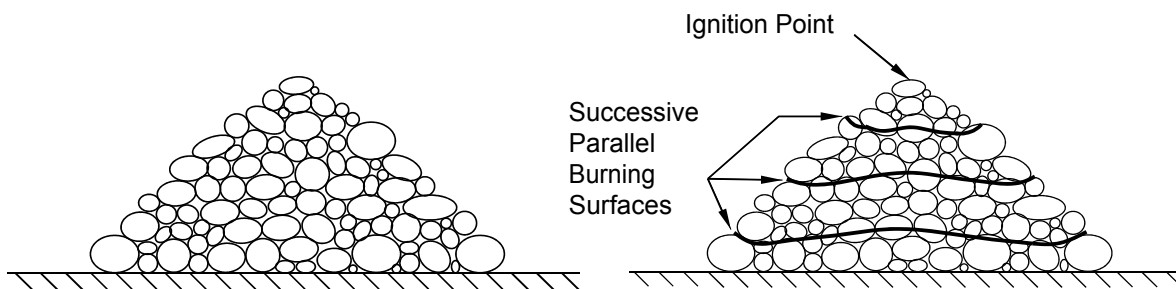


Figure 6. Loose pile of fine powder experiencing parallel burning.

will accelerate to an explosion, but generally only for larger amounts of material.

There is a third general class of pyrotechnic materials, for which predictions about output upon burning are even less reliable. That third class consists of loose, fine-grained, pyrotechnic compositions such as raw star composition. Generally the individual grains will be the components of a pyrotechnic composition (i.e., individual grains of fuel and oxidizer). However, each small grain could also be a complete pyrotechnic in itself such as commercial meal powder. Figure 6 is a representation of how a small pile of such material might appear in cross-section. One important characteristic of the material shown is that it has a wide range of particle sizes (in actuality, this is almost always the case). The smaller particles tend to plug the gaps between the larger ones, thus tending to fill in the fire paths and blocking the penetration of hot gasses when the material is burned. In many cases, such loose powders, once started, will experience parallel burning in a relatively mild fashion. This is illustrated in the right half of Figure 6, where the material is ignited at the top of the pile and then burns downward, as shown by the burning surfaces at three subsequent times during the burning process. In such an instance, the rate of burning does increase somewhat as a result of the increasing burning surface area of the pile; however, it does not become propagative.

At any time during the parallel burning of such a pile of loose composition, there exists the possibility that there will be a transition to propagative burning. This is most likely to occur if the material is disturbed in any way while burning; or the area of burning becomes the least bit confined, perhaps by nothing more than the weight of slag produced during the burning. No matter what the cause, whenever there is a significant penetration of hot combustion gases into the pile, a transition to propagative burning will almost certainly occur. The mechanism for this is illustrated in Figure 7. The pile is ignited on top and first experiences parallel burning as shown. However, as soon as there is penetration of combustion gasses, more material becomes ignited, resulting in a slight rise in local pressure. If the pressure rise is suf-

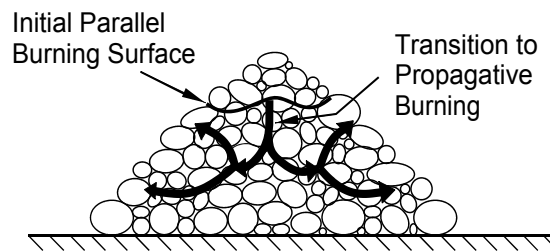


Figure 7. Loose pile of fine powder with a transition to propagative burning.

ficient to separate the loose grains of material, thus opening more fire paths, there will be further penetration of combustion gas, leading to an even greater spread of ignition, still higher local pressure and even greater fire penetration. Very soon all remaining material is consumed, and at a potentially explosive rate. Predictions concerning the likelihood of a transition from parallel to propagative burning are generally not possible for fine-grained pyrotechnic powders. However, some very general guidance can still be given for this third class of material.

3) A Loose Pile of Very Fine Powder (e.g., blended pyrotechnic powders awaiting final processing or flash powder):

- It is not possible to predict with certainty whether the burning will undergo a transition to propagative burning, or whether it will remain parallel throughout the burn. However, it becomes more likely there will be a transition to propagative burning when: large amounts of material are present, the material is of a type that produces a large percentage of gaseous combustion products, or the material burns very rapidly even when it is undergoing parallel burning.
- Based on a small test burn, it is not possible to predict with certainty how long a larger burn will last or the fire output of that burn. If the burning remains parallel, it could scale up as predicted above. However, at any instant it might undergo a transition to propagative burning and accelerate catastrophically.
- These materials present the greatest danger of unexpected explosive output.



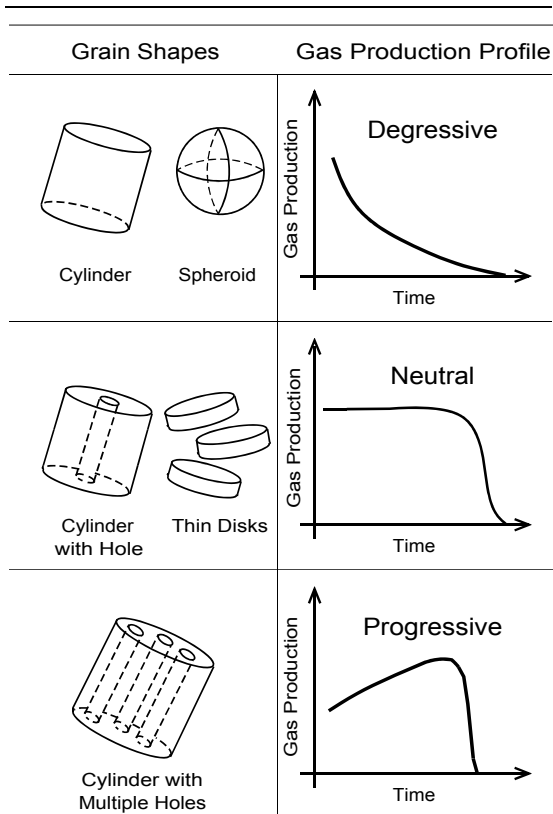


Figure A-1. Propellant powder burning.

## Appendix: Propellant Burning<sup>6,7</sup>

In the terms used in this article, each individual grain of propellant powder experiences parallel burning, but a collection of propellant powder grains burns propagatively, with fire rapidly spreading across the surfaces of all the grains. The amount of propellant gas produced per unit time is proportional to the surface area of the burning powder grains at the time. The propellant powder industry uses the terms degressive (also regressive), neutral (also steady), and progressive to describe the time dependent production of propellant gas by their powders. The use of these terms can be explained by considering some typical powder shapes. For powder grains that are solid particles, such as cylinders or spheroids as shown at the upper left of Figure A-1, as each grain burns, it becomes smaller and its surface area decreases. Thus the surface area of a burning collection of grains, and the rate of gas production, decreases with time as the individual grains become smaller

and smaller. Shown in the upper right of Figure A-1 is a curve of gas production as a function of time illustrating the decreasing rate of gas produced by a collection of solid powder grains. Propellant powders, which generate such a decreasing curve, are called “degressive.”

In the case of propellant grains that are either thin disks or cylinders with an axial hole, roughly the same rate of gas production occurs throughout the period of their burning. This is illustrated in the middle of Figure A-1. For these particle shapes the surface area remains roughly constant as the individual grains are consumed during burning. Propellant powders producing an approximately constant gas production curve are called “neutral.”

In the case of propellant grains that have multiple lateral holes, an increasing rate of gas production occurs throughout the period of their burning. This is because the surface area of each grain increases during burning. Propellant powders producing gas at an increasing rate are called “progressive.”

Another term used in discussing propellant powders is “erosive” burning. This term is used to describe a situation when burning rate is accelerated because of the passage of jets of hot gases across a burning surface. Consider a propellant grain with an axial hole, as the grain burns along the interior of the hole, gas is produced, which exits by jetting out through the ends of the core hole. Because of this jet of hot gas, across the burning surface inside the hole, the rate of energy transfer to unburned propellant is increased. This manifests itself as an increased rate of inward (parallel) burning, beyond what would occur without the jet of gas.

## Acknowledgments

The authors wish to gratefully acknowledge the technical and editorial comments of J. Bergman, R. Winokur, and D. Haarmann in the preparation of this article.

## References

- 1) K.L. and B.J. Kosanke, "Introduction to the Chemistry and Physics of Low Explosives," *PGI Bulletin*, Nos. 68, 69 & 70, 1990.
  - 2) Urbanski, *The Chemistry and Techniques of Explosives*. Pergamon Press, 1967.
  - 3) K.L. & B.J. Kosanke, "Fuse Burn Rates" *PGI Bulletin* No. 76, 1991.
  - 4) T. Shimizu, *Fireworks from a Physical Standpoint, Part 1*, Reprinted by Pyrotechnica Publications, 1981.
  - 5) T. Shimizu, *Fireworks, The Art, Science and Technique*, Reprinted by Pyrotechnica Publications, 1988.
  - 6) A. Bailey and S.G. Murray, *Explosives, Propellants and Pyrotechnics*, Brassey's (UK) 1989.
  - 7) *Military Explosives*, Dept. of the Army Technical Manual, TM 9-1300-214, June, 1979.
-

## Dautriche — Shock Tube Measurement of High Propagation Rates in Pyrotechnic Materials

by K.L. and B.K. Kosanke

### Introduction

There are times when it is of interest to measure propagation rates in highly energetic pyrotechnic materials, such as flash powder. These rates tend to range from less than 1000 to about 5000 feet per second. Conventional means of making such velocity of propagation (VOP) measurements involve the application of techniques developed for use with high explosives in order to make velocity of detonation (VOD) measurements. Some examples of the equipment used are high speed framing cameras, streak cameras, continuous velocity probes, and any of the various so-called “pin” techniques. These approaches require expensive instruments and in some cases may not be entirely reliable in the lower reaction pressure regime of pyrotechnics, especially when weakly confined.<sup>1,2,3</sup>

In searching for an inexpensive alternative for making pyrotechnic VOP measurements, and after attending a seminar by Chris Cherry<sup>4</sup> dealing with some novel applications of Nonel shock tube, the authors have developed a method using shock tube. The method is based on the old Dautriche method for making VOD measurements.

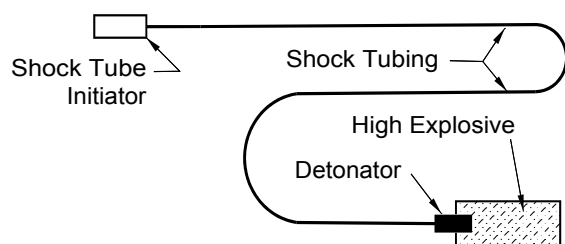


Figure 1. Shock tube initiation system for high explosives.

Shock tube systems, such as Nonel Trunkline from Ensign-Bickford, are non-electric initiation systems for high explosives (see Figure 1). The basic component is a thin tube (1/8-inch OD), which has a very thin inner coating<sup>5</sup> ( $\approx$ one pound per 100,000 feet) of a mixture of aluminum metal powder and HMX, a high explosive. When subjected to simultaneous application of heat and pressure, as can be provided by a shotgun primer, a shock wave initiates and propagates along the inside of the tube at about 6500 feet per second, according to Ensign-Bickford's technical bulletin.<sup>5</sup> However, according to their Technical Services personnel, the actual rate is somewhat greater, and maybe subject to environmental conditions and other factors such as length. Passage of the shock wave normally leaves the tube intact and essentially unaffected, except for the barely detectable appearance of a carbonyl film on its inner surface. However, in the event that a shock wave is initiated at both ends of the tube, the point where the waves collide is evidenced by a small rupture (burst) of the tube at that point. The cost of Nonel shock tube is about \$0.04 per foot in large quantities. It can be shipped as a non-hazardous material (plastic tubing, NOS). [See References 5 and 6 for more information concerning non-electric shock tube, and Reference 7 for a discussion of the channel effect, which is the basis of operation of shock tube.]

The Dautriche (D'Autriche) method for measuring detonation velocity pre-dates the availability of high-speed cameras and digital electronics. It involves the use of detonating cord (detonating fuse, det-cord, prima-cord), and is illustrated in Figure 2. In essence, two ends of a piece of detonating cord are inserted some distance apart into a column of high explosive, such as a stick of dynamite. When the

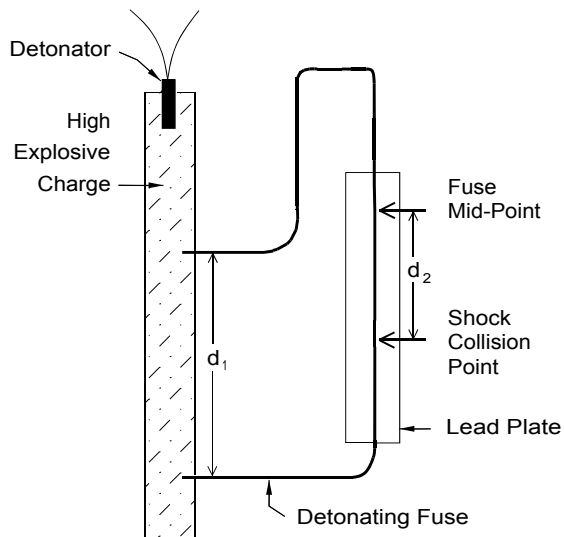


Figure 2. Dautriche method for measuring detonation velocity.

explosive is detonated, the shock wave propagates along its length, first encountering and initiating one end of the detonating cord. Then, after the shock wave in the explosive has propagated further, it encounters and initiates the other end of the detonating cord. At this time there are two shock waves propagating along the detonating fuse, one from each end. If the detonating fuse has been laid along the surface of a lead plate, the point where the two shock waves eventually collide will be witnessed by the lead plate as a point of increased deformation. If the VOD of the detonating cord, the distance between the points where the cord was inserted into the explosive column, and the distance from the mid point of the cord to the point of collision of the two shock waves, are all known, then the unknown VOD of the explosive column can be calculated using Equation 1. [See References 8 or 9 for more information on the Dautriche method.]

$$D_u = D_f (d_1/2d_2) \quad (1)$$

where

- $D_u$  is the unknown VOD of the column of explosive,
- $D_f$  is the VOD of the detonating fuse,
- $d_1$  is the distance along the column of explosive between points of attachment of the detonating fuse, and

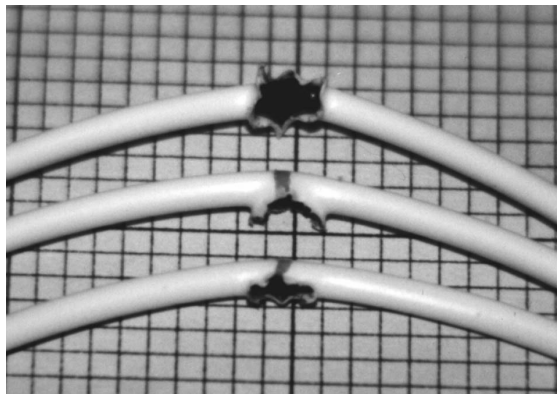


Photo 1. Pieces of Nonel Shock Tube, illustrating the rupturing (bursts) caused by the collision of two shock waves.

$d_2$  is the distance from the midpoint of the detonating fuse to where the shock waves meet.

There are a number of reasons why the Dautriche method is poorly suited for use with pyrotechnic materials. Most importantly, pyrotechnic materials generally do not produce the shock pressures needed to initiate detonating fuse. However, even if this were somehow overcome, the expense and effort required with the use of lead plates, and explosive output from the detonating fuse, make the Dautriche method less than desirable.

### Shock Tube Method of VOP Measurement

For the most part, pyrotechnic VOP measurements can be made by simply substituting shock tube for detonating cord in the Dautriche method, but without the lead plate. The point of collision of the two shock waves is indicated by the burst point of the tube. Examples of this are shown in Photo 1. To allow measurement of the collision point from the center of the length of the shock tube, it is important to mark the midpoint on the tube before the explosive is initiated, since the explosion may destroy a short section of shock tube at each point of attachment to the explosive column.

It is possible that the migration of small amounts of loose powdered explosive mixtures into the open end of the shock tube at its point of attachment, could introduce errors into the

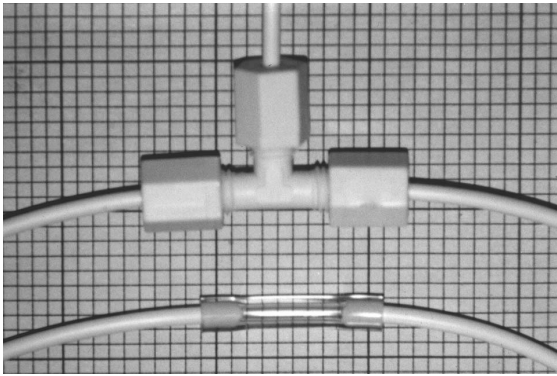


Photo 2. Coupling methods for shock tube; a straight coupling using Tygon tubing as a sleeve, and a three-way coupling using a plastic tee.

measurement. This can be avoided by placing a small piece of 1-mil polyethylene film over the end of the shock tube before it is attached to the tube, which will eventually contain the explosive charge. (In these experiments the tubes used to contain the explosive charge were convolute tubes made of kraft paper.) In attaching the shock tube to the empty paper tube, hot-melt glue has proven to be effective.

The VOP in the pyrotechnic explosive charge may not be constant and the reaction front is likely to have an irregular and changing shape as it moves along the charge. Thus, it is desirable to have the benefit of several VOP measurements along the length of the charge. This can be accomplished by using any number of lengths of shock tube attached along the explosive. However, because of operational difficulties, it is undesirable to have all the lengths of tube attached at the time the paper tube is filled with the explosive being studied. This problem can be largely eliminated and the number of attachment points reduced to nearly half, by taking advantage of another characteristic of shock tube.

Pieces of shock tube can be joined by merely inserting both ends into a sleeve made of material such as Tygon tubing. Also the ends need not be in direct contact with one another (i.e. the shock wave can successfully jump an inert gap and reestablish itself in the continuing shock tube). This allows interesting and useful possibilities in joining and fanning shock tube.<sup>4,6</sup> For example, one piece of tube can successfully

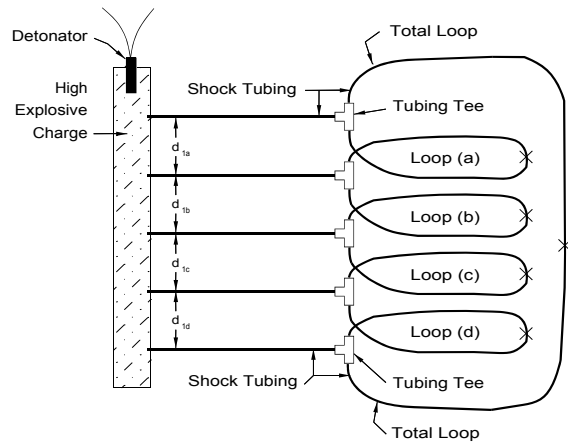


Figure 3. Shock tube method for measuring propagation velocity.

pass a shock wave to two pieces of tube by using a 1/8-inch tubing tee such as might be purchased in a hardware store. Photo 2 illustrates such an arrangement using a plastic tee from a laboratory supply house. It is important to note that when a propagating shock wave encounters an inert gap, such as inside a tee, the strength of the wave weakens causing its velocity to be reduced. A distance of perhaps a foot may be required before the shock wave regains a steady state velocity.<sup>4</sup> Thus, in order to get accurate results, it is necessary to use a symmetric setup, so that delays, introduced when the shock waves cross gaps, will cancel.

The problem of having numerous long lengths of shock tube attached to the paper tube when loading the explosive, can be reduced by initially only attaching a series of relatively short lengths of shock tube. Then after the paper tube has been loaded with the pyrotechnic explosive, tees can be attached to the already installed short lengths of shock tube and other lengths of shock tube (with their mid-points marked) can be attached between the tees. This is shown schematically in Figure 3. (Not shown in Figure 3 is a barrier used to protect the tees and shock tube loops from damage when the device is exploded.) When the pyrotechnic explosive is initiated, and the reaction front reaches the first shock tube attachment point, a shock wave begins to propagate down that tube. When the shock wave enters the tee it initiates shock waves in both pieces of the shock tube

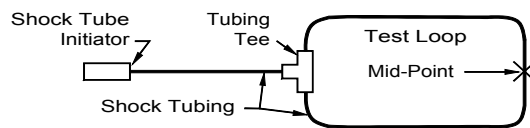


Figure 4. Timing consistency determination for shock tube method.

attached to the tee. One piece is the beginning of loop(a) and one piece is the beginning of a loop for the total length of explosive. This provides a measurement of the VOP for the total length of explosive. It also provides the needed symmetry to be certain that the timing of the passage of the shock wave through the first tee will be the same as for all subsequent tees. A little later, when the reaction front in the pyrotechnic explosive reaches the second shock tube attachment point, a shock wave begins to propagate down that tube. At the tee on that line, shock waves are initiated on the end of loop(a) and the beginning of loop(b). At this time, provided loop(a) is sufficiently long, there will be two shock waves moving along it from opposite ends. The point where the two waves eventually meet will be revealed by a burst point (see Photo 1). In this same way, as the pyrotechnic reaction front passes through the explosive charge, pairs of shock waves are initiated in each of the succeeding loops. At the completion of the experiment, after the explosive charge has been consumed, the lengths of shock tube are collected and the distance from each mid-point to its respective burst point is measured. Finally, using Equation 1, the average VOP between each pair of attachment points is calculated.

## Results

Before VOP measurements were made it was appropriate to first verify the reproducibility of the timing that could be achieved. This was a concern because the method relies on there being a fairly constant and reproducible time between the entry of a shock wave into the tee and the initiation of shock waves in both pieces of tube connected to it. One set-up used to examine this is shown schematically in Figure 4. The shock initiator in this case was a .22

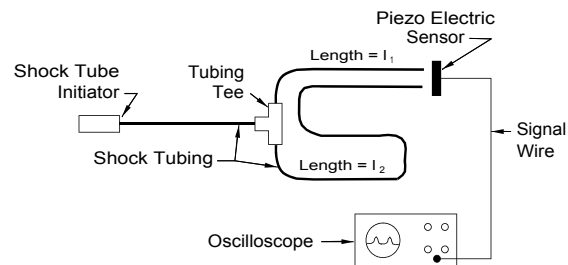


Figure 5. Determination of shock velocity within shock tube.

caliber starter pistol, with the shock tube in close proximity to the end of the blank cartridge. The mid-point of the loop had been marked, and, after firing, the distance to the burst point in the shock tube was measured. In a series of five tests, the burst point was never more than 0.04 inch (1 mm) from the mid-point mark. Thus, it would seem that the time of passage of the shock wave was always essentially equal through both legs of the tee.

The quoted rate of propagation through Nonel shock tube was known to be an understatement of its true speed. Also, the actual speed was known to be somewhat dependent on conditions, such as length of shock tube, temperature, pressure, etc. Thus it was appropriate to measure its speed under conditions similar to those anticipated during the experiments. The apparatus used to accomplish this, is shown schematically in Figure 5. The shock tube set-up is similar to that in Figure 4; however, in this case the test loop was cut and the ends positioned just above the surface of the piezoelectric sensor. This sensor produces a current pulse whenever a pressure wave impacts the sensor. In each test, the shorter length ( $l_1$ ) was a constant 11.8 inches (30 cm), and the longer length ( $l_2$ ) was varied in the range expected for future experiments. Because the lengths of the two legs were different, the arrival of the shock waves at the piezoelectric sensor occurred at different times. The difference in arrival times was recorded using a digital oscilloscope. The propagation velocity of the shock tube was calculated using Equation 2.

$$VOP_{st} = (l_2 - l_1)/t_d, \quad (2)$$

where

$VOP_{st}$  is the velocity of propagation of the shock tube,  
 $l_1$  and  $l_2$  are as indicated in Figure 5, and  
 $t_d$  is the time difference between arrival of the shock waves.

Table 1 is a listing of VOP data for Nonel shock tube. It does not appear that the VOP is length dependent over the range examined, and the average VOP is 7090 feet per second (2.16 mm/ $\mu$ s).

**Table 1. Velocity of Propagation Data for Nonel Shock Tube.**

Length ( $l_2$ ) inches (cm)	Time Dif. ( $t_d$ ) milliseconds	VOP <sub>Nonel</sub> ft/sec (mm/ $\mu$ s)
129.9 (330)	1.38	7120 (2.17)
169.3 (430)	1.85	7090 (2.16)
198.9 (530)	2.30	7120 (2.17)
236.2 (630)	2.79	7050 (2.15)
	Average	7090 (2.16)

Two attempts were made to use the shock tube method to measure the VOP of a flash powder. In both cases the setup was essentially as shown in Figure 3. The flash powder was 70:30 potassium perchlorate (Chinese) and German Blackhead aluminum. The explosive containing tube was  $\frac{1}{4}$ -inch (1.6 cm) inside di-

**Table 2. Velocity of Propagation Determinations for a Flash Powder.**

Distance ( $d_1$ ) inches (cm)	Distance ( $d_2$ ) inches (cm)	VOP <sub>flash</sub> ft/sec (mm/ $\mu$ s)
Test 1		
0.80 (2.0)	2.64 (6.7)	1060 (0.32)
0.80 (2.0)	2.32 (5.9)	1220 (0.37)
0.80 (2.0)	2.76 (7.0)	1030 (0.31)
0.80 (2.0)	3.66 (9.3)	770 (0.23)
	Average	1040 (0.31)
Test 2		
1.13 (2.9)	3.50 (8.9)	1140 (0.35)
1.04 (2.6)	2.01 (5.1)	1830 (0.55)
0.91 (2.3)	3.39 (8.6)	950 (0.29)
	Average	1270 (0.40)

ameter with a 5/8-inch (0.32 cm) wall. The flash powder was slightly compacted using gravity by tapping the loaded paper tube on a tabletop; however, the loading density of the powder was not determined. A No. 8 electric detonator (blasting cap) was used to initiate the charge. The results of the two experiments are reported in Table 2.

## Conclusion

The results of the above VOP measurements seem reasonable in both magnitude and precision, considering the likely nature of propagation reactions in a flash powder.<sup>2,3,10,11,12</sup> However, more study remains before results from the shock tube method should be considered completely reliable.

The work reported here was completed about a year and a half ago, with no additional measurements made in the interim because of the press of other activities. The authors hope to devote more effort to this study in the future but have chosen to publish these preliminary results for fear that other work will continue to prevent further development of the method and in hope that others may benefit from the work being reported.

## Acknowledgments

The authors gratefully acknowledge the technical and/or editorial assistance of Ettore Contestabile of the Canadian Explosives Research Laboratory, Chris Cherry and Paul Cooper of Sandia National Laboratory, and Don Haarmann.

## References

- 1) R.W. Gipson and A. Macek, "Flame fronts and compression waves during transition for deflagration to detonation in solids," *Eighth Symposium on Combustion*, 1962.
- 2) E. Hay, *Bullet Sensitivity Testing of Class B Fireworks and Ingredients and Detonability Testing of Flash Powders*, US Bureau of Mines, Report No. 4573.

- 3) A.J. Tulis, D.E. Baker and D.J. Hrdina, "Investigation of physical and chemical effects in energetic fuel-oxidizer powder compositions I. Stoichiometry vs. Particle size relationship," *Eleventh International Pyrotechnics Seminar*, 1986.
  - 4) C. Cherry, "Nonel firing systems," IABTI Region 2 Training conference, 1990.
  - 5) Ensign-Bickford Technical Bulletin, "Noiseless Trunkline," 2000-6/89, 6000-Rev. 7/90. Ensign-Bickford Co., 660 Hopmeadow St., Simsbury, CT 06070.
  - 6) E. Contestabile, "A new non-electric blasting system — Nonel," Department of Energy, Mines and Resources, Canada, MRL/75-20, 1975.
  - 7) C.J. Johansson and P.A. Persson, *Detonics of High Explosives*, Academic Press, 1970.
  - 8) A. Bailey and S.G. Murray, *Explosives, Propellants & Pyrotechnics*, Brassey's (UK), 1989.
  - 9) R. Meyer, *Explosives*, Verlagsgesellschaft, 1987.
  - 10) J. Hershkowitz, F. Schwartz and J.V.R. Kaufman, "Combustion in loose granular mixtures of potassium perchlorate and aluminum," *Eighth Symposium on Combustion*, 1962.
  - 11) D.J. Haarmann, "Hazards from salute/flash/star compositions — A brief literature survey," *Pyrotechnics Guild Bulletin* No. 65, 1989.
  - 12) A.A. Shidlovskiy, *Fundamentals of Pyrotechnics*, 1961. Reprinted by American Fireworks News.
-



## Repeat Firing of 10.2 cm (4 in.), SDR-17, HDPE Mortars

K.L. Kosanke and B.J. Kosanke

PyroLabs, Inc., 1775 Blair Road, Whitewater, CO 81527, USA

### ABSTRACT

*High Density Polyethylene (HDPE) mortars are beginning to find wide use because of their desirable characteristics. They are relatively inexpensive, lightweight, have a long service life, and some consider them to be among the safest mortars presently in use. Initially HDPE mortars were only recommended for use in electrically fired displays, where each mortar is fired only once. This was done because of a desire to take a cautious approach with this relatively new mortar material, even though the mortars had successfully passed some repeat firing tests. Now, it is becoming increasingly common to use HDPE mortars for manually discharged displays, in which individual mortars are fired repeatedly. The mortars heat up during firing, and, being a thermoplastic, they lose strength with increasing temperature. If mortar temperature rises sufficiently high, they will burst during use, venting the lift gases needed to propel shells to safe altitudes. To date there has been no systematic study of HDPE mortars under conditions of repeat firings, in order to determine the safe limits for their use. Thus it is appropriate to more carefully examine the performance of HDPE mortars under conditions of repeat firing and to offer guidance for their use. Measurements were made of the thermal energy deposited in a mortar during the process of firing 10.2 cm (4 in.) aerial shells and of the distribution of that thermal energy along the length of mortars for typical aerial shell firings. Then, measurements were made of the rate of heat dissipation from HDPE mortars freely exposed to air and when buried in dry sand. Finally, data was collected regarding the ability of HDPE mortars to survive shell firings as a function of temperature. With this information, very rough guidelines are proposed for*

*repeat firing of thick-walled, 10.2 cm (4 in.), SDR-17, HDPE mortars.*

### Introduction

The use of High Density Polyethylene (HDPE) for fireworks mortars has been independently discovered by several individuals around the world. For example, S. Howard of Australia sets the date of his first use sometime before 1970,<sup>1</sup> R. Lancaster of Great Britain reports his use as beginning about 1976,<sup>2</sup> and P. Spielbauer and the authors first use in the United States dates to about 1985.<sup>3</sup> However, most people in the fireworks industry were probably unaware of the potential of HDPE mortars until articles describing their use began to appear in the mid to late 1980s.<sup>4,5,6</sup>

Initially the authors limited their endorsement of HDPE mortars to use in electrically fired displays, where each mortar fires only once during a show. Since then, the use of HDPE mortars has become fairly widespread, and they are now being used with increasing frequency in manually fired displays. With repeated shell firings over a short interval, the mortar's interior surface can heat to temperatures exceeding 100 °C (212 °F). Since it is known that the strength of HDPE falls with increasing temperature, at some temperature, the mortar's strength must fall to an unacceptably low value. At that point, use of the mortar must be interrupted until the mortar cools to a sufficiently low temperature.

In an attempt to determine the safe operating temperature for HDPE mortars and to set guidelines for their use when fired repeatedly, the authors undertook the present study. However, in order to limit the scope, the initial work has only been to establish the experimental method to be used in future studies and to briefly exam-

ine repeat firing of 10.2 cm (4 in.) mortars with fairly thick walls (pipe with an SDR of 17). It is anticipated that the present work will soon be expanded and will include other wall thickness and other mortar sizes.

## Background Information

Aerial shells are propelled from a mortar because of the gas pressure produced by burning the black powder lift charge. It is the function of the mortar to successfully contain these high pressures while the shell is being discharged. Ignoring end effects, a pipe's strength is a function of its wall thickness, the safe tensile strength (yield strength) of the material from which it is constructed and the inside diameter of the pipe. This functional relationship for thin-walled pipe is shown in Equation 1.<sup>7,8</sup>

$$P_b = 2 \cdot S_t \cdot t_w / d_i \quad (1)$$

where,

- $P_b$  is burst strength (pressure),
- $S_t$  is safe tensile strength of the pipe material,
- $t_w$  is wall thickness, and
- $d_i$  is the inside diameter of the pipe (occasionally the more conservative outside diameter is used.).

From Equation 1, it is apparent that burst

strength for a pipe is proportional to its wall thickness. Thus it is appropriate to consider the wall thickness for typical 10.2 cm (4 in.) HDPE mortars; these are listed in Table 1.

Equation 1 also identifies burst strength as proportional to the safe tensile strength (yield strength) of the pipe material. High Density Polyethylene resin type PE-3408 has the highest rated tensile strength commonly available. Thus this is the resin type of choice, and the one used for mortars in this study.

The use of HDPE for fireworks mortars pressure-stresses the pipe in a substantially different manner than typical plumbing applications. Probably the most significant difference is the very short duration of the pressure generated by shell firings, typically less than about 0.03 seconds.<sup>9,10</sup> This is less than one 10-billionth the time of a typical plumbing application. The resiliency of HDPE, coupled with the very brief interval of the pressure pulse from shell firings, seems to provide it with significantly greater strength than would be predicted from Equation 1.<sup>10</sup>

HDPE is a thermoplastic (i.e., it melts at high temperature); thus its strength diminishes as temperature rises. The temperature-rating factor for HDPE pipe is its relative strength as a function of temperature in typical plumbing applications. Figure 1 illustrates the effect of temperature on the burst strength of HDPE pipe.<sup>11</sup> As can be seen, the strength factor has

**Table 1. Wall Thickness for Typical 10.2 cm (4 in.), HDPE Mortars.**

Source – Designation	Minimum Specified Wall Thickness		Typical Wall Thickness <sup>[c]</sup>	
	cm	(in)	cm	(in)
Commercial Pipe – SDR = 17 <sup>[a]</sup>	0.67	(0.26)	0.74	(0.29)
Mighty-Mite Molded Mortar	n/a	n/a	0.66 <sup>[b]</sup>	(0.26)
Commercial Pipe – SDR = 21 <sup>[a]</sup>	0.54	(0.21)	0.58	(0.23)

Notes:

- [a] SDR stands for Standard Dimensional Ratio and equals the pipe outside diameter divided by the minimum wall thickness.
- [b] Mighty-Mite Mortars have a wall that varies in thickness, grading from thickest at the bottom to thinnest at the top. The value reported is for 8.9 cm (3.5 in) above the bottom.
- [c] Manufacturers tend to extrude HDPE pipe with walls that exceed the minimum specified thickness. The thickness reported here are those measured on the mortars used in this and future studies.

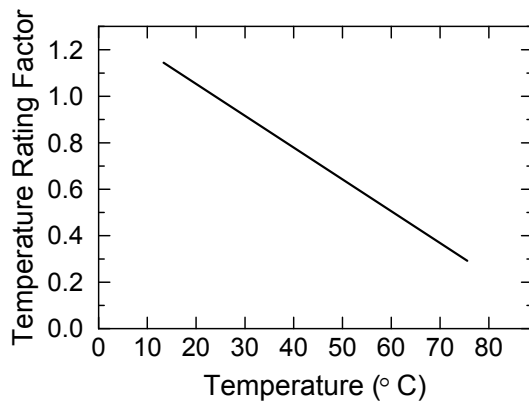


Figure 1. Temperature rating factor for HDPE pipe, derived from Reference 11.

been normalized to 1.0 at 23.9 °C (75 °F), and it falls by 10% for every 7.2 °C (13 °F) rise in temperature. Figure 1 is greatly simplified and not a completely accurate representation of the manner in which HDPE pipe loses strength with increasing temperature. Nonetheless, it clearly suggests that the strength of HDPE mortars must fall to dangerously low levels as their temperature rises. With each shell fired, the mortar absorbs a portion of the thermal energy released from the burning Black Powder; this manifests itself as a rise in the temperature of the mortar. Thus, unless the mortar is allowed to cool between repeated shell firings, the mortar will lose strength with each firing, as its temperature rises.

### Experimental method

The first portion of this study was conducted to learn how measurements should be made. One piece of information needed was, how long after thermal energy (heat) is deposited on the inside of a mortar does it become evenly distributed throughout the wall of the mortar? This information was needed to design intelligent shell firing and temperature measuring sequences. Another piece of information needed was, at what point on the mortar does the highest temperature occur? This is the point where the mortar is most likely to fail and where the temperature needs to be monitored most closely. Finally, in preparation for destructive testing, what method should be used to raise the

temperature of the mortars to near their failure temperature?

In the second portion of this study, the basic data needed to help establish the safe limits for repeat firing was collected. This consisted of determining: how much thermal energy is deposited in the mortar with each shell firing; what is the rate of heat loss from the mortar as a function of mortar temperature and its environment, and what is the mortar temperature at which failures could be expected to occur for typical spherical and cylindrical shells.

Finally, based on the data collected, rough guidance was offered for safe limits of repeat firing of 10.2 cm (4 in.), SDR-17, HDPE mortars.

## Tests and Measurements

### Thermal Equilibration Time

When an aerial shell is first fired from a mortar, the inside of the mortar is very hot and the outside has not begun to warm-up. As time passes, heat energy is distributed more evenly throughout the wall. Eventually, if essentially no energy is lost from either the inside or the outside of the mortar, the temperature will be the same at every point in the wall. The first measurement in this study was of the time required to distribute the thermal pulse from a shell firing throughout the wall of the mortar. This was needed to establish the appropriate time delay after shell firings before other measurements could reliably be made. It was also needed to design the shell firing sequences for some of the tests that would follow.

For an HDPE mortar, the time it takes to reach thermal equilibrium is a function of wall thickness, with thicker walls requiring longer times to equilibrate. Thus, the thickest-walled mortar (commercial pipe with SDR-17) was examined first. For this determination, a single thermocouple was attached to the exterior of the mortar, a few centimeters above its mortar plug. The thermocouple was attached with a narrow strip of PVC tape. Then the mortar was loosely wrapped with fiberglass insulation and mounted in an enclosure to hold the mortar and prevent

drafts from affecting the measurement. At this point, the mortar was ready for a series of test firings. After each firing, a plug was inserted into the mouth of the mortar to reduce thermal loss (from convection) from inside the mortar. Each measurement consisted of monitoring the temperature rise of the exterior of the mortar as a function of time. The data from a series of tests are shown in Figure 2 as the percent of maximum temperature reached.

As can be seen, the maximum temperature is reached in about two minutes and certainly within three minutes. At that time, it is assumed that the mortar has reached essentially a constant temperature throughout the thickness of the wall. In the data reported below, if a time after firing is not given for a temperature measurement, that time is approximately three minutes.

### Distribution of Thermal Energy Along the Length of a Mortar

All else being equal, the most likely point of failure for an over-heated HDPE mortar will be where it is hottest. Thus it is important to examine the distribution of temperature along the length of a mortar to determine where the temperature is highest.

For this determination, a series of six thermocouples were attached along the length of the test mortar (SDR-17). Attachment points were at 0.0, 2.5, 7.6, 15.2, 27.9, and 45.7 cm (0, 1, 3, 6, 11, and 18 in.) above the mortar plug,

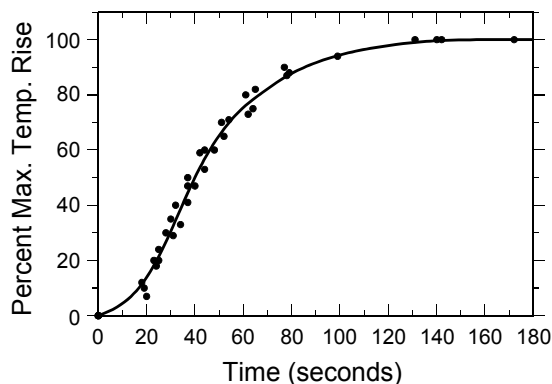


Figure 2. HDPE mortar warm-up curve from test firings of aerial shells.

which was made of 3.8 cm (1.5 in.) thick wood. Thermocouple attachment was again made using narrow strips of PVC tape. Then the mortar was loosely wrapped with fiberglass insulation and mounted in an enclosure to hold the mortar and prevent drafts from affecting the measurements. At this point, the mortar was ready for a series of test firings. After each firing, a plug was inserted into the mouth of the mortar to reduce thermal energy loss. Each measurement consisted of recording the exterior temperature of the mortar approximately three minutes after the test firing.

Both spherical and cylindrical test shells were used. Spherical shells were tested with and without a lift cup, to raise the shell above the bottom of the mortar; also, both 2F-A and 4F-A Black Powder were used for lifting

Table 2. Test Shell Configurations Used in Determining Mortar Temperature Profiles.

Type	Shell				Lift			Dead Volume	
	Mass		Diameter		Type	Mass		[a]	
	g	(oz)	cm	(in.)		g	(oz)	cm <sup>3</sup>	(in <sup>3</sup> )
Sph.	363	(12.8)	9.4	3.7	2F-A	28	(1)	345	(21.6)
	363	(12.8)	9.4	3.7	2F-A	28	(1)	559	(34.1)
	363	(12.8)	9.4	3.7	4F-A	28	(1)	345	(21.6)
	363	(12.8)	9.4	3.7	4F-A	28	(1)	559	(34.1)
Cyl	500	(17.6)	9.2	3.6	2F-A	55	(2)	257	(15.7)

[a] Dead volume is the space below an aerial shell when resting in a mortar. Dead volume affects the maximum mortar pressure and the distance above the bottom of the mortar where maximum mortar pressure is reached. For more information about pressure profiles and the effect of dead volume, see References 9 and 12.

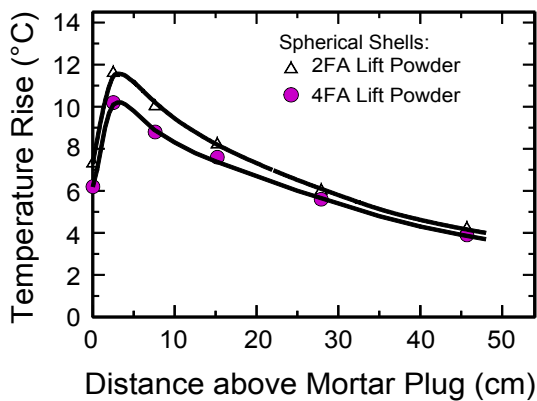


Figure 3. Average mortar temperature profiles for spherical test shells without lift cups.

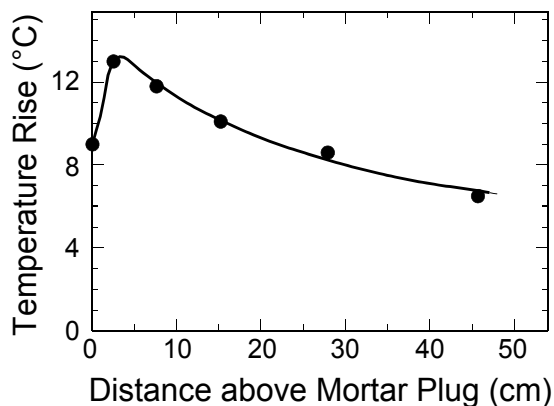


Figure 5. Average mortar temperature profile for cylindrical test shells.

spherical shells. Table 2 lists the various shell and lift configurations used.

Test results are summarized in Figures 3, 4 and 5, where each data point is the average result from at least three test shell firings. Figure 3 presents the mortar temperature profiles for spherical shells fired without a lift cup (dead volume = 345 cm<sup>3</sup>) when using 4F-A and 2F-A Black Powder. Figure 4 presents the results for spherical shells with lift cups (dead volume = 559 cm<sup>3</sup>), and Figure 5 presents the results for cylindrical shells.

The curves in Figures 3, 4 and 5 should only be considered approximations of actual mortar temperature profiles. This is because only a limited number of tests were averaged together and only a limited number of thermocouples were used near the bottom of the mortar where

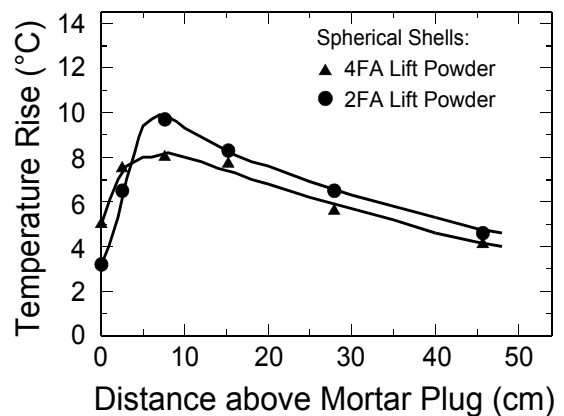


Figure 4. Average mortar temperature profiles for spherical test shells with lift cups.

the profile is rapidly changing. Nonetheless, the curves are quite consistent and appear essentially as expected. For example:

1. Mortar temperature slowly increases as one proceeds along the length of the mortar toward the bottom. Presumably, this is because as one moves down the length of the mortar, it has been exposed to the high-pressure lift gases for longer periods of time. (The amount of thermal energy transferred to the mortar is a function of both the temperature and the pressure of the lift gases, and the duration of that exposure.)
2. The mortar temperature suddenly decreases just before reaching the plug. Presumably this is because some of the heat initially deposited there has been conducted away. (The test mortar was closed on the bottom with a wooden plug, which, along with the mortar wall below the top of the plug, constitutes a heat sink.)
3. The distance above the plug to where maximum temperature occurs is roughly proportional to dead volume. Presumably this is because as dead volume increases more of the mortar just above the plug receives the maximum exposure to the hot lift gases, with the effect that the point of greatest average exposure moves upward.
4. The maximum temperature detected is greatest for cylindrical shells, followed by spherical shells without a lift cup, and is least for spherical shells with a lift cup.

Presumably this corresponds to the relationship for expected mortar pressures for those types of shells. (The amount of thermal energy transferred to the mortar is a function of the pressure of lift gases.)

In the following results, a point 5.1 cm (2 in.) above the mortar plug was chosen for measurement of maximum mortar temperature.

### Method for Pre-Heating the Test Mortars

It might seem that the best way to heat HDPE mortars to near their failure temperature, in preparation for determining the conditions resulting in their failure, would be to repeatedly fire shells from them. One obvious problem with this is the expense of preparing the large number of test shells, which would be considerable. However, there are other technical and operational problems. For example, the amount of thermal energy deposited in the mortar during test firings of identical shells seems to vary significantly from shot to shot. Figure 6 presents the results from six test firings of spherical shells with lift cups and using 4F-A lift powder. The temperature rise for each thermocouple is shown for each test. The gridded area illustrates the range of values observed.

At present, the authors do not fully understand the reason for the range of measured temperatures in the above tests. However, it is likely that it is related to the dynamics of the gas flow in the mortar during its firing. It is possible that much of the variability is merely an artifact caused by only measuring temperature at a series of points along one side of the mortar. The authors speculate that when a shell is propelled up the mortar, it moves somewhat from side to side, within the constraint imposed by the walls of the mortar. As it follows this zigzag path, the gap between the shell and mortar varies from place to place and moment to moment. As a result, the amount of high temperature lift gas escaping between the shell and the wall varies in similar fashion. If this is the case, then it is likely that the amount of thermal energy received by the mortar wall at various points depends on the details of the shell's motion within the mortar, which will be different for each shell firing. Thus if measurements are made along a line of points up one side of the

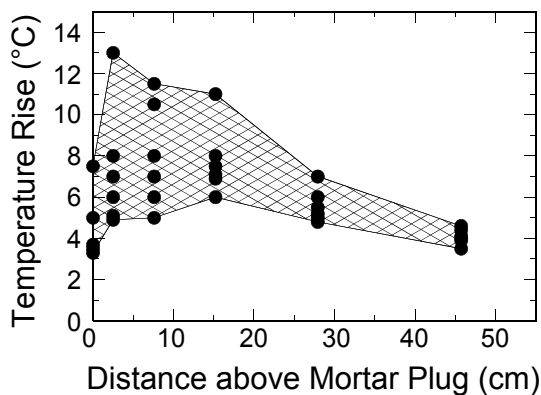


Figure 6. Range of mortar temperature values observed during test shell firings. [Spherical shells with 4F-A lift powder and with lift cups.]

mortar, it seems likely that significant variations from shot to shot could be expected.

Partially as a test of the above hypothesis, but primarily to find a more predictable method of heating mortars, another series of measurements were made. In these tests, bags of lift powder, without attached test shells, were placed in the test mortar and fired. The results from these tests are shown in Figure 7. On average there was slightly less thermal energy transferred to the mortar, but the most striking difference is that the values for the points are more closely grouped. For this reason, plus the cost savings from firing only lift powder and not test shells, it was decided to pre-heat test

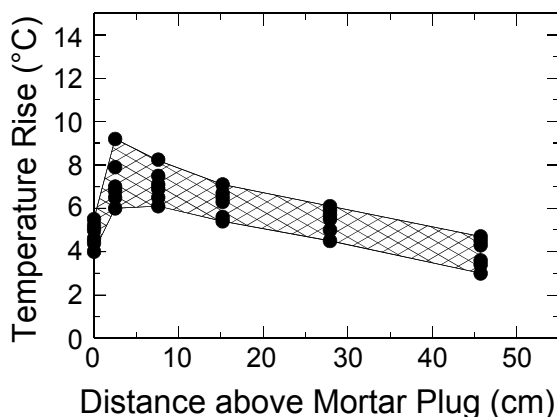


Figure 7. Range of mortar values observed during test burning of bags of lift powder alone [28 g (1 oz) of 4F-A lift powder].

mortars by repeatedly burning bags of lift powder in them. So-called B-blasting powder (sodium nitrate oxidizer) is slower burning and was found to produce greater mortar temperature increases than normal A-blasting powder (potassium nitrate oxidizer). The average temperature rise for 28 g (1 oz) of 4F-A powder is about 7 °C (13 °F), while that for 1F-B powder is about 37 °C (66 °F). Thus B-blasting powder was chosen to preheat the test mortars.

### Amount of Thermal Energy Deposited in Mortar During Shell Firing

The data needed for this determination, is the same as already reported to establish the mortar temperature profiles shown in Figures 3, 4 and 5. Knowing the temperature rise of an object, its mass, and its heat capacity (specific heat), it is a simple matter to calculate the amount of heat (thermal energy) absorbed, see Equation 2.

$$q = m \cdot C \cdot \Delta T \quad (2)$$

where,

- q is the heat transferred in calories,
- m is the mass of the object in grams,
- C is the heat capacity in cal/g °C (0.50 cal/g °C for HDPE<sup>13</sup>), and
- ΔT is the change in temperature in °C.

Considering a 1-cm<sup>2</sup> section of a SDR-17 mortar, with a typical wall thickness of 0.74 cm [Table 1], and given that the density of HDPE averages<sup>13</sup> 0.95 g/cm<sup>3</sup>, the heat required for a 1 °C (1.8 °F) temperature rise is 0.35 calories. The maximum temperature rise seen in the various profiles shown in Figures 3, 4, and 5, averages about 10 °C (18 °F) for spherical shells and about 13 °C (23 °F) for cylindrical shells. The thermal energy deposited in the mortar at the point of maximum temperature rise is approximately 3.5 and 4.5 cal/cm<sup>2</sup> for spherical and cylindrical shells, respectively.

As an aside, it was felt that it might be of interest to determine the fraction of thermal energy, which is produced by burning the Black Powder lift that is absorbed by the mortar. This was calculated by mathematically dividing the mortar into six sections of varying length, one section centered on each thermocouple. Then,

assuming the temperature rise of each section was that observed by the thermocouple, Equation 2 was used to calculate the heat deposited in that section. The total thermal energy absorbed was determined by summing the individual values. This resulted in estimates that, typically, the mortar absorbs 1.2 and 1.6 kcal of energy when firing spherical and cylindrical shells, respectively. Knowing the amount of lift powder used, and that the heat of reaction for Black Powder<sup>14</sup> is 0.66 kcal/g, the total heat produced was calculated. This amounts to about 18 and 36 kcal for spherical and cylindrical shell firings, respectively. Thus the mortar absorbs approximately 6.7 and 4.4 percent of the total thermal energy produced by the lift powder during the firing of spherical and cylindrical shells, respectively.

### Rate of Thermal Energy Loss from Mortars

Thermal energy always migrates from hotter to cooler areas, and the rate of heat transfer is a function of the temperature difference (temperature gradient) between the two areas. Thus in the examination of the heat loss from mortars, the rate of loss was always considered in terms of temperature gradients, and not specifically in terms of mortar and environment temperatures. This provides solutions that are more generally applicable, instead of requiring data for each different mortar and environmental temperature.

There are three mechanisms for transferring thermal energy: radiation, convection, and conduction. For above ground mortars, only convection is significant; the hot mortar is in contact with cool air, which acquires heat from the mortar and then drifts away. For buried mortars, only conduction is significant; the hot mortar is in contact with the cool ground, which acquires heat from the mortar and passes it from layer to layer through the ground. Heat transfer problems are often fairly simple to solve analytically; however, in this case there are complexities that make an analytic solution impractical and possibly unreliable as well. Thus an empirical approach has been taken. For this, mortars were instrumented with thermocouples at six locations, attached in the manner described above. However, for above ground mortars, a rubber band was placed around the mortar and

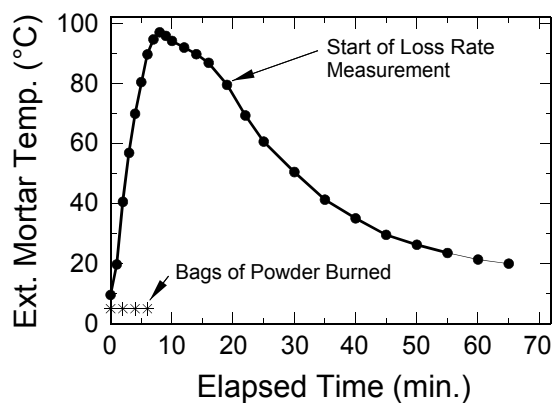


Figure 8. Temperature history recorded by TC2 for an above ground HDPE mortar.

over the thermocouple to augment its attachment. This was necessary because, at the temperatures during testing, the adhesive on the tape failed to provide sufficient attachment strength. The test mortar was then placed in the environment to be studied.

To study above ground mortars, a stake was used for mortar support. The mortar was attached to the stake so as not to interfere with or distort the temperature measurements. Shields were erected around the test mortar to shade the mortar from direct sunlight and breezes. However, the shields were not close enough to restrict free air circulation around the mortar. At this stage of work, no attempt was made to account for effects that would be produced by having mortars in racks. (Racks would restrict air circulation to some extent, insulate some spots on the mortar, and may place heated mortars close to one another.)

To study buried mortars, a wooden box was used to support the mortar. The box provided about 16 cm (6.5 in.) of space around the mortar; the space was filled with dry sand. (Hopefully, data will eventually be collected using wet sand, which will have greater thermal conductivity and a higher heat capacity.)

To begin the process of taking measurements, the mortars were heated by burning packets of Black Powder in them. The packets were small enough and their burning separated enough in time so as not to damage the mortar by localized over-heating. Generally, 28 g (1 oz) packets of 1F-B powder were used, with

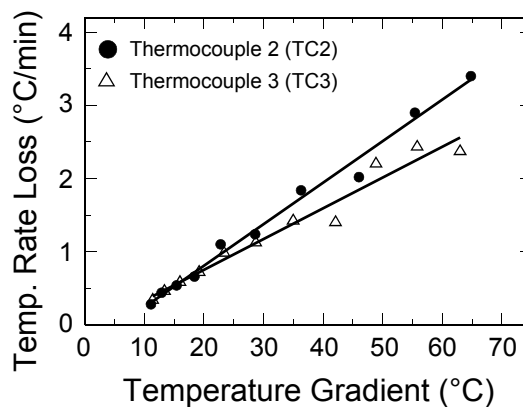


Figure 9. Temperature loss rate at TC2 and TC3 for an above ground HDPE mortar.

two minutes elapsing between burnings. Figure 8 is an example of the temperature history recorded by thermocouple number two (TC2) in one above ground thermal energy loss experiment.

It is at the approximate location of TC2 and TC3 where the mortar is hottest and is expected to fail during use. Thus this is where attention was focused. Figure 9 presents the results from one of three above ground tests. Here, temperature gradient is the difference between mortar exterior and air temperatures. The rate of heat loss is reported as temperature loss rate because the two are proportional (see Equation 2) and because this information will be of more direct use later in this report.

It appears that the temperature loss rate at TC2 and TC3 is a linear function of temperature gradient. Also the loss rates at TC2 and TC3 is similar, but not precisely the same. Considering that the mechanism for heat loss is convection, it is not surprising there is a difference and that the rate of heat loss at TC3 is less than at TC2. The heat being convected away from near TC2 would be expected to raise the air temperature over TC3 higher than ambient air temperature, thus reducing the efficiency of heat loss at that point.

Of necessity, the rate of temperature loss (heat loss) must be zero when the temperature gradient is zero. However, the Y-intercept for the lines in Figure 9 are about  $-0.3$  °C/min. It is believed that this is an artifact of fitting the data to a linear relationship and not including data



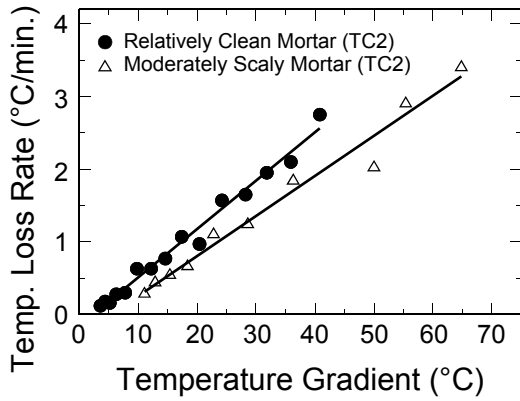


Figure 10. Temperature loss rate as a function of cleanliness of an above ground mortar.

for near zero temperature gradients. Nonetheless, in the temperature gradient range of greatest interest, this should be of no concern.

When Figure 9 results were compared with those of earlier experiments, it was observed that the temperature loss rate had fallen about 20 percent for the same mortar (see Figure 10). Upon examination of the mortar, apparently a scale of combustion products had built up on the interior mortar walls. While the direction of the change is what would be expected, its magnitude is larger than would have been expected. Thus, in predicting the safe limits for repeat firing, it seems that the cleanliness of the HDPE mortar also must be considered. The temperature loss rate ( $R_{TL}$ ) for a clean mortar, shown in Figure 10, is:

$$R_{TL} (\text{°C/min}) = 6.7 \times 10^{-2} (\Delta T) - 0.16 \quad (3)$$

For a buried mortar, the rate of heat loss was observed to be almost exactly the same for both TC2 and TC3, see Figure 11. When compared with above ground mortars, the most significant difference is that the temperature loss rate is only about one-third as much for the same gradient. Also different is that the relationship is not linear, the curve is very nearly a parabola and the temperature loss rate is given in Equation 4.

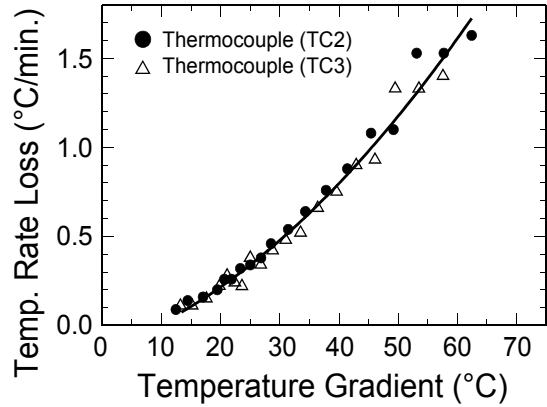


Figure 11. Temperature loss rate at TC2 and TC3 for a buried mortar.

$$R_{TL} (\text{°C/min}) = 5.0 \times 10^{-4} (\Delta T)^2 \quad (4)$$

With above ground mortars, because even minor air currents continually carry heated air away, the ability of the air to absorb thermal energy does not diminish with time. However, this is not the case for buried mortars, where the ground nearest the mortars tends to become saturated with heat. To examine this effect, a series of three thermal energy loss experiments were conducted, one immediately following the other, see Figure 12. Using this data, three loss rate curves were derived illustrating that the ability of the ground to absorb heat diminishes with each cycle, see Figure 13. This is an effect that must be considered when attempting to define limits for repeat firing of buried HDPE mortars.

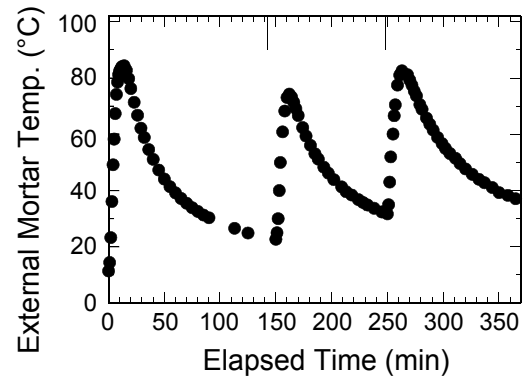


Figure 12. Three consecutive temperature loss rate experiments for a buried mortar.

### Failure Temperature of HDPE Mortars

For these measurements, two mortar configurations were used. In some tests, the mortar was insulated, essentially reducing the rate of heat loss to zero. This represents the extreme case of completely thermal-saturated ground. In other tests, the mortars were not insulated and were exposed to cool air, 0 °C – 20 °C (30 °F – 70 °F). In these tests, the mortars were pre-heated to near their expected failure temperatures; then aerial shells were fired to test whether the strength of the mortars had remained high enough to survive. Mortars that survived were heated to still higher temperatures and tested again. This process was continued until each mortar had failed. Because the firing of cylindrical shells pressure-stresses mortars more than spherical shells, information was collected for both types of shells. In this way, data was collected identifying the highest mortar temperature for which mortars survived and the temperatures at which they failed. Results from those experiments are listed in Table 3.

During the tests reported in Table 3, in at least one case, a mortar had visibly bulged, ~0.3 cm (0.12 in.), during preheating. Recall that no significant pressure is produced when bags of Black Powder are burned in the mortars. Thus, the bulging in that one case cannot be attributed

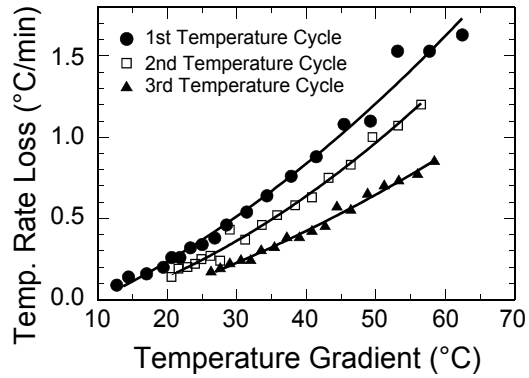


Figure 13. Temperature loss rate at TC2 and TC3 for a buried mortar illustrating the effect of thermal saturation.

to the high pressure of shell firing. In other tests, after the mortars had bulged slightly, they continued to fire shells successfully even though the temperature had been raised significantly. For example, the mortar that bulged at 76 °C (169 °F), while firing a cylindrical shell, continued to withstand cylindrical shell firings at 88 °C and 92 °C. The bulges were small both in terms of change in diameter [~0.3 cm (0.12 in.)] and mortar length affected [~5 cm (2 in.)]. Accordingly, it seems likely that the mortar pressure during subsequent shell firings was about the same as for unbulged mortars. Thus the survival of the mortar during subsequent

Table 3. Survival and Failure Temperatures for 10.2 cm (4 in.), SDR-17, HDPE Mortars.

Shell Type	Maximum Temperature Survived		Temperature Where Mortar Bulged or Burst	
	°C	(°F)	°C	(°F)
Spherical	88	(190)	86	[b] (187)
	99	(210)	88	[b] (190)
	92	(198)	97	(207)
	102	[a] (216)	96	(205)
			97	(207)
		108	[a] (226)	
Cylindrical	96	(205)	76	[b] (169)
	88	(190)	90	(194)
			103	[a] (217)

[a] The mortar was wrapped in insulation for the test.

[b] The mortar only bulged; it did not burst.

firings at higher temperatures, probably cannot be attributed to those firings putting significantly less stress on the mortars. At present, the authors do not fully understand the bulging phenomenon.

It might be of interest to note that on average the mortar burst points were 2.9 cm (1.1 in.) above the plug and ranged from 2.2 to 5.5 cm (0.9 to 2.0 in.) above the plug. Based on the estimated point of highest mortar temperature, temperatures reported in Table 3 were recorded at about 5 cm (2 in.) above the mortar plug. The location of the burst points, which corresponds to the point of highest mortar temperature, suggests that a point slightly closer to the plug should be used in future tests.

The overall strength of an HDPE mortar at high temperature depends on the temperature of the pipe throughout the thickness of its wall. As an example of the complexity this introduces, consider the case where the mortar is exposed to relatively cool air on its exterior. In this case, the temperature measured on its exterior wall is a complex function of both the temperature of the mortar, the air temperature, and the degree to which the air is in motion or is stagnant. The data for non-insulated mortars in Table 3 do not consider this complication, and thus must be considered only as a general guide. Based on the work performed to date for 10.2 cm (4 in.), SDR-17, HDPE mortars exposed to relatively cool and calm air, it seems that the maximum service temperature (as measured on their exterior) is not more than about 75 °C (167 °F) for typical cylindrical shells and about 85 °C (185 °F) for typical spherical shells. For insulated mortars, with near zero heat loss, these temperatures are probably about 15 °C (27 °F) higher. For mortars in dry sand (roughly equivalent to dry soil) the rate of heat loss should be somewhere between that for cool air exposed mortars and insulated mortars. Thus, it seems that the maximum service temperature of buried mortars, as measured on their exteriors, would be no more than about 80 °C (176 °F) for typical cylindrical shells and 90 °C (194 °F) for typical spherical shells.

## Preliminary Results

The authors feel that the results generated to date are only barely sufficient to suggest even the most preliminary guidelines for repeat firing of 10.2 cm (4 in.), SDR-17, HDPE mortars with wooden plugs. It is only because this subject is of considerable interest to some and has important safety ramifications that an attempt was made to offer any guidance at this time.

During repeat firing of HDPE mortars, some amount of heat will be lost from the mortar between firings. Therefore, a worst-case scenario would be the case of a well-insulated mortar when no heat loss occurred. Thus, if it is determined how many shells of a given type can be successfully fired from an insulated mortar, then surely at least the same number could be successfully fired during a fireworks display. If it is assumed that:

- the initial temperature of the mortar is 20 °C (68 °F);
  - only spherical shells of typical weight and normal lift charges are fired;
  - the maximum mortar temperature rise produced by these shells is 10 °C (18 °F) per firing;
  - the maximum temperature rise for such shells before mortar damage occurs is 100 °C (212 °F) [insulated mortar results]; and
  - the thermal energy lost during the process of shell firing, from a non-insulated mortar, provides a sufficient safety margin;
- ⇒ then it could be concluded that eight typical spherical shells could be rapidly fired from the same mortar without it failing.

If a greater safety margin were felt appropriate, the number of shells could be reduced to seven. For each 10 °C (18 °F) increase in initial mortar temperature, the number of shells should be reduced by one, and conversely, could be increased by one for each 10 °C (18 °F) decrease in initial mortar temperature. Following similar logic, and for similar conditions for cylindrical shells, it could be suggested that as many as five typical cylindrical shells could be safely fired in rapid succession.

Having once raised an HDPE mortar to its limiting service temperature, the question might then be how long to wait between subsequent firings. For above ground mortars, if it assumed that:

- air temperature is 20 °C (68 °F);
  - air flow around the base of the mortar is not obstructed;
  - adjacent mortars are not hot enough or close enough to affect the mortar of interest;
  - the interior of the mortar is fairly free of scale; and
  - during repeat firing, because of heat loss during the process, the exterior temperature of the mortar had risen to approximately 70 °C (158 °F), producing a temperature loss rate of a little more than 3 °C (36 °F) per minute;
- ⇒ then subsequent shells could be fired every three or four minutes.

Following similar logic, and for similar conditions for cylindrical shells, it could be suggested that subsequent cylindrical shells could be fired every four or five minutes.

For buried mortars, the rate of heat loss for the same temperature gradient is about one-third that for above ground mortars. Accordingly, the time between subsequent firings should then be about three-times as long as that for unobstructed above ground mortars with the same temperature gradient.

### Acknowledgments

The authors gratefully acknowledge that Mighty-Mite Marketing and Hercules Pipe (Grande Finale Fireworks) have contributed test mortars for this and subsequent studies. In addition, the Pyrotechnics Guild International, Inc. and Hercules Pipe have underwritten a portion of the cost of this study.

### References

- 1) Sid Howard, Private communication, 1992).
- 2) Ron Lancaster, Private communication, 1986).
- 3) Paul Spielbauer, Private communication, 1992).
- 4) K.L. Kosanke, "HDPE mortars for electrically fired displays," *Pyrotechnics Guild International Bulletin*, No. 54, 1986.
- 5) K.L. Kosanke, "Destructive testing and field experience with HDPE mortars," *American Fireworks News*, No. 72, 1987.
- 6) K.L. Kosanke, "Further information about HDPE mortars," *Fireworks Business*, No. 60, 1989.
- 7) M.G. Bassin, S.M. Brodsky, H. Wolkoff, *Statics and Strength of Materials*, McGraw-Hill, 1969.
- 8) E.A. Avallone and T. Baumeister III, *Mark's Standard Handbook for Mechanical Engineers*, 9th Edition, 1986.
- 9) E. Contestabile, R.A. Augsten, T.R. Craig and J.G. McIndoe, "A study of the firing characteristics of high altitude display fireworks," *Proceedings of 13th International Pyrotechnics Society Seminar*, IIT Research Institute, Chicago, 1988.
- 10) K.L. and B.K. Kosanke, "Measurements of aerial shell mortar pressure and muzzle velocity," in preparation.
- 11) Polypipe Technical Bulletin, "Pressure design," Polypipe Industries, Inc., Gainesville, TX.
- 12) K.L. and B.J. Kosanke, "Shimizu aerial shell ballistic predictions, Parts 1 & 2," *Pyrotechnics Guild International Bulletin*, Nos. 72 & 73, 1990.
- 13) A.J. Moses, *The Practicing Scientist's Handbook*, Van Nostrand Reinhold, 1978.
- 14) J.A. Conkling, *Chemistry of Pyrotechnics*, Marcel Dekker, 1985.

## Aerial Shell Drift Effects

K.L. and B.J. Kosanke

PyroLabs, Inc., 1775 Blair Road, Whitewater, CO 81527, USA

---

### ABSTRACT

*A prime consideration in determining separation distance requirements for aerial fireworks displays is where fallout of dangerous debris is likely to occur. Certainly the most dangerous single piece of fallout is a dud aerial shell. Thus it is important to have knowledge of where duds may fall during typical displays. This would be a relatively simple situation if aerial shells were ballistically stable, and they precisely followed the path determined by mortar orientation, shell muzzle velocity, and atmospheric conditions. Unfortunately, however, aerial shells tend to drift from their ideal (predicted) path, and that drift is greater than most realize. In order to determine where dud shells fall, a large number of aerial shells, both spherical and cylindrical, were fired into the air after having been rendered incapable of bursting at altitude. Most firings were from mortars that were positioned vertically and under calm wind conditions; however, some firings were from angled mortars. For spherical aerial shells, 7.6 cm to 25.4 cm (3 in. to 10 in.) it was found that, on average, duds fall 3.8 m per cm (32 ft per in.) of shell size, from the point ballistically predicted. Further the data suggests that drifts as great as 12 m per cm (100 ft per in.) of shell size may occur nearly 1 percent of the time. For cylindrical shells, 7.6 cm to 15.2 cm (3 in. to 6 in.) it was found that, on average, duds fall 2.4 m per cm (20 ft per in.) of shell size, from the point ballistically predicted. Finally, a large number of 10.2-cm (4-in.) cylindrical shells were fired in order to determine the effect of shell weight, shell length, and lift powder weight on drift distance.*

### Introduction

When aerial shells are fired from a mortar, fairly accurate predictions can be made about their ideal (average or typical) trajectories, providing the necessary input information is available. The type of information needed includes the shell's shape, weight, amount and type of lift, mortar tilt angle and azimuth, wind speed and direction. These ballistic predictions could be based on empirical data, but more often they are based on mathematical calculations.<sup>1,2,3</sup> The accuracy of the predictions generally improve with more and better input information. However, at present, the exact trajectory for an individual shell is not predictable. This is because, for each individual shell being fired, other needed input information is unknown or unknowable, and the mathematical models presently available lack the degree of sophistication to use the information even if it were known. For the purpose of this paper, the difference between the ballistically predicted path of an aerial shell and its actual path will be termed drift distance.

Knowledge of aerial shell drift distance is important in establishing appropriate spectator separation distances for fireworks displays. For example, if it were possible to align all of one's mortars so as to cause all shells to be propelled toward one specific fallout point, then it would be easy to avoid injuries from duds falling into the crowd. However, because individual shell drifts cannot be predicted, it is not possible to aim each mortar to compensate for drift. Thus, dud shells occurring during a show will be scattered about the fallout area. In establishing appropriate spectator separation distances, it is

important to know how widely those duds are likely to be scattered.

The reason aerial shells drift or wander from their ideal trajectories is not completely known, at least by the authors. However, the cause of drift is of less concern than is its magnitude. The reason aerial shell drift has more than mere academic interest, is that drift effects are considerably greater than many in the fireworks display business realize. This, in turn, means that appropriate spectator separation distances are greater than many realize. This paper summarizes information presented earlier by the authors<sup>4,5</sup> and others<sup>6,7</sup> and presents the results of new work by the authors and others<sup>8</sup>.

## Background Information

### Magnus Effect

While there may be many causes for aerial shell drift, it may be useful to discuss one cause as an example of how drift forces arise. Aerial shells generally tumble through the air after they are fired from a mortar. This tumbling (spinning) produces an effect analogous to that when a baseball pitcher throws a curve ball. The tumbling shell follows a trajectory which curves (drifts) away from that predicted based solely on mortar tilt and wind effects. This tumbling or curve-ball effect is technically known as the Magnus effect.

The magnitude of the drift derived from the

Magnus effect depends on the rate of spin of the shell and its velocity through the air. To better understand why this is the case, consider Figure 1(A). Here a rotating aerial shell is depicted with air flowing past it. (From a physics standpoint this is the same as if the shell were moving through still air, but a stationary shell and the forces acting on it are easier to visualize and draw.) As the shell rotates, a thin layer of air, called the boundary layer, rotates along with the shell. When this air motion is combined with that moving past the shell, the resulting air velocity will not be the same on both sides of the shell. In effect, the two air motions add on the left side of the shell producing a higher overall velocity, and they subtract on the right side producing a lower velocity. Bernoulli's Principle states that the pressure in a moving column of fluid is inversely proportional to its velocity. Although not completely applicable in this case, it suggests that the pressure acting on the left side of the shell ( $P_1$ ) will be less than that on the right side ( $P_2$ ), see Figure 1(B). This pressure differential produces a net force ( $F$ ) acting on the shell toward the left. This is the Magnus force, and it acts to push a rotating shell off course. The magnitude of the drift depends on the magnitude of the force and the length of time the force is applied. This depends on the combination of the shell's velocity through the air, its rate of spin, and the duration of the flight of the shell (with greater flight times resulting in greater drifts).

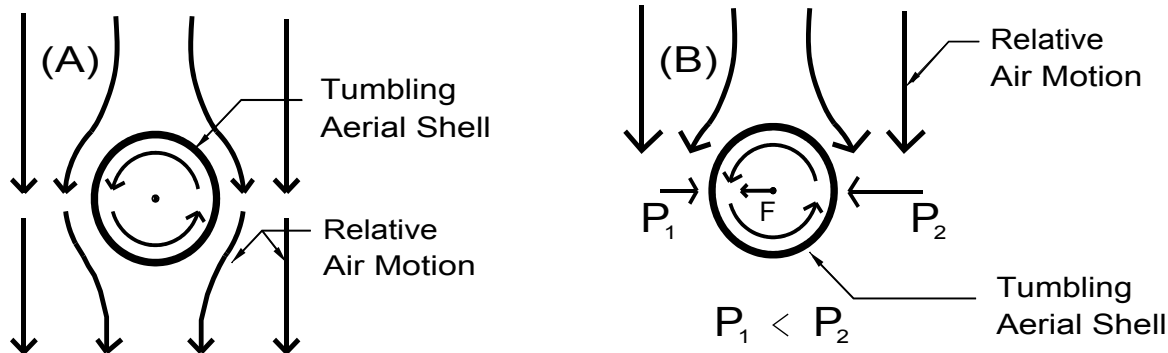


Figure 1. Rotating spherical aerial shell with air flowing past it, and the force produced as a result of pressure differential ( $P_2 - P_1$ ).

**Table 1. Characteristics of Mortars Used in Aerial Shell Drift Tests.**

Shell Size		Mortar Length <sup>(a)</sup>		Mortar I.D.		Mortar Material <sup>(b)</sup>	Type of Shell Fired Used
cm	(in.)	cm	(in.)	cm	(in.)		
7.6	(3)	57.2	(22.5)	7.3	(2.89)	HDPE	All
10.1	(4)	56.9	(22.4)	9.9	(3.88)	HDPE	Spherical
10.1	(4)	61.0	(24.0)	10.4	(4.10)	HDPE <sup>(c)</sup>	Cylindrical
12.7	(5)	68.6	(27.0)	12.5	(4.92)	HDPE	All
15.2	(6)	68.6	(27.0)	15.0	(5.91)	HDPE	Spherical
15.2	(6)	75.7	(29.8)	15.5	(6.10)	Steel	Both
20.3	(8)	98.6	(38.8)	20.3	(8.00)	Steel	Spherical
25.4	(10)	118.9	(46.8)	25.6	(10.06)	Steel	Spherical

(a) Mortar length is measured from the top of the mortar plug to the mouth of the mortar.

(b) HDPE = High Density Polyethylene.

(c) Mighty-Mite mortar with a slightly tapering ID. Reported ID is an average.

### Mortar Characteristics

The velocity of a shell and its time of flight depend (to some extent) on the characteristics of the mortar being used. For this reason, Table 1 gives characteristics of the mortars used in these tests and indicates on which shell drift tests they were used.

### Air Density

Another factor possibly influencing drift distance is air density, which depends on the elevation above sea level at which shells are fired. As air density decreases, so does the magnitude of forces acting on the shell; drift forces will be less, but so will aerodynamic drag (which means the flight time of shells will be greater). The combined effect of increased elevation is to have a smaller drift force acting for a longer time. At the time of writing this paper, the authors have not evaluated the precise net effect of changes in elevation; however, it is felt that any elevation dependence is small. (Except as noted, the tests reported here were conducted in Whitewater, CO at approximately 4600 ft above sea level.)

The effect of temperature and pressure variations, which affect air density, is also expected to be small.

### Absolute Drift Predictions

The speed of an aerial shell as it leaves the mortar and then travels through the air is roughly predictable based on calculations using typical shell parameters,<sup>1,2</sup> or it can be measured.<sup>9,10</sup> However, as suggested in the introduction, the magnitude and orientation of a shell's drift are not absolutely predictable. In part, this is because no one has developed an adequate mathematical model. However, more importantly, when a shell is fired, one does not have details of the shell's exact position in the mortar, the shell's internal mass distribution, the smoothness and symmetry of the shell's surface and the mortar's interior, etc., all of which would be needed to perform a drift calculation (assuming an appropriate mathematical model existed). For this reason, it may never be possible to calculate drift distance for an individual shell. As an alternative it is possible to measure typical aerial shell drifts; then to use this information in a general way to predict the average drifts of shells to be fired. However, it must be recognized that those predictions will only be accurate in a statistical sense. For example, it might be possible to state for a given type of shell, that 5% of the time it will drift between 30 and 60 meters in a direction between north and east. Similarly, the likelihood for other drifts could be stated. However, for any particular shell, it is not possible to predict the precise

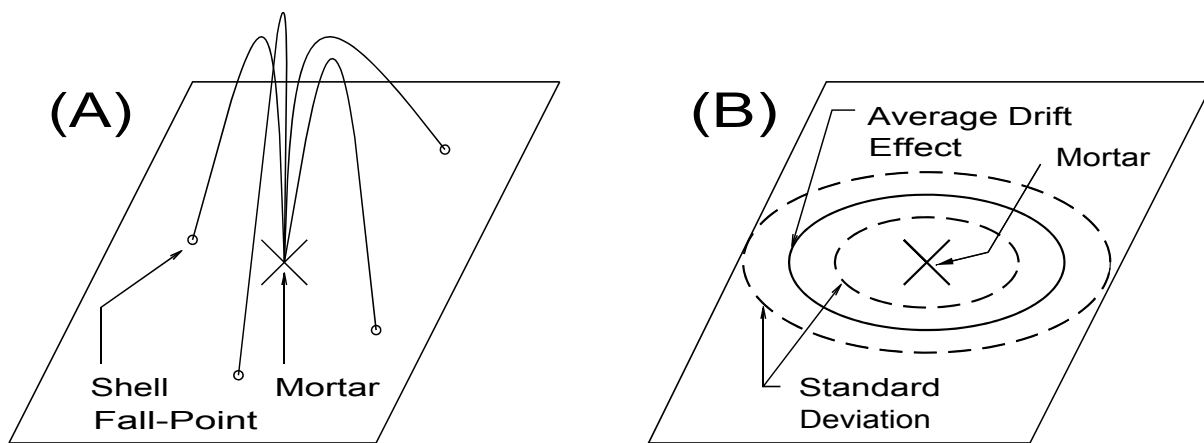


Figure 2. Method of determining aerial shell drift distance.

magnitude or direction of its drift. For this reason, drift distances reported in this paper can only be stated in a statistical or probabilistic sense.

## Experimental Method

### Shell Firings

Except in a few cases, the only mortar orientation used in this study was vertical. Also, tests were generally performed under calm surface wind conditions, i.e., winds measured at 6.1 meters (20 ft) above ground were less than 3.2 km/h (2 mph). Both spherical and cylindrical shells were tested. The spherical aerial shells were commercially produced and ranged in size from 7.6 cm (3 in.) to 25.4 cm (10 in.). Before being fired, the shells were altered so as not to burst during their flight (i.e., they were made into duds). (In most cases this was accomplished by injecting water into each shell's time fuse.) Also, a variety of shells from different manufacturers were used, so that the results would tend to be independent of peculiarities of any one manufacturer. (The brands or manufacturers used were Onda, Yung Feng, Horse, Temple of Heaven, and Flying Dragon.) The shells were fired using an electric match to replace the quick match shell leader installed by the manufacturer. All the cylindrical shells were specifically made for these tests and were inert. They ranged in size from 7.6 cm (3 in.) to 15.2 cm (6 in.). These

cm (6 in.). These shells were also fired electrically.

Each test consisted of the firing of from 8 to 10 shells of one size. After firing and upon the shell's return to ground, the approximate point of impact of each shell was noted. Following the completion of firing of a series of shells of one size, the exact points of impact were determined relative to a coordinate grid system. This process is illustrated in Figure 2(A).

### Data Reduction

If one could be assured that experimental conditions were ideal (perfect mortar alignment and absolutely no wind from the surface through the maximum height reached by the shell), there would be little data processing to perform. For each shell size, it would only be necessary to calculate the average displacements from the mortar, their standard deviation and standard error, as illustrated in Figure 2(B).

Unfortunately, conditions were not perfect; for example, there were usually winds aloft that pushed the shells somewhat off course. Accordingly, some mechanism was needed to separate systematic effects (such as winds aloft) from the randomly oriented shell drift effects. It was decided to shift the original coordinate grid in order to correct for systematic errors. This was accomplished by first calculating the mathematical center for the distribution of shell impact points and then assigning that as the origin



**Table 2. 15.2-cm (6-in.) Spherical Shell Drift Effect Data.**

Shell No.	Shell Displacement from Mortar (m)		Shell Displacement in Shifted Grid (m)		Distance from Center (m)
	North	East	North	East	
1	-22.9	-61.0	8.5	-26.2	27.4
2	0.6	-82.4	30.0	-47.6	57.3
3	15.6	-24.7	47.0	10.1	48.2
4a	—	—	—	—	—
5	-46.1	-29.0	-14.6	5.8	15.9
6	-56.4	-33.6	-25.0	1.2	25.0
7	13.7	-20.1	45.1	14.6	47.6
8	-132.7	-22.9	-101.3	11.9	101.9
9	-22.3	-5.2	9.2	29.6	31.1
Average	-31.4	-34.8	≈0	≈0	44.2

(a) Shell burst at altitude, thus no drift data was produced.

of a new (shifted) coordinate system. In effect, what that does is to say that the distribution of shell impact points in the shifted coordinate system is the distribution that would have occurred had there not been systematic errors.

If the tests for each type of aerial shell had included many shells, and if one could be certain that wind conditions did not change during the tests, then this grid adjustment method should work very well. However, in this study, only a limited number of shells were used and

wind conditions probably did change at least a little during the time it took to fire the shells. Thus there is some uncertainty as to how accurately the impact points in the shifted coordinate system represent actual shell drift effects. Having given this matter considerable thought, the authors feel that the average drifts presented in this paper probably are slightly underestimated, while the reported standard deviations probably are slightly over-estimated. (For a more complete discussion of this subject, see Notes A and B of Reference 4.)

Figure 3 and Table 2 illustrate the process for the first set of shells fired, 15.2-cm (6-in.) spherical shells. The mortar was placed at the origin of the coordinate system, indicated by the large  $\times$  in Figure 3. The points of fall of the shells fired are indicated as small circles, which are located primarily in the southwest quadrant. The center of the pattern of these points, the average displacements, was determined to be 31.4 m (103 ft) south and 34.7 m (114 ft) west and is indicated as the smaller  $\times$  in Figure 3. Next, for each point of fall, the distance from the center of the pattern was determined and the average of those distances was calculated. In the case of these 15.2-cm (6-in.) spherical shells, the average is 44.2 m (145 ft) and is shown as the heavy solid line circle in Figure 3. [Note that in this initial test series an error had been made in the vertical positioning of the mortar. That is the primary reason for the center

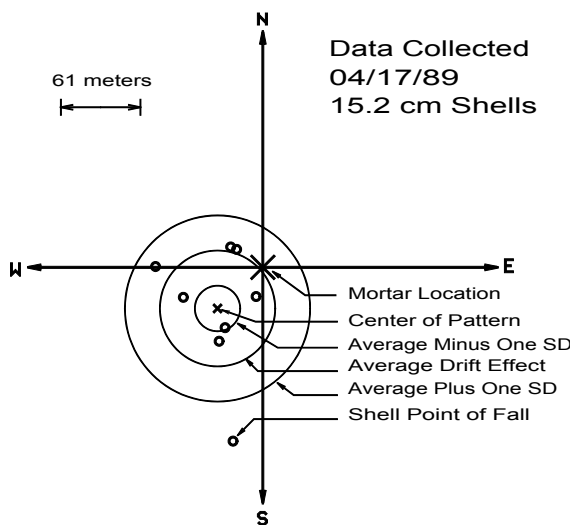


Figure 3. Illustration of 15.2-cm (6-in.) spherical aerial shell drift distance determination.

**Table 3. Average Spherical Aerial Shell Drift Distance.**

Shell Size		Mean Drift		Standard Error <sup>(a)</sup>	
cm	(in.)	m	(ft)	m	(ft)
7.6	(3)	45.4	(149)	6.7	(22)
7.6 <sup>(b)</sup>	(3)	19.2	(63)	4.3	(14)
10.2	(4)	38.7	(127)	11.0	(36)
12.7	(5)	40.7	(140)	6.7	(22)
15.2	(6)	44.2	(145)	9.4	(31)
15.2 <sup>(c)</sup>	(6)	50.9	(167)	12.2	(40)
20.3	(8)	81.7	(268)	14.9	(49)
25.4	(10)	104.5	(343)	18.9	(62)

- (a) Standard error is equal to the observed standard deviation, using the n-1 method, divided by the square root of the number of shells fired for that measurement.
- (b) Because the first set of 7.6-cm (3-in.) aerial shells demonstrated unexpectedly high drifts, a second series of shells were fired the next day.
- (c) One set of 15.2-cm (6-in.) aerial shells was intentionally fired with a mortar tilt of 24°, causing the shells to be propelled down range.

of the fall points being located about 47 m (154 ft) from the mortar.]

Even though the distribution of points about the average cannot be a true normal distribution, it is still useful to estimate the width of the distribution by calculating its standard deviation. The standard deviation, using the n-1 method, for the 15.2-cm (6-in.) spherical shells is 27 m (88 ft) and is shown in Figure 3 as the dashed circles. It is also useful to estimate the uncertainty in the average drift by calculating its standard error, which is 9.4 m (31 ft). Thus, the results for this series of shells is a drift effect of 44.2±9.4 m (145±31 ft).

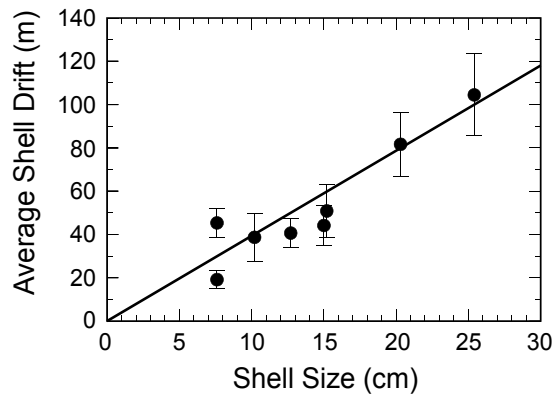


*Figure 4. Average spherical aerial shell drift distance as a function of shell size.*

Using this method, data was collected for nearly 50 groups of about 10 shells each.

## Results

### Spherical Shells, Average Drift Distance

Eight groups of spherical fireworks shells (75 shells in total) were fired during the determination of average drift distances. Table 3 and Figure 4 present the results for these measurements of drift distance for spherical aerial shells. In Figure 4, the fit to the data was accomplished by a linear least squares regression, and equals 3.8 m of drift per cm (32 ft per in.) of shell size.

### Statistical Distribution of Spherical Shell Drift Distances

Not enough aerial shells of any one size were fired to determine the nature of the statistical distribution for any individual size group. However, if it is assumed that the distributions are independent of shell size, the data from all shells fired could be used by standardizing the results for each of the groups. (This is a reasonable assumption, but not one that is assured.) To accomplish this standardization, each individual shell drift was expressed as a percent of the mean (average) for that size shell, as determined previously by a linear least squares fit of

**Table 4. Standardized Spherical Shell Drift Data by Class Interval.**

Shell Size cm (in.)		Class Intervals (Percent of Mean Drift for Each Shell Size)											
		0-25	25-50	50-75	75-100	100-125	125-150	150-175	175-200	200-225	225-250	250-275	275-300
7.6	(3)	3	2	0	2	2	1	0	0	0	0	0	0
7.6	(3)	0	0	1	3	1	0	0	2	1	1	1	0
10.2	(4)	0	5	1	0	1	1	0	0	1	0	0	1
12.7	(5)	1	1	1	3	2	1	1	0	0	0	0	0
15.2	(6)	0	3	2	2	0	0	1	0	0	0	0	0
16.2	(6)	1	1	3	1	0	0	1	1	0	0	0	0
20.3	(8)	0	1	4	2	0	0	1	1	1	1	0	0
25.4	(10)	0	1	3	1	0	2	1	0	1	0	0	0
Totals		5	14	15	14	6	5	5	4	3	2	1	1
Cum. Tot.		5	19	34	48	54	59	64	68	71	73	74	75
Cum. %		7	25	45	64	72	79	85	91	95	97	99	100

all the data. The standardized drift results for all 75 shells were then divided into twelve class intervals as shown in Table 4.

Figure 5 is a graph of the cumulative frequency of the standardized drift distances, against upper class interval limits, on a linear probability graph. The appearance of such a graph gives an indication of the nature of the statistical distribution. For example, a statistically normal distribution would appear as a straight line. Other distributions, such as log-normal, appear as curves unless plotted using a log axis. When a distribution is normal bimodal, it appears as two straight-line segments with different slopes. The distribution of aerial shell drift distances in Figure 5 has the appearance of two normal distributions, with the break

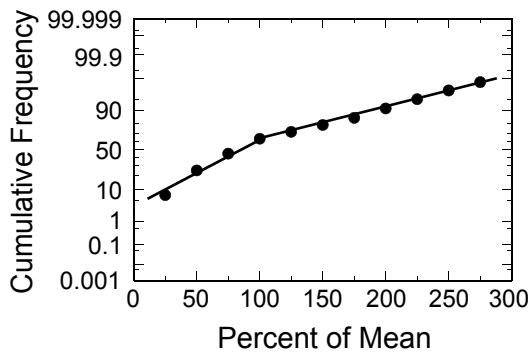


Figure 5. Cumulative frequency as a function of standardized spherical shell drift.

occurring at the average shell drift distance. Thus from Figure 5, it can be seen that nearly 65% of the time shell drifts will be less than the mean, and that shell drifts as great as about 300% of the mean will occur nearly 1% of the time. In Table 4, it can be seen that the shells with the greatest relative drifts were for 7.6-cm (3-in.) and 10.2-cm (4-in.) shells. Thus it is possible that only the smaller sized shells experience such extreme drifts. Unfortunately, the present collection of data is not sufficiently large to allow that to be established with certainty.

#### 10.2 cm (4 in.) Cylindrical Shells, Average Drift Distances

With cylindrical shells, length as well as diameter plays a role in determining drift distances. Also, shell mass and lift powder amounts can vary significantly with shell length. For this reason, the study of cylindrical shells was begun with a rather lengthy examination of the effects of shell length, shell mass, and lift amount for 10.2-cm (4-in.) shells. All of the shells used in this effort were plastic (so-called RAP™ Shells) with relatively smooth exterior surfaces, 9.2 cm (3.62 in.) in diameter, without lift-cup, and using 2F-A blasting Black Powder. Table 5 is a listing of the shell parameter values and the average drift distance for each group of ten shells fired.

**Table 5. Shell Parameter Values and Drift Distance for 10.2-cm (4-in.) Cylindrical Shells.**

Group Number	Shell Parameters							
	Shell mass		Shell Length		Lift Mass		Drift Distance	
	g	(oz)	cm	(in.)	g	(oz)	m	(ft)
1	250	(8.8)	7.6	(3.0)	25	(0.9)	10.6	(34.7)
2	250	(8.8)	7.6	(3.0)	38	(1.3)	20.2	(66.1)
3	250	(8.8)	7.6	(3.0)	50	(1.8)	27.5	(90.1)
4	250	(8.8)	7.6	(3.0)	75	(2.6)	35.2	(115.)
5	250	(8.8)	7.6	(3.0)	100	(3.5)	37.6	(123.)
6	250	(8.8)	15.2	(6.0)	38	(1.3)	7.8	(25.5)
7	250	(8.8)	15.2	(6.0)	75	(2.6)	13.6	(44.7)
8	250	(8.8)	30.5	(12.0)	38	(1.3)	9.1	(29.9)
9	250	(8.8)	30.5	(12.0)	75	(2.6)	13.0	(43.0)
10	500	(17.6)	7.6	(3.0)	25	(0.9)	3.8	(12.6)
11	500	(17.6)	7.6	(3.0)	38	(1.3)	13.3	(43.6)
12	500	(17.6)	7.6	(3.0)	50	(1.8)	11.2	(36.8)
13	500	(17.6)	7.6	(3.0)	50	(1.8)	19.5	(63.9)
14	500	(17.6)	7.6	(3.0)	50	(1.8)	17.9	(58.8)
15	500	(17.6)	7.6	(3.0)	50	(1.8)	21.4	(70.0)
16	500	(17.6)	7.6	(3.0)	50	(1.8)	17.2	(56.4)
17	500	(17.6)	7.6	(3.0)	75	(2.6)	25.4	(83.4)
18	500	(17.6)	7.6	(3.0)	100	(3.5)	32.1	(105.)
19	475	(16.8)	15.2	(6.0)	38	(1.3)	8.9	(29.4)
20	475	(16.8)	15.2	(6.0)	50	(1.8)	14.0	(46.0)
21	475	(16.8)	15.2	(6.0)	75	(2.6)	20.5	(67.4)
22	475	(16.8)	15.2	(6.0)	75	(2.6)	13.6	(44.6)
23	475	(16.8)	15.2	(6.0)	100	(3.5)	27.6	(90.5)
24	500	(17.6)	30.5	(12.0)	38	(1.3)	9.5	(31.3)
25	750	(26.5)	22.8	(9.0)	38	(1.3)	4.7	(15.4)
26	750	(26.5)	22.8	(9.0)	75	(2.6)	14.5	(47.6)
27	925	(32.6)	7.6	(3.0)	50	(1.8)	11.4	(37.4)
28	925	(32.6)	7.6	(3.0)	100	(3.5)	18.6	(61.0)
29	1000	(35.2)	15.2	(6.0)	50	(1.8)	9.0	(29.5)
30	1000	(35.2)	15.2	(6.0)	100	(3.5)	24.8	(81.6)
31	980	(34.6)	30.5	(12.0)	50	(1.8)	7.2	(23.6)
32	980	(34.6)	30.5	(12.0)	75	(2.6)	15.4	(50.5)
33	980	(34.6)	30.5	(12.0)	100	(3.5)	20.1	(66.0)

In order to determine the functional relationship between drift distance and the various shell parameters, multivariate analysis was performed.<sup>9</sup> Although 33 sets of 10 shells were fired in this test series, this is not a particularly large number considering the variability in the results and number of shell variables. Thus, it would be preferable to seek only linear relationships between drift distance and the shell variables. However, only for moderate amounts of lift powder is the relationship essentially linear; at low amounts of lift (2% or 3% of shell mass),

drift distance falls very rapidly to near zero. In order to incorporate this effect, an additional (composite) variable, incorporating both shell lift and mass, was introduced into the multivariate analysis. The regression formula fitted in the analysis was

$$D_d = a + b \cdot M_s + c \cdot L_s + d \cdot M_l + \frac{e}{(M_l - 0.03 \cdot M_s)}$$

where,

$$D_d = \text{drift distance in m (ft),}$$

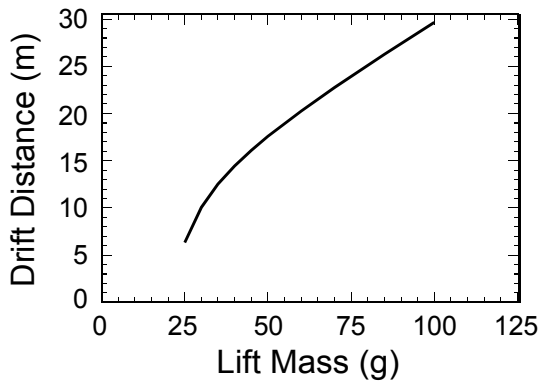


Figure 6A. Effect of varying lift powder mass for a typical 10.2 cm (4-in.) cylindrical shell.

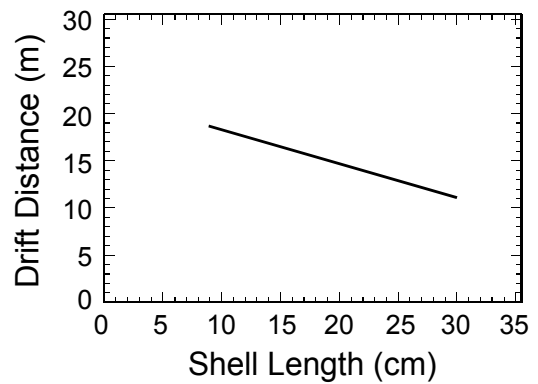


Figure 6B. Effect of varying shell length for a typical 10.2 cm (4-in.) cylindrical shell.

$M_s$  = shell mass in gm (oz),  
 $L_s$  = shell length in cm (in.),  
 $M_l$  = lift amount in gm (oz), and

a, b, c, d and e are constants.

The constants, as determined by multivariate analysis, are:

- a = 16.4 m (54 ft)
- b = -0.0075 m/gm (-0.69 ft/oz)
- c = -0.36 m/cm (-3.0 ft/in.)
- d = 0.21 m/gm (18 ft/oz)
- e = -99 m/gm (9100 ft/oz).

The correlation coefficient for the multivariate regression is 0.86, which indicates quite a good fit of the data to Equation 1. (Note that a perfect fit would have produced a correlation coefficient of 1.00.) As an indication of the uncertainty in drift distance predictions made us-

ing Equation 1, it should be noted that the average deviation between the experimental results and predicted value was 22 percent.

If it is assumed that a typical 10.2 cm (4 in.) cylindrical shell weighs 454 g (16 oz), is 8.9 cm (3.5 in.) long, and uses 54 g (1.9 oz) of lift powder, Equation 1 predicts the average drift distance to be 18.7 m (61.3 ft). As shell weight, length and lift amount are varied, the average drift distance should change as suggested by the constants b through e above. Figures 6A through 6C demonstrate the expected result of varying these shell parameters.

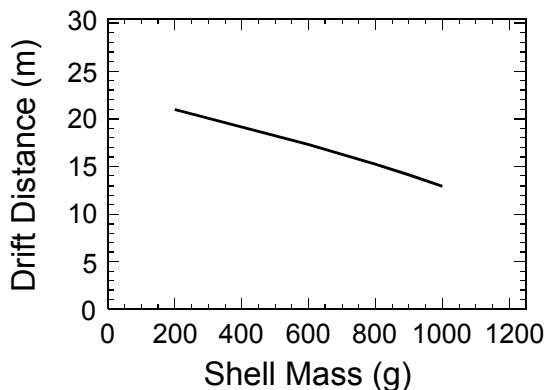


Figure 6C. Effect of varying shell mass for a typical 10.2-cm (4-in.) cylindrical shell.

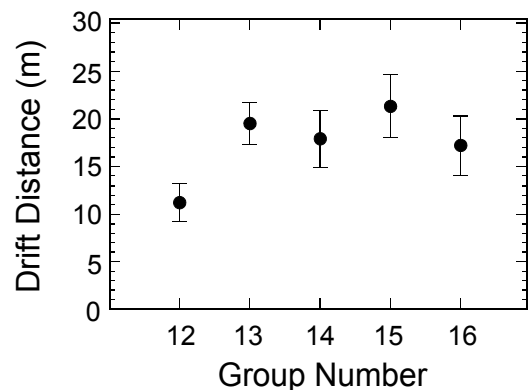


Figure 7. Reproducibility of results from five groups of ten identical 10.2-cm (4-in.) cylindrical shells.

**Table 6. Shell Parameter Values and Drift Distances for Cylindrical Shells.**

Shell Size	Shell Diameter	Shell Length	Shell Mass	Lift Mass	Drift Distance
cm (in.)	cm (in.)	cm (in.)	g (oz)	g (oz)	m (ft)
7.6 (3)	6.7 (2.62)	6.9 (2.7)	180 (6.5)	28 (1)	20 (64)
7.6 (3)	6.7 (2.62) <sup>[a]</sup>	6.9 (2.7)	180 (6.5)	28 (1)	5 (49)
10.2 (4)	9.2 (3.62) <sup>[b]</sup>	8.9 (3.5)	460 (16.)	56 (2)	190 (63)
12.7 (5)	11.4 (4.5)	10.2 (4.0)	910 (32.)	84 (3)	30 (98)
12.7 (5)	11.4 (4.5) <sup>[a]</sup>	10.2 (4.0)	910 (32.)	84 (3)	36 (120)
15.2 (6)	14.1 (5.56)	12.7 (5.0)	1800 (64.)	75 (2.7)	22 (72)
15.2 (6)	14.1 (5.56)	12.7 (5.0)	1800 (64.)	100 (3.6)	36 (120)
15.2 (6)	14.1 (5.56)	12.7 (5.0)	1800 (64.)	130 (4.5)	58 (190)
15.2 (6)	14.1 (5.56)	12.7 (5.0)	1800 (64.)	130 (4.5)	49 (160)

[a] These shells were fired from non-vertical (tilted) mortars.

[b] Typical shell parameters and calculated drift distances using Equation 1.

**Drift Distance Reproducibility**

In a brief discussion of aerial shell drift experiments, Shimizu reports<sup>12</sup> that significantly different test results were observed on different occasions. Specifically, he observed that the drift of dud shells was about twice as great on one occasion as it was on another. He speculated that a possible reason for this might have been turbulent air currents experienced on one of the days. The authors also observed a similar situation; a second set of measurements was made on 7.6-cm (3-in.) spherical shells because results from the first set were unexpectedly high. The two sets of drift distances differed by more than a factor of two. This was enough

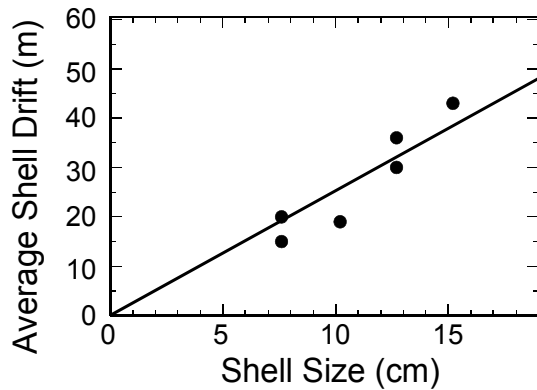


Figure 8. Average cylindrical aerial shell drift distance as a function of size.

greater than the calculated standard errors (see Figure 4), to suggest that the difference may not be the result of a random statistical occurrence. A brief attempt was made to look at this further. Five identical groups of shells, numbers 12 through 16 in Table 5, were fired on five different days. Figure 7 displays the average drift distances for these five measurements, along with their standard errors. Again there is about a factor of two in the spread of the data. However, considering the standard errors, one cannot be certain that the difference was more than a random statistical occurrence.

**Cylindrical Shells, Average Drift Distance**

In addition to the drift distance for 10.2-cm (4-in.) cylindrical shells, data was also collected for 7.6, 12.7, and 15.2-cm (3, 5, and 6-in.) shells. These too were inert shells made especially for testing. Varying shell parameters significantly affects drift distance, thus information on shell diameter, shell length, shell mass and mass of 2 F-A lift powder was included in Table 6 along with the results of drift distance measurements.

Table 6 reports results for a series of 15.2-cm (6-in.) shell tests, using varying amounts of lift powder. The observed drift distances follow a relationship similar to that shown in Figure 6A. If it is assumed that the typical amount of lift used for 15.2-cm (6-in.) cylindrical shells, with other parameters as listed in Table 6, is

**Table 7. Comparison of the Yamamoto Spherical Shell Drift Results with Those of This Study.**

Conditions	Drift Distance		This Study's Results		Difference
	m	(ft)	m	(ft)	
5 Light Shells with smoke candle attached (wind = 0.7 m/s) (size = 3 in.)	25.0	(82)	29.3	(96)	-15%
5 Heavy Shells with smoke candle attached (wind = 0.7 m/s) (size = 3 in.)	38.9	(128)	29.3	(96)	+33%
15 Heavy Shells with smoke candle attached (wind = 0.7 m/s) (size = 3 sun)	35.8	(117)	35.1	(115)	+2%
15 Light Shells with smoke candle attached (wind = 2 m/s) (size = 3 sun)	39.9	(130)	35.1	(115)	+13%
15 Heavy Shells with smoke candle attached (wind = 2.5 m/s) (size = 5 sun)	54.2	(178)	58.5	(192)	-7%

(a) Note that 1 sun = 3 cm (1.2 in.).

112 g (4 oz) then the expected drift distances will be about 43 m (140 ft). This result and the others reported in Table 6 are plotted in Figure 8, and have the appearance of a roughly linear relationship with a slope of approximately 2.4 m per cm (20 ft per in.) of shell size.

#### Comparison with the Results of Others

Approximately 30 years ago T. Shimizu, working at the request of Professor S. Yamamoto at Tokyo University<sup>6,7</sup> studied the drift of spherical aerial shells for the purpose of determining appropriate separation distances. In order to simulate typical conditions, many of the measurements were made using mortars angled to about 10° and in many cases a significant wind was blowing. In some tests, efforts were made to restrict the normal spin of the shells after firing; also the grid adjustment method used in this study was not employed. Thus although they were excellent studies, most of the data is not directly comparable with the results of this study. However, Table 7 presents the results from those cases that are the most comparable.

On average, the drift distance results of Yamamoto (Shimizu) are about 5 percent greater than those predicted from this study. Considering the differences between the two bodies of work, this is amazingly good agreement and serves to increase the authors' confidence in their results.

In 1989, E. Contestabile, at the Canadian Explosives Research Laboratory, conducted a series of aerial shell ballistics tests.<sup>8</sup> Only 15.5-cm (6-in.) shells were used. They weighed 1340 g (48 oz) and were fired from a 4-m (13-ft) long mortar using 42.5, 56.7 or 99.1 g (1.5, 2.0, or 3.5 oz) of lift powder. The shells were of an unusual geometry, having a relatively short cylindrical wall and domed ends, one end having a concave recess to contain the lift charge. Thus, it would be anticipated that the drift distances for these intermediately shaped shells might be somewhere between those reported here for spherical and cylindrical shells. The results from the Contestabile tests are listed in Table 8.

**Table 8. Contestabile Shell Drift Results.**

Lift Weight		Number of Shells Fired	Drift Distance	
g	(oz)		m	(ft)
42.5	(1.5)	7	11.8	(39)
56.7	(2.0)	7	28.2	(93)
99.2	(3.5)	12	53.5	(176)

In order to compare Contestabile's data with the results from this study, it is necessary to adjust for what would be expected for a more typical 15.2-cm (6-in.) cylindrical shell. In the present study this was considered to be a shell weighing about 1800 g (64 oz) and using 112 g

**Table 9. Effect of Mortar Tilt on Drift Distance.**

Shell		Shell Shape	Mortar Tilt Angle (°)	Drift Distance		Difference
cm	(in.)			m	(ft)	
7.6	(3)	Cyl.	0	19	(64)	- 23%
			15	15	(49)	
12.5	(5)	Cyl.	0	30	(98)	+ 21%
			10	36	(119)	
15.2	(6)	Sph.	0	44	(146)	+ 15%
			24	30	(167)	

(4.0 oz) of lift powder. Based on the effect of shell mass and lift observed for 10.2-cm (4-in.) shells, and the effect of lift mass for 15.2-cm (6-in.) shells observed in this study, the authors estimate that Contestabile would have observed a drift distance of about 46 m (150 ft) for such shell and lift mass. This compares well with the prediction from the present study of 58 m (190 ft) for spherical shells and 36 m (120 ft) for cylindrical shells, particularly when it is recalled that the Contestabile shells were expected to experience drifts somewhere between those for cylindrical and spherical shells.

**Effect of Mortar Tilt on Drift Distance**

On three occasions, groups of the same size shells were fired from both vertical and tilted mortars. This brief study was conducted to discover the approximate magnitude of any strong dependence of shell drift distance on mortar tilt angle. Table 9 lists the results of this study. Although some differences were observed, the results are not consistent. Thus it would seem that if there is a dependency of drift distance on mortar tilt angle, the effect is too small to have been observed in this brief study.

**Discussion**

In research there always seems to be more data that could (should) be collected. However, the data collected to date are probably sufficient and should be used to consider the important question of the adequacy of spectator separation distances. Unfortunately, doing that is more complex than might at first be realized. For example, it involves making assumptions about such things as:

- How accurately can a typically skilled display operator predict the ideal trajectory of aerial shells?
- How precisely can a typically skilled display operator align his mortars?
- To what extent will mortar alignment change during firing?
- How different are winds aloft likely to be than those experienced at ground level, which were considered in deciding how the mortars should be aimed?
- What percentage of dud shells falling outside the secured boundary is acceptable, recognizing that choosing 0% would probably require about 18 m per cm (150 ft per in.) of shell size?

Because of these complexities, a discussion of appropriate spectator separation distances is beyond the scope of this article. Hopefully, the authors or others will soon undertake this important task.

Another area of application for the results reported here is in statistically predicting the trajectory of aerial shells. Armed with information about drift distances, it is possible to use a relatively simple computer model to predict the average trajectory of aerial shells and then super-impose on those results the empirically determined and statistically distributed drift distances.<sup>3</sup> This has been performed in a number of cases to determine the likelihood of various accident scenarios.

**Acknowledgments**

The authors wish to acknowledge the Pyrotechnics Guild International for assisting with some of the material costs of this study.



The authors also wish to acknowledge the technical and editorial assistance of W.D. Smith and C. Jennings-White in the preparation of this article.

The authors are also indebted to T. Shimizu and E. Contestabile for making their data available.

## References

- 1) T. Shimizu, *Fireworks from a Physical Standpoint (Part III)*, Pyrotechnica Publications, 1985.
- 2) K.L. and B.J. Kosanke, "Shimizu aerial shell ballistic predictions," *PGI Bulletin*, Nos. 72 and 73, 1990 and 1991.
- 3) K.L. and B.J. Kosanke, "Computer modeling of aerial shell ballistics." Accepted for publication in *Pyrotechnica XIV*, Pyrotechnica Publications, 1992.
- 4) K.L. and B.J. Kosanke, "'Drift Effect' for spherical aerial shells," *PGI Bulletin*, No. 74, 1991.
- 5) K.L. and B.J. Kosanke, "Statistical distribution of spherical aerial shell lateral drift effects," *Proceedings of the 17th International Pyrotechnics Society Seminar*, Beijing Institute of Technology Press, 1991.
- 6) S. Yamamoto (T. Shimizu), "Studies to obtain a standard for the safety distances to avoid accidents from blind shells," Tokyo University, 1960.
- 7) S. Yamamoto (T. Shimizu), "Studies on the safety of firework shell trajectory (Studies on minimizing drift)," Tokyo University, 1962.
- 8) E. Contestabile, Canadian Explosives Research Laboratory, Unpublished data, Private Communication, 1989.
- 9) E. Contestabile, R.A. Augsten, T.R. Craig and J.G. McIndoe, "A study of the firing characteristics of high altitude display fireworks," *Proceedings of the 13th International Pyrotechnics Society Seminar*, IIT Research Institute, Chicago, 1988.
- 10) K.L. and B.J. Kosanke, "Measurement of aerial shell muzzle velocities," in preparation.
- 11) J.C. Davis, *Statistics and Data Analysis in Geology*, John Wiley & Sons, 1973.
- 12) T. Shimizu, *Fireworks, The Art, Science and Technique*, Published by T. Shimizu, 1981.

## Computer Modeling of Aerial Shell Ballistics

by K.L. and B.J. Kosanke

### **ABSTRACT**

*If one has a reasonably accurate computer model, it is usually appropriate (cheaper and faster) to rely primarily on modeled results, supplemented with limited experimental results. The case of aerial shell ballistics is no exception. The mathematical basis for such a ballistics model is derived, and the simplifications and assumptions of the model are considered. The necessary input parameters are developed and some modeling results are presented. Finally, the use of the model is demonstrated by performing a series of calculations, including the effect of mortar tilt angle and wind speed.*

### **Introduction**

A knowledge of fireworks aerial shell ballistics is of more than academic interest. It is the basis for answering several important questions dealing with fireworks displays. For example: (1) What is the appropriate mortar tilt angle to use to compensate for a given wind condition? (2) Under a given set of conditions, where in the sky will properly performing aerial shells break? (3) In the event that a shell fails to break (is a dud), where will it fall to earth? (4) For shells properly breaking at a given altitude, where will the shell debris fall to earth? (5) For a specific time delay, provided by the time fuse, how near the apogee (highest point) will the shell be when it bursts? Answering questions such as these requires information about aerial shell ballistics. The needed information can come from guesses based on experience (generally unreliable), from specific field experiments (always expensive), or from ballistics calculations (generally reliable and always inexpensive). Thus the use of ballistics calculations, guided by practical experience and occasionally

verified empirically, is the best choice for answering questions such as those posed above.

Following a general discussion of computer modeling, this paper presents a derivation of the equations used in the authors' computer modeling of aerial shell ballistics. The model is three-dimensional and includes the effects of mortar angle and wind conditions. Also presented is an empirical determination of the drag coefficient for spherical shells, information about tests of the computer model, and some results determined through its use.

### **Computer Modeling Analogy**

Before computers were available, physicists solved problems analytically. They solved complex equations using high-level mathematics and obtained exact answers. The difficulty was that only the very simplest of problems could be solved in this way. For the more interesting and complex problems, simplifying assumptions and approximations had to be made. At best this resulted in only approximate answers; and, often, even after simplifying the problems they remained unsolvable.

Now that computers are available, the whole approach to problem solving has changed. Computers do not make it easier to get analytic (exact mathematical) solutions to complex problems, but they offer a level of "brute force" arithmetic that is simply astounding. Even the most inexpensive personal computers can perform more arithmetic calculations in a few hours than a physicist could in a lifetime. This has made it practical to use a much simpler (if also less elegant) approach to problem solving; that approach is termed modeling. While computer modeling is not an exact solution to a problem, it can yield results as close to the ex-

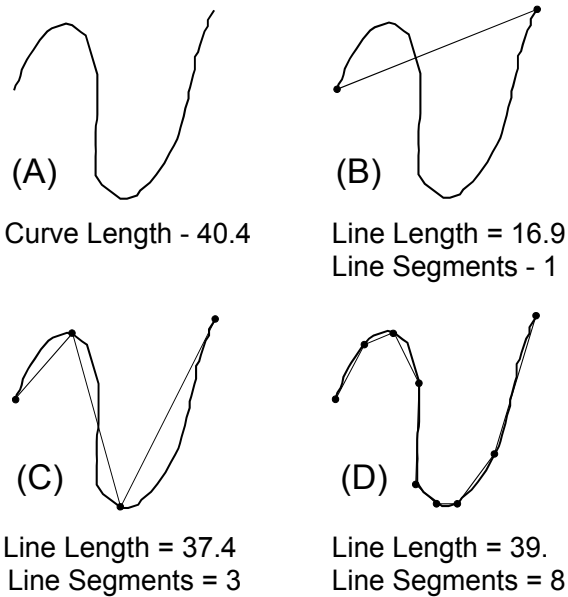


Figure 1. Determining the length of a curved line with a ruler.

act solution as necessary, provided enough computer time is used. In computer modeling there is always a trade-off between the time needed to produce an answer and the accuracy of that answer. The nature of this trade-off is illustrated in the following example.

Imagine that the problem to be solved is to determine the length of the curved line shown in Figure 1a, and the only tool available is a ruler. The easiest approach is simply to place the ruler from the start to the end and read the result (see Figure 1b). This is fast, but obviously seriously underestimates the length of the curved line. Suppose instead, that the ruler was laid along the line as shown in Figure 1c. In this case three measurements are taken and summed. This took longer but obviously produced a much better estimate of the length of the curved line. In Figure 1d this approach is carried further; here eight measurements are taken and summed. Again more time was taken, but now a good estimate of the length of the curved line has resulted. If it were only necessary to know the length to within a few percent, then this would be sufficient. If still greater accuracy is needed, all that would be required is to measure even more individual segments. Theoretically, no matter how much accuracy is needed, greater and greater numbers of line

segments could be measured until their total yielded an answer with the required accuracy; the only limitation is the amount of time available for the measurements.

The above example illustrates how this same problem might be solved on a computer. Problems are broken into very many small steps and solved in a brute force fashion. It is not elegant, but it works, and it allows solutions to many problems that cannot be solved analytically.

When complex problems are solved using computers by dividing the problem into smaller and smaller parts, it is important to know when the individual parts are small enough. The above example also illustrates how this is done. Consider the change upon increasing from using one line segment to using three line segments. In this case the estimate of length increased considerably, about 120%. Now consider the change upon increasing from using three to eight line segments. This time the estimate of length only increased slightly, approximately 5%. In computer modeling, when calculated results change very little as the problem is broken into ever smaller parts, the modeled result is generally very close to the exact solution.

## Computer Modeling of Aerial Shell Ballistics

Problems in classical mechanics, such as aerial shell ballistics, are well suited to computer modeling and excellent results can be attained. In general, this type of problem can be stated as: given the force laws operating, determine the acceleration of the object; from that and initial conditions for position and velocity determine its path. In a computer model of aerial shell ballistics this is accomplished as a repeating series of steps:

- 1) Start at the muzzle of the mortar with the shell having its initial (muzzle) velocity ( $v$ ).
- 2) Choose the small time interval ( $\Delta t$ ) to be used.
- 3) Calculate the force ( $F$ ) acting on the shell at the start of the time interval.

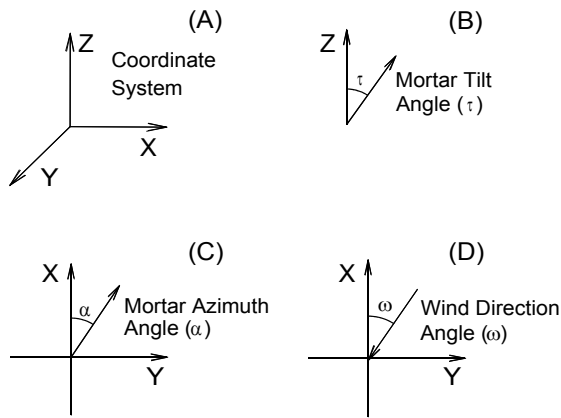


Figure 2. Coordinate system with mortar tilt angle ( $\tau$ ), mortar azimuth angle ( $\alpha$ ), and wind direction angle ( $\omega$ ) defined.

- 4) Using Newton's Second Law of Motion ( $\mathbf{F}=\mathbf{ma}$ ), calculate the acceleration ( $\mathbf{a}$ ) of the shell during that time interval.
- 5) Calculate the change in velocity ( $\Delta\mathbf{v} = \mathbf{a}\Delta t$ ), and the average velocity ( $\bar{\mathbf{v}} = \mathbf{v} + \frac{1}{2}\Delta\mathbf{v}$ ) of the shell.
- 6) Calculate the change in shell position ( $\Delta\mathbf{r} = \bar{\mathbf{v}}\Delta t$ ).
- 7) The velocity and position for the shell at the end of the time interval are  $\mathbf{v} + \Delta\mathbf{v}$  and  $\mathbf{r} + \Delta\mathbf{r}$ , and the time is now  $t + \Delta t$ .
- 8) Unless the shell has returned to the ground, return to step 3 and continue the calculations using the new values from step 7.

Following this procedure the aerial shell is stepped along its trajectory until it returns to the ground. In the limit as  $\Delta t$  approaches zero, the modeled trajectory is exactly equal to the actual trajectory of the shell. Of course, this means there would be an infinite number of steps along the trajectory, which would require an infinite time to run on a computer. As a practical matter, when  $\Delta t$  is set to 0.01 second, the errors in the modeled results are vanishingly small in comparison to errors resulting from uncertainties in initial conditions such as muzzle velocity, wind speed and direction, mortar tilt and direction, air mass density, and the shell's drag coefficient.

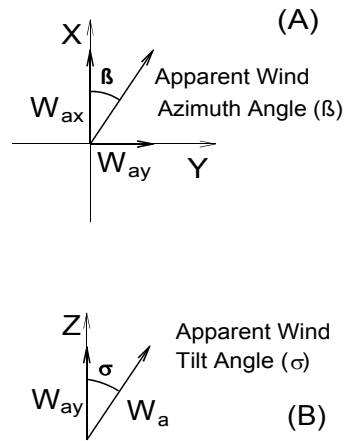


Figure 3. Apparent wind azimuth angle ( $\beta$ ) and apparent wind tilt angle ( $\sigma$ ) defined.

In the above steps, two types of variables are used, scalars such as  $t$  (shown in normal typeface), and vectors such as  $\mathbf{F}$ ,  $\mathbf{a}$ ,  $\mathbf{v}$ , and  $\mathbf{r}$  (shown in bold italic typeface). It is important to understand the difference between the two types of variables. Time ( $t$ ) is a scalar because, while it has magnitude, it does not have a direction in three-dimensional space. Similarly, speed ( $v$ ) is a scalar quantity because it is used without reference to direction. On the other hand, velocity ( $\mathbf{v}$ ) is a vector because it has both magnitude and direction. (The concept of scalars and vectors is not an easy one to grasp. If the reader does not have experience with these, it may become clearer in the next section of this paper. If after completing this paper, the reader wishes more information about scalar and vector quantities and how they are used mathematically, a college physics text should be consulted.)

### Derivation of the Computer Model Equations

Readers wishing to be spared the tedium of the derivation should skip to the next section. Before beginning the actual derivation of the computer model equations, it is first necessary to define some parameters and lay some additional groundwork.

- A) The model uses Cartesian coordinates, with the mortar located at the origin, and the Z-direction corresponds to the height, see Figure 2A.

B) The placement of the mortar is defined by two angles, tilt ( $\tau$ ) and azimuth ( $\alpha$ ).

- 1) The tilt angle is measured in degrees from vertical (the Z-axis) i.e.,  $\tau = 0^\circ$  corresponds to vertical mortar placement, see Figure 2B.
- 2) The azimuth is the mortar angle projected onto the X–Y plane, measured from the X-axis, with clockwise rotation corresponding to positive angles, see Figure 2C. For example, a mortar tilted in the X-direction has  $\alpha = 0^\circ$ , and a mortar tilted in the Y-direction has  $\alpha = 90^\circ$ .

C) It is assumed that the wind has no vertical component. Thus only one angle is needed for its direction. The wind direction ( $\omega$ ) is the direction of the origin of the wind, measured from the X-axis, with clockwise rotation corresponding to positive angles. For example, a wind coming from the X-direction has  $\omega = 0^\circ$ , and a wind coming from the minus Y-direction has  $\omega = 270^\circ$ .

D) The model uses metric units internally, but all input and output are converted to English units for convenience.

As the aerial shell emerges from the mortar, it is acted on by a net force ( $F_s$ ), which is the sum of two forces, gravity ( $F_g$ ) and the aerodynamic drag ( $F_d$ ):

$$F_s = F_g + F_d \quad (1)$$

The gravitational force (or weight) is simply

$$F_g = m g, \quad (2)$$

where  $m$  is the mass of the shell in kilograms, and  $g$  is the acceleration due to gravity (9.8 meters per second<sup>2</sup>).

The magnitude of the aerodynamic drag force is<sup>1,2</sup>

$$F_d = \frac{1}{2} C_d \rho_m S v_a^2, \quad (3)$$

where  $C_d$  is the drag coefficient for the shell (a dimensionless constant which must be determined empirically),  $\rho_m$  is the mass density of air (1.28 kg/m<sup>3</sup> at sea level),  $S$  is the projected area of the shell, and  $v_a$  is the relative speed of the air past the shell.

Converting Equation 3 into vector notation

$$F_d = \frac{1}{2} C_d \rho_m S \mathbf{u}_a v_a^2, \quad (4)$$

where  $\mathbf{u}_a$  is the air velocity unit vector (which has the same direction as  $\mathbf{v}_a$ ).

The air flowing past an aerial shell ( $\mathbf{v}_a$ ), arises in part from the wind  $W$ , but more significantly from the motion of the shell itself. The component of air velocity resulting from the shell's motion is equal in magnitude to the velocity of the shell  $\mathbf{v}_s$  but opposite in direction. Thus,

$$\mathbf{v}_a = W - \mathbf{v}_s. \quad (5)$$

By substitution of Equations 2 and 4 into Equation 1, the force acting on the aerial shell is

$$F_s = m g + \frac{1}{2} C_d \rho_m S \mathbf{u}_a v_a^2. \quad (6)$$

Using Newton's Second Law of Motion ( $F = m\mathbf{a}$ ), the resulting acceleration of the shell  $\mathbf{a}_s$  is

$$\mathbf{a}_s = \mathbf{g} + K \mathbf{u}_a v_a^2, \quad (7)$$

where the constant  $K$  has been substituted for the quantity ( $\frac{1}{2} C_d \rho_m S/m$ ).

From general physics,  $\Delta \mathbf{v} = \mathbf{a} \Delta t$ , where  $\Delta \mathbf{v}$  is the change in velocity produced by constant acceleration. Thus the change in shell velocity  $\Delta \mathbf{v}_s$  occurring during the short time interval  $\Delta t$  is

$$\Delta \mathbf{v}_s = \mathbf{g} \Delta t + K \mathbf{u}_a v_a^2 \Delta t. \quad (8)$$

For constant acceleration, the average shell velocity  $\bar{\mathbf{v}}_s$ , during the time interval  $\Delta t$ , is simply

$$\bar{\mathbf{v}}_s = \mathbf{v}_s + \frac{1}{2} \Delta \mathbf{v}_s, \quad (9)$$

where  $\mathbf{v}_s$  is the shell velocity at the start of the time interval.

At the start of the first time interval, shell velocity  $\mathbf{v}_s$  is the muzzle velocity. For all subsequent time intervals, the starting shell velocity is simply the starting shell velocity for the previous interval plus the change in shell velocity  $\Delta \mathbf{v}_s$  (Equation 8) occurring during that previous time interval.

Again from general physics,  $\Delta \mathbf{r} = \bar{\mathbf{v}} \Delta t$ , where  $\Delta \mathbf{r}$  is the change in position. Thus, the change in shell position  $\Delta \mathbf{r}_s$  occurring during the short time interval is

$$\Delta \mathbf{r}_s = \bar{\mathbf{v}}_s \Delta t. \quad (10)$$

At the start of the first time interval, the shell position is at the mortar muzzle, which is the origin for the coordinate system. For all subsequent time intervals, starting shell position is simply the starting shell position for the previous interval plus the change in position  $\Delta \mathbf{r}_s$  (Equation 10) occurring in the previous time interval.

The next (and most tedious) step in deriving the equations for the model is to resolve Equations 8 and 10, which contain vector quantities, into sets of three equations containing only scalar variables. In the coordinate system defined above, any of the vector quantities can be resolved into three component vectors, one along each axis. For example, the shell's vector velocity can be expressed as

$$\mathbf{v}_s = \mathbf{v}_{sx} + \mathbf{v}_{sy} + \mathbf{v}_{sz}. \quad (11)$$

Further, each of the three component vectors can be expressed as the product of its scalar magnitude and a unit vector  $\mathbf{u}$  along the axis,

$$\mathbf{v}_s = v_{sx} \mathbf{u}_x + v_{sy} \mathbf{u}_y + v_{sz} \mathbf{u}_z. \quad (12)$$

At time zero, when the shell has just exited the mortar, its velocity will be the muzzle velocity. Using basic trigonometric relationships, the magnitudes of the three initial velocity components are:

$$v_{sz} = v_m \cos(\tau), \quad (13)$$

$$v_{sx} = v_m \sin(\tau) \cos(\alpha), \text{ and} \quad (14)$$

$$v_{sy} = v_m \sin(\tau) \sin(\alpha), \quad (15)$$

where  $v_m$  is the scalar muzzle velocity of the shell.

Using basic trigonometric relationships, and recalling that it is assumed that there is no Z-component, the three components for the true wind  $W$  are:

$$W_z = 0, \quad (16)$$

$$W_x = -W \cos(\omega), \text{ and} \quad (17)$$

$$W_y = -W \sin(\omega), \quad (18)$$

where  $W$  is the scalar true wind velocity, and the minus sign converts the direction for the origin of the wind to the direction toward which the wind is blowing.

Thus using Equation 5 and the above equations, the magnitudes of the three components of the air velocity are:

$$v_{az} = -v_{sz}, \quad (19)$$

$$v_{ax} = [-W \cos(\omega)] - v_{sx}, \text{ and} \quad (20)$$

$$v_{ay} = [-W \sin(\omega)] - v_{sy}. \quad (21)$$

To calculate the change in shell velocity using Equation 8, the magnitude of the air velocity is also needed, which by combining its components, is:

$$v_a = [v_{ax}^2 + v_{ay}^2 + v_{az}^2]^{1/2}. \quad (22)$$

To resolve  $\mathbf{u}_a$  into its components along the coordinate axes, it is necessary to determine its tilt angle  $\sigma$  and azimuth angle  $\beta$ , see Figure 3. Using basic trigonometric relationships:

$$\sigma = \cos^{-1}(v_{az}/v_a), \text{ and} \quad (23)$$

$$\beta = \tan^{-1}(v_{ay}/v_{ax}). \quad (24)$$

Then, again using basic trigonometric relationships, the magnitudes of the projections of  $\mathbf{u}_a$  are:

$$u_{ax} = \sin(\sigma) \cos(\beta), \quad (25)$$

$$u_{ay} = \sin(\sigma) \sin(\beta), \text{ and} \quad (26)$$

$$u_{az} = \cos(\sigma). \quad (27)$$

The set of model equations for velocity change during the time interval  $\Delta t$ , result from substitution of the above equations into Equation 8 and recalling that the only non-zero component of  $\mathbf{g}$  is  $\mathbf{g}_z$  which is in the minus Z-direction:

$$\Delta v_{sx} = K v_a^2 \sin(\sigma) \cos(\beta) \Delta t, \quad (28)$$

$$\Delta v_{sy} = K v_a^2 \sin(\sigma) \sin(\beta) \Delta t, \text{ and} \quad (29)$$

$$\Delta v_{sz} = -\mathbf{g}_z \Delta t + K v_a^2 \cos(\sigma) \Delta t. \quad (30)$$

The set of model equations for position change during the same time interval is just Equation 10 resolved into its components:

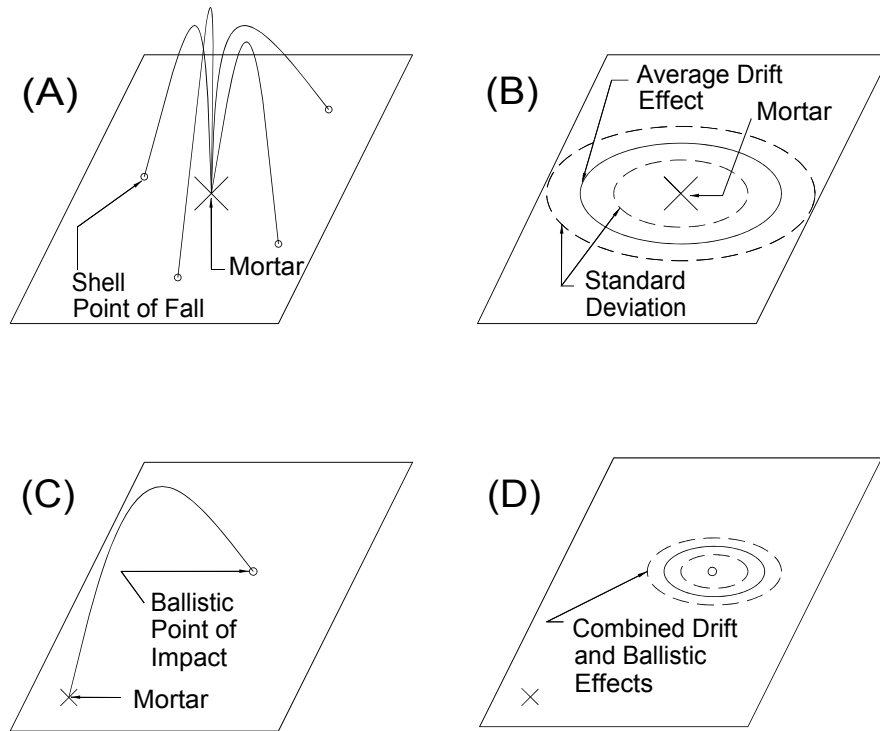


Figure 4. Inclusion of drift effects into ballistic results from a model.

$$\Delta r_{sx} = (v_{sx} + \frac{1}{2} \Delta v_{sx}) \Delta t, \quad (31)$$

$$\Delta r_{sy} = (v_{sy} + \frac{1}{2} \Delta v_{sy}) \Delta t, \text{ and} \quad (32)$$

$$\Delta r_{sz} = (v_{sz} + \frac{1}{2} \Delta v_{sz}) \Delta t. \quad (33)$$

In Equations 19 through 21 and 31 through 33, the  $v_s$  terms are the shell velocity components at the start of the time interval. During the very first time interval, these values are calculated using the muzzle velocity and Equations 13 through 15. Subsequently, they are just the velocity components after the previous time interval.

The authors have not included a copy of their computer program in this paper because it is considered proprietary. However, using Equations 28 through 33 and following the procedural steps for the model listed in the previous section, it is a relatively simple matter to write a computer program to implement the model.

### Model Simplifications and Assumptions

As aerial shells are propelled from a mortar, they almost always begin to tumble (spin), sometimes a little, sometimes a lot. The magnitude of the tumbling is impossible to predict; also unpredictable is the orientation of the spinning. The effect of shell spinning is similar to a curve-ball pitch in baseball; it will deviate from its ballistically predicted path. In addition, there are other factors that also contribute to an aerial shell “drifting” away from its ballistically predicted path. Because the magnitude and orientation of these “drift effects” cannot be known in advance, it is not possible to include the drift effect into the model without first determining the probability of various drifts occurring and then using so-called Monte Carlo techniques in the computer model. (A discussion of Monte Carlo modeling techniques is beyond the scope of this article. Suffice it to say that: it is a method by which effects that are only knowable on a statistical level can be in-

corporated into a computer model; a factor of about 100 more computer time is required for the calculations; and those modeled results are not absolute but only statistical in nature. Readers wishing more information on Monte Carlo techniques are referred to a university level text on numerical analysis.) Fortunately, there is an easier and faster way to include drift effects into computer modeled results. Many physics problems, which are difficult to solve, can be made easier by separating the problem into parts, finding answers for each part, and then combining the parts to get the overall solution. This method was attempted by the authors.

The method by which drift effects are included in the ballistic results from the model is illustrated in Figure 4. First, (Figure 4A) a series of dud aerial shells of a given shape and size are fired into the air. The shells were rendered duds by having water injected into their time fuses. The locations at which the shells fall to the ground are recorded. From this information, statistical parameters (the average distance of the points-of-fall from the mortar and the standard deviation about the average) are calculated (Figure 4B). Next, (Figure 4C) the ballistics model is used to predict the trajectory of a non-drifting shell. Finally, (Figure 4D) drift effects are added to the ballistic result, predicting the center of probable points-of-fall, how far from the center an average shell will fall, and the statistical distribution of points-of-fall about the average.

When complex problems can be separated into parts, solved separately, and then successfully recombined to give accurate results, they are said to be linear. While it is unlikely that the drifting aerial shell problem is absolutely linear, tests such as one described later in this article, indicate that the effects of any non-linearity in this problem are small enough to be safely ignored.

Another simplifying assumption (presently being made) is that the aerodynamic drag coefficient ( $C_d$ ) for the aerial shell is constant, independent of air velocity. This is certainly not true. At the high speed of a typical aerial shell as it leaves the mortar, the airflow around the shell will be turbulent. Whereas, near the apex of its trajectory, when the speed of the shell is low, the airflow will be nearly laminar. The

drag coefficients for these two cases are significantly different. In the present model, an average value for the drag coefficient, or what might be called an effective drag coefficient, is used. This works well, providing the conditions being modeled and those operating when the effective drag coefficient was determined are similar regarding the magnitude of air velocity. Fortunately, such close similarity exists for most of the situations of interest in aerial shell ballistics modeling. (In the event that cases for study required a velocity-dependent drag coefficient that upgrade to the model can easily be made.)

Finally, the model assumes the true wind is constant, independent of height above the ground and unchanging over the time-of-flight of the aerial shell being modeled. Rarely is this ever the case, and it would be a simple matter to include such effects into the model. However, this was not done for two reasons: wind effects on an intact aerial shell are relatively small in comparison with other effects such as mortar angle; and, more importantly, one essentially never has even crude information regarding wind conditions aloft.

For this model, the above simplifying assumptions will occasionally introduce errors into the results. However, uncertainties in other parameters, such as muzzle velocity for an individual shell can introduce significantly larger errors. Thus the simplifying assumptions are appropriate.

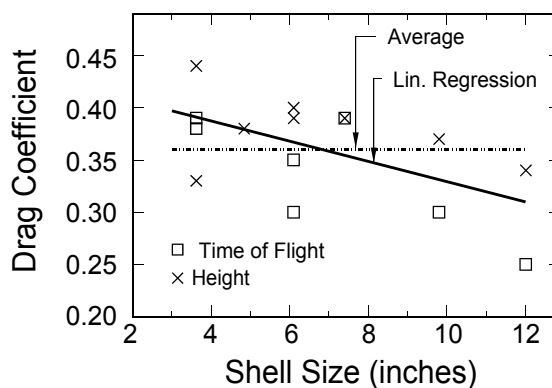


Figure 5. Drag coefficients for spherical aerial shells.



## Determination of Aerial Shell Drift Effects

The determination of drift effects of aerial shells is underway. Drift effects for spherical shells from three-inch to ten-inch have been determined.<sup>3</sup> For spherical shells fired from vertical mortars with no wind, the drift effect would cause them to fall at an average of 32 feet away from the mortar for each inch of shell size. Thus, on average, a three-inch dud shell would fall approximately 100 feet from the point-of-fall predicted for a non-drifting shell. Finally, the coefficient of variation of the distribution of the points-of-fall averages 42% for fall points below the mean and 97% for fall points above the mean.<sup>34</sup> (Note: the coefficient of variation is standard deviation expressed as a percentage of the mean.) As further studies are completed, their results will be reported.

## Determination of Aerial Shell Drag Coefficients

The drag coefficient for spherical aerial shells was determined empirically using T. Shimizu's published shell performance data in.<sup>35</sup> Using Shimizu's values for muzzle velocity, mass, and projected area, the drag coefficient of the model was adjusted until there was agreement with Shimizu's measurements of shell apogee and then flight time to impact. In this way 15 drag coefficients were determined. These results are plotted in Figure 5. (Note that Japanese shell sizes are measured in "suns," with 1 sun = 1.19 inches, and is the reason the shell sizes are not integer inches. Also, it should be noted that Shimizu occasionally reported two sets of results for the same size shell; this corresponds to normal and low mass shells.) There is a fair amount of scatter in the drag coefficient data in Figure 5. This makes it difficult to determine whether the drag coefficients for spherical shells are a function of shell size. When a linear least squares fit was attempted with the data, the correlation coefficient was -0.69, suggesting only a moderate degree of correlation between drag coefficient and shell size. (A full discussion of correlation coefficients is beyond the scope of this article. Suffice it to say that correlation coefficients range from -1 to 0

to +1 with: -1 indicating a perfect inverse correlation, 0 indicating absolutely no correlation, +1 indicating a perfect direct correlation, and values between suggesting correlations with varying degrees of certainty.) Table 1 lists drag coefficients as a function of shell size, as determined using the slope and intercept from the least squares fit.

**Table 1. Spherical Aerial Shell Drag Coefficient as a Function of Shell Size.**

Aerial Shell Size (inches)	Drag Coefficient
3	0.397
4	0.387
5	0.377
6	0.368
8	0.348
10	0.329
12	0.310
Average of all Data Points = 0.359	

As a check on the appropriateness of these drag coefficients, they were used in an attempt to reproduce Shimizu's measured times to apogee and heights of apogee. Note that this should work well because this is the same data that was originally used in determining the drag coefficients. It was found that the average deviations between modeled and measured times to apogee and heights of apogee were 0.1 second and 39 feet, respectively. As a point of reference, when Shimizu's outer ballistics equations (Shimizu, 1985, Section 12.3) were used with the same data, the average deviations between calculated and measured times to apogee and heights of apogee were 0.6 seconds and 48 feet, respectively. Thus, at least with the Shimizu data, the above drag coefficients work well.

Because the degree of correlation between shell size and drag coefficient was not particularly good, it was decided to investigate whether the use of a single average drag coefficient would result in a significant increase in average deviations reported above. When a coefficient of 0.36 was used, the average deviations between modeled and measured times to apogee and heights of apogee were 0.3 second and 34 feet, respectively. This corresponds to a moderate worsening of average deviation in

times to apogee and a slight improvement in the deviation of heights of apogee. While these results are not quite as good as when shell size dependent drag coefficients were used, they are not so bad as to reject the use of an average drag coefficient independent of spherical shell size. The limited results given herein as examples were produced using 0.36 as the drag coefficient.

Drag coefficients for cylindrical shells could be determined in much the same way as above, providing one has access to similar empirical data. Unfortunately, the authors are not aware of any such data. The situation is further complicated because the average drag coefficient for cylindrical shells will be a function of the shell's aspect ratio (ratio of the shell's length to diameter), and shell aspect ratios vary significantly between different types of shells. At the time of submission of this article, the authors have just started work to determine drag coefficients for cylindrical shells.

### Determination of Optimum Time Interval for Model Iterations

In the computer modeling analogy at the beginning of this article, it was demonstrated that as the problem is broken into ever-smaller steps (iterations), the modeled result approaches the true (analytic) solution to the problem. It was also demonstrated that the law of diminishing returns plays an important role, and that there soon comes a point where the gains resulting from ever smaller steps becomes insignificant, especially when considering the added time necessary to achieve those slight improvements. Thus, one way to establish when the problem has been broken into small enough steps is to observe the results as one uses ever-smaller steps.

In this computer model, the iteration interval (step size) is a time interval. To establish the optimum time interval the following problem (from Shimizu's data) was considered:

- Shell Muzzle Velocity = 390 feet/second,
- Shell Size = 6.85 inches,
- Shell Weight = 4.65 pounds,
- Mortar Tilt Angle = 0°,

- Wind Speed = 0 miles/hour,
- Drag Coefficient = 0.36, and
- Elevation Above Sea-Level ≈ 0 feet.

Table 2 lists the results of a series of modeled results using ever-shorter time intervals.

**Table 2. Modeled Results for Various Iteration Time Intervals.**

Time Interval (seconds)	Time to Apogee (seconds)	Apogee Height (feet)	Time to Impact (seconds)
1.0	5.8	775	13.4
0.1	6.71	949	15.43
0.01	6.78	965	15.60
0.001	6.79	966	15.62

Only an insignificant change resulted from reducing the time interval by the factor of ten from 0.01 to 0.001 second. Using 0.001 second as the time interval, the computer program required nearly 27 minutes to run, whereas when the time interval was 0.01 second it required only a little more than 2.5 minutes. (Note that these times are for a 286 CPU, IBM-compatible computer without a math co-processor.) Obviously time intervals of 0.01 second are optimum in terms of run time and accuracy. In the modeling results reported in the remainder of this article, 0.01 second was used as the time interval.

### Model Testing

In those imaginary cases when aerodynamic drag is zero, the problem of aerial shell ballistics becomes so simple that it is possible to calculate exact mathematical solutions. Thus the first test of the model was to verify that it successfully reproduced those analytic results. For example, with  $C_d = 0$ , for any projectile (independent of mass or projected area) fired vertically into the air, from general physics it is known that:

$$t_a = v_m / g, \quad (34)$$

where  $t_a$  is the time to apogee;  $v_m$  is muzzle velocity, and  $g$  is the acceleration due to gravity.

$$Z_a = v_m^2 / 2 g, \quad (35)$$

where  $Z_a$  is the height of apogee;

$$t_i = 2 t_a, \quad (36)$$

where  $t_i$  is the time to impact; and

$$v_i = -v_m, \quad (37)$$

where  $v_i$  is the velocity on impact.

When results were computed, there was exact agreement between modeled results and Equations 34 through 37.

The next series of tests confirmed that individual model calculations were in exact agreement with hand-generated results. In this manner, each section of the computer program was tested and verified to have properly implemented the model equations when non-zero drag coefficients were used.

Tests were also conducted to evaluate the “reasonableness” of computer-modeled results. For example, checks were made to verify that the effects of wind on an aerial shell fired vertically are consistent with the shell’s speed, i.e., are greatest just after the shell leaves the mortar, then decrease until the shell reaches its apogee where the effects begin to increase again until the shell returns to the ground. The model successfully passed this series of tests.

The final and most definitive test was whether the model successfully reproduced results from field tests with real shells. This test also established that shell drift effects can be treated separately from ballistic results, i.e., that the problem is linear. The first set of results was for six-inch spherical shells. In this test, the mortar was angled to 24.5°, the azimuth was approximately south, and surface winds were ≤ 2 mph. Eight shells weighing an average of 39.4 ounces were fired. Their average flight time was 12.5 seconds and their average point-of-fall was 850 feet down range.

To determine the ballistic trajectory for these shells using the computer model, it was necessary to input a value for the shell’s muzzle velocity. Average muzzle velocity was determined using the times of flight of the six-inch aerial shells fired previously when measuring

shell drift effects. In this manner, an average muzzle velocity of 320 feet per second was established. Using this muzzle velocity and the measured average shell weight, the computer model predicted the average point of impact would be 825 feet down range. This level of agreement (within 3%) is exceptionally good considering the uncertainty in winds aloft and actual muzzle velocities.

When the distribution in the points of fall were considered, it was found that the average drift effect for shells propelled down range was 167 feet with a standard deviation of 113 feet. This is in comparison with<sup>4</sup> 192 and 117-feet for the mean and standard deviation found in the previously reported study of spherical aerial shell drift effects. Considering the uncertainty in the reported results, the agreement between the two drift effect determinations is also exceptionally good.

Upon consideration of the above results and other similar tests, two conclusions were reached. The first is that the aerial shell ballistics problem is very nearly linear, and the other is that the model works well in predicting the average ballistic path of spherical aerial shells.

### Sample Aerial Shell Ballistics Modeling Results

While it is not the purpose of this article to present an extensive series of modeled results, a few cases will be presented as examples of how the model can be of use.

One simple application of the model is the examination of trajectory parameters for spherical aerial shells for various mortar tilt angles. The modeled results to follow are for the conditions:

- Muzzle velocity = 320 feet per second,
- Shell diameter = 5.62 inches,
- Shell weight = 2.5 pounds,
- Wind speed = 0 miles per hour,
- Sea level drag coefficient = 0.36, and
- Elevation above sea level = 1,000 feet.

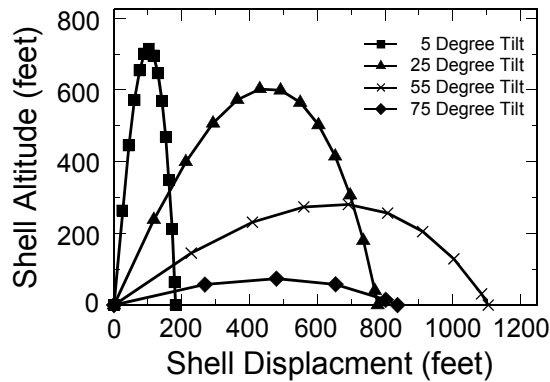


Figure 6. Ballistically predicted trajectories for shells fired from tilted mortars.

Figure 6 illustrates the ballistically predicted trajectories for shells fired from mortars with tilt angles of 5°, 25°, 55°, and 75° from vertical and azimuths of 0°. The various curves are plotted in the X-Z plane and thus form scaled representatives of the actual trajectories. The points shown on each curve are the locations of the shells for each second in time elapsed since firing. Thus, the distance between points is an indication of relative shell velocity. (Note, however, that in each case the final time interval just before impact is not a full second.)

The curve for a 5° mortar tilt can be used to make a point about proper timing of bursts of aerial shells. Notice that the shell spends about four seconds traveling up and down only 70 feet about its apogee. Throughout this period of four seconds, the shell is traveling slowly, and the symmetry of its burst any time during this period would not be distorted by the shell's velocity. Some manufacturers feel that the optimum timing of a shell's burst is just after it reaches its apogee, which means the shell is already starting to come down. If the shell had lost some lift powder or there was a brief hang fire in the time fuse, such a shell could be dangerously close to the ground at the time of its burst. Obviously a more appropriate time (just as effective but safer) for the shell burst would be one (or even two) seconds before the shell reaches its apogee.

Figures 7 and 8 graphically present a collection of ballistic trajectory parameters for typical six-inch spherical aerial shells as a function of mortar tilt angle. Those parameters are apogee

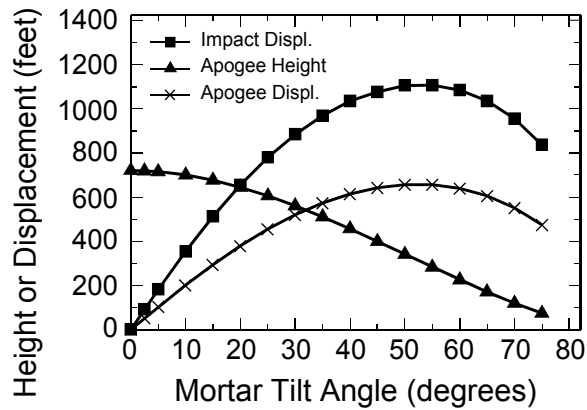


Figure 7. Ballistic trajectory parameters for 6" spherical aerial shells as a function of mortar tilt angle.

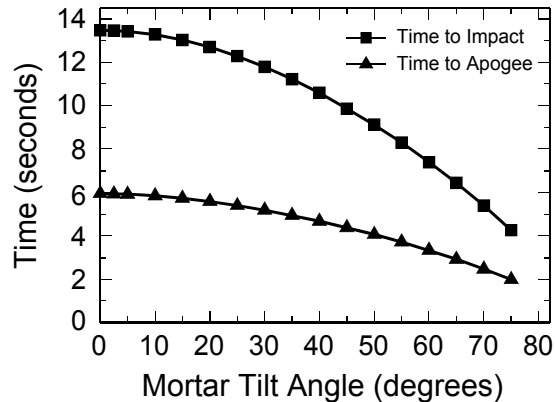


Figure 8. Ballistic trajectory parameters for 6" spherical aerial shells as a function of mortar tilt angle.

height, apogee displacement (the distance the shell has traveled down range at the time it reaches its apogee), impact point displacement (assuming the shell has not already burst), time to apogee, and time to impact. Besides demonstrating a capability of the modeling program, these graphs predict the effect of angled mortars on the location of normal shell bursts and the point where duds could fall. It is perhaps of some interest to note that the greatest impact point displacement is just over 1,100 feet (not considering drift effects) and occurs for a mortar tilt angle of approximately 53°, not at 45° as is often assumed. The reason for this is a result of drag force being proportional to velocity

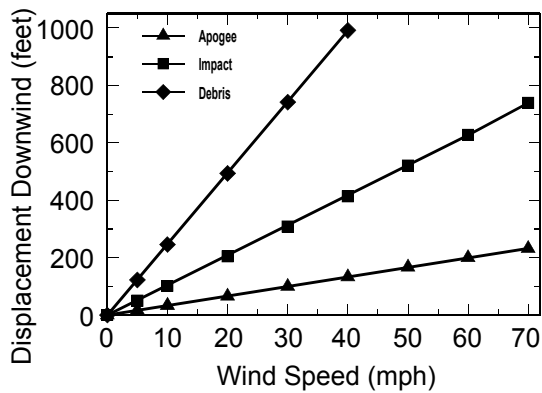


Figure 9. Displacement of 6" spherical aerial shell in wind.

squared (see Equation 3), and the trajectory not being symmetric about the apogee.

Another aspect of fireworks displays that is of considerable interest is the effect of wind on the trajectory of aerial shells and the debris created at the time of their bursts. Figure 9 graphs the displacement of typical six-inch spherical shells and their debris downwind as the result of varying wind conditions. Three sets of values are plotted, shell displacement at the time of apogee, shell displacement at the time of impact for a dud shell, and, for a normally functioning shell, debris displacement at the time the debris falls to the ground. In calculating the debris trajectory, after the shell reaches its apogee, new values for projectile mass, projected area, and drag coefficient are used by the computer-modeling program. Obviously, when a shell breaks the debris will have a great range of values for these three parameters, thus not all debris will fall at the same point. In addition, the debris will have a great range of velocities resulting from the exploding shell. Thus, the calculation of landing points for debris should be seen as only the very approximate center of the distribution. Nonetheless, it is instructive to consider the expected fallout point for debris, when examining the difficulty in performing a display in even moderate winds. In an attempt to be conservative with respect to the range of debris fallout, it was decided to track one of the most dense pieces of debris that would be expected. In these calculations the piece of debris has a mass equal to 3% of the shell, a projected area equal to 15% of the shell, and a drag coef-

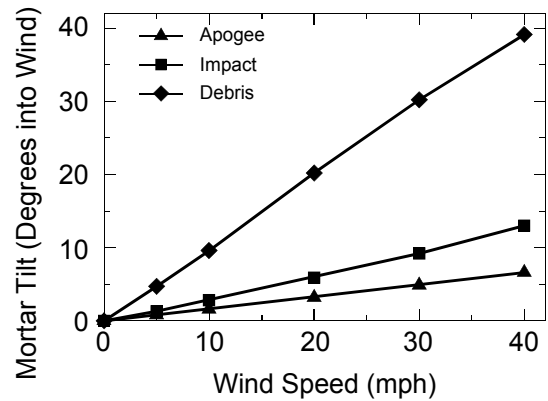


Figure 10. Amount of mortar tilt to correct for wind displacement.

ficient equal to 3 times that of the shell. Figure 9 shows that the effects of wind on a shell's displacement at apogee are relatively minor; the effect on a dud shell's impact point is more significant; and the effect on a dense piece of debris is very substantial. (Note that while graphs in Figure 9 appear as straight lines, they are actually curving slightly.)

Information concerning the amount of mortar tilt needed to correct for the wind displacement effects is shown in Figure 10. The amount of mortar tilt indicated in Figure 10 for correction of shell apogee may be less than common experience might suggest. The reason for this is that the wind speed sensed by a display operator is the speed very near the ground. Because of obstructions to the wind (trees, buildings, people, etc.) the wind speed within five feet of the ground will usually be only a fraction of that above the obstructions. Perhaps a very crude rule of thumb is that the wind at chest height is only half of what it is at 50 feet. This underestimation of true wind speed makes it appear that the wind effect on a shell's displacement is somewhat greater than it actually is.

The really important information in Figure 10 is that except for the trivial case of zero wind, there is no one mortar tilt angle that will completely correct for both the displacement of the a dud shell on impact and the point-of-fallout for dense debris. Figure 11 illustrates the ballistic trajectory for the case of a six-inch shell fired from a mortar tilted  $6.6^\circ$  into a 40 mph wind. This is the case where the mortar has suf-

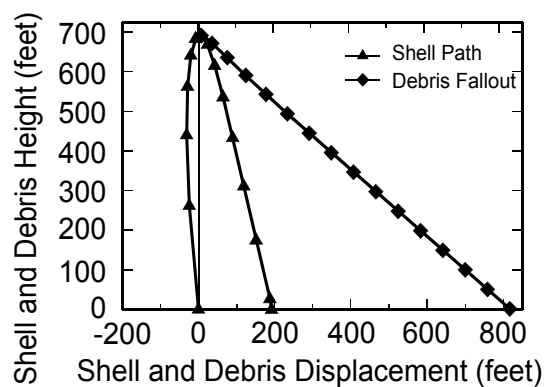


Figure 11. Ballistic trajectory of a 6" shell fired from a mortar tilted 6.6° into a 40 mph wind.

ficient tilt to compensate for the displacement of the shell's apogee. However, the tilt is significantly less than would be required to compensate for the drift in the landing point for a dud shell or for the debris from a properly functioning shell. Table 3 gives the required mortar tilts needed to compensate for the extreme case of a 40 mph wind.

**Table 3. Mortar Tilt Needed to Compensate for Effects of 40 mph Wind on a Typical 6" Spherical Shell.**

Mortar Tilt Angle (degrees)	Displacement Down Wind (ft)		
	Shell at Apogee	Dud Shell at Impact	Debris Fallout
6.6	0	195	820
13.0	-115	0	650
39.1	-460	-590	0

From Table 3, it should be clear why it is not acceptable to fire a display in a 40 mph wind, unless spectators are kept at extremely great distances or are only upwind from the display. That is because, although it is possible to correct for any one of the displacements, the others can still present serious public safety concerns. A display can only be safely per-

formed when the wind conditions are such that shells are not propelled toward spectators, and both duds and debris will fall safely within the secured area for the display.

## Conclusion

The computer-modeling program presented in this article has been verified by both field experiment and analytical calculation. The modeling program has been used to generate some interesting and useful information that would have been too expensive to produce experimentally. The authors intend to continue their work and make further results available to the fireworks industry as they are completed.

## Acknowledgments

The authors gratefully wish to acknowledge the technical and/or editorial suggestions made by E. Contestabile, T. Shimizu, R. Winokur, J. Bergman, and J. Taylor.

## References

- 1) *Handbook of Physics*, Edited by E.V. Condon and H. Odishaw, McGraw Hill, NY, 1967.
- 2) *Van Nostrand's Scientific Encyclopedia*, Fifth edition. Van Nostrand, NY, 1976.
- 3) K.L. and B.J. Kosanke, "Drift Effect for Spherical Aerial Shells," *Pyrotechnics Guild International Bulletin*, No. 74, 1991.
- 4) K.L. and B.J. Kosanke, "Statistical Distribution of Spherical Aerial Fireworks Shell Lateral Drift Effects," Presented at the *17th International Pyrotechnics Society Symposium*, Beijing, China, 1991.
- 5) T. Shimizu, *Fireworks from a Physical Standpoint*, Part 3, Table 35, Pyrotechnica Publications, Austin, TX, 1985.

## Pyrotechnic Accelerants

by K.L. Kosanke

---

Conventional accelerants used in arson crimes, such as gasoline, readily burn in air producing flame temperatures of about 3000 °F. Yet these accelerants generally lack the ability to produce major involvements in short times. This is because, like most combustion reactions, they must rely on a continuing supply of air to provide the needed oxygen. Thus, even when there is a large amount of accelerant, it is of little value unless there is a corresponding large supply of fresh air.

One special class of combustion reactions, “pyrotechnic” reactions, proceeds without having to draw oxygen from the air. This is because pyrotechnic materials are mixtures containing both oxidizer and fuel. Generally the oxidizer is an inorganic oxygen-rich chemical, such as potassium nitrate or ammonium perchlorate. Perhaps the most familiar pyrotechnic reaction is the striking (ignition) of a safety match, whose pyrotechnic composition burns to produce a flame temperature of about 4000 °F. With the addition of high-energy fuels, such as powdered metals, flame temperatures can ex-

ceed 6000 °F. As accelerants, pyrotechnic materials are less efficient than typical accelerants on a pound for pound basis, because they contain an oxidizer in addition to fuel. However, they can generate much higher flame temperatures, and can deliver all their thermal energy in very short times.

As an example of the very high temperature and horrendous quantity of heat that can be generated pyrotechnically, consider the “Pyronol Torch.” This is a device that was originally developed for underwater salvage operations. Although fairly simple in its construction, this item’s chemistry is quite unusual. Its fuel consists of a mixture of aluminum and nickel powders; unusual in that they can react together in an alloying reaction to produce heat, even without an oxidizer. Its oxidizers are iron oxide (rust) and Teflon; unusual in that few would recognize either of these chemicals as being an oxidizer. When a Pyronol Torch is ignited, it produces a jet of vaporized iron which reportedly can penetrate four inches of steel in less than a second, even under 2000 feet of water!

---

## Timing Aerial Shell Bursts for Maximum Safety and Performance





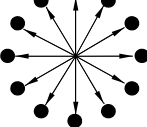
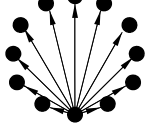
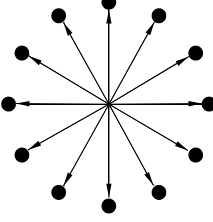
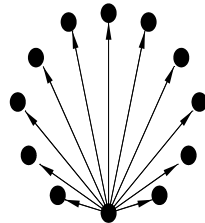
K.L. and B.J. Kosanke

The time chosen for the interval between a shell firing and its burst is sometimes given less thought than it deserves. By carefully choosing the delay interval provided by the time fuse, it may be possible to produce undistorted bursts, with a higher level of safety.

When an aerial shell bursts, while it is nearly stationary, its stars are propelled outward, each experiencing nearly the same aerodynamic drag. Thus the symmetry of the burst is determined only by the construction of the shell, and the pattern will appear to be suspended in the air for its duration. That is to say, a properly made peony will appear as an ex-

panding, near-perfect sphere and will seem to hang motionless in the air as it spreads. See the left column of Figure 1, which is intended to appear as a timed sequence of the burst and expanding pattern of stars from a near stationary spherical shell. On the other hand, if the same shell were to burst while it was in rapid motion, the star pattern would be distorted. This is because the spreading stars would be subjected to a little different aerodynamic forces depending on which way they were traveling relative to the motion of the shell. The star pattern will appear smaller and somewhat elliptical. Also, the star pattern will be slightly more sparse on the bottom than on the top. Perhaps, most noticeably, the developing star pattern will move in the direction of the original shell motion, and will appear to expand from a point, which is not at the center of the pattern. See the right column of Figure 1 for an illustration of the case where the upward motion of the shell approximately equals the burst velocity of the stars. (Readers wishing to learn more about star ballistics are referred to Reference 1.) Thus there are aesthetic reasons why aerial shells are normally intended to burst near their apogee, when their upward motion has essentially stopped.

The time interval during which the vertical motion of an aerial shell has virtually stopped is longer than many may realize. Aerial shells spend more than four seconds traveling up and down only 70 feet at their apogee, and this is independent of shell size, see Figure 2. These results were generated using the computer model described in an earlier article<sup>2</sup>. This illustrates the trajectory of typical 3, 6, and 12-inch aerial shells fired from slightly angled mortars, where the time elapsing between each point is one second. The plotting of the shell trajectory data is terminated a few seconds after the shell's apogee.

Stationary Shell	Time Seq.	Rapidly Moving Shell
	0	
	1	
	2	
	3	

*Figure 1. Time sequence views of stationary and rapidly moving aerial shell bursts.*



**Table 1. Input Parameters and Results of Computer Modeling.**

Nominal Shell Size:	3"	6"	12"
<b>Input Parameters:</b>			
Shell shape	Spherical	Spherical	Spherical
Shell Diameter (inches)	2.75	5.56	11.50
Shell Weight (pounds)	0.3	2.5	18.0
Drag Coefficient[a]	0.40	0.37	0.31
Muzzle Velocity (ft/sec)	300	340	360
<b>Results:</b>			
Apogee Height (feet)	440	760	1100
Time to Apogee (seconds)	4.5	6.0	7.6
± 70 ft Time Interval (sec)	4.1	4.2	4.2
Approx. Ideal Burst Times (sec)	2.5–3.0	4.0–4.5	5.5–6.0
Experimental Burst Height (ft)[b]	406±50	776±52	1164±134

[a] Empirically determined from published data<sup>2</sup>

[b] Experimentally determined aerial shell burst heights were reported earlier<sup>3</sup>.

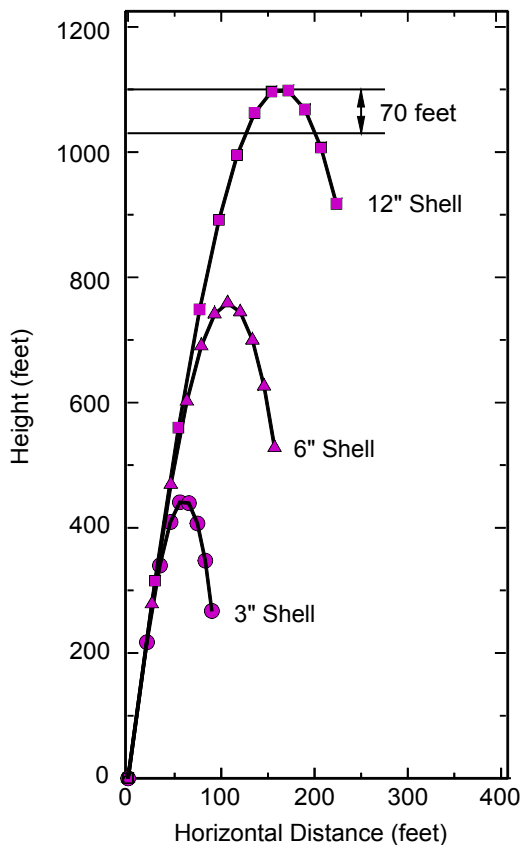


*Figure 2. Trajectories of spherical aerial shells illustrating the approximate 4-second, near-stationary, interval about the apogee.*

Table 1 presents the input data for the computer model, as well as, the results. Included in the results is the approximate time for the shell to travel up and then back down the last 70 feet about its apogee. In each case, this time is about 4.2 seconds, independent of shell size. Thus it is relatively easy to time the burst of an aerial shell to occur during this 4-second period. In terms of fullness and symmetry of the star pattern, because the shell is moving so slowly during this interval, a burst at any time is equivalent. In terms of safety, however, all times are not equivalent. If the burst is planned to occur at or near the start of this interval, there will be added time to allow a damp or sputtering time fuse to complete its task before the shell falls too close to the ground for its stars or components to burn out before endangering people or property. Similarly, on those occasions when shells are mistakenly fired from over-sized mortars, the amount of burning debris reaching the ground will be lessened if the shell has been designed to burst early during the 4-second interval about its intended apogee.

Thus, by selecting the time-fuse delay (length) so that bursts occur 1.5 to 2.0 seconds prior to apogee, safety may be increased without loss in aesthetic performance. These times are included in Table 1 as approximate ideal burst times for the stated input parameters. Ob-

viously, the actual time delays need to be determined by experimentation and will depend on individual shell and mortar parameters.

#### References

- 1) T. Shimizu, *Fireworks from a Physical Standpoint, Part III*, Pyrotechnica Publications, Austin, TX, 1985.
  - 2) K.L. and B.J. Kosanke, "Aerial Shell Ballistic Computer Modeling," *Pyrotechnica XIV*, Pyrotechnica Publications, Austin, TX, 1992.
  - 3) K.L. Kosanke, L.A. Schwertly and B.J. Kosanke, "Report of Aerial Shell Burst Height Measurements," *PGI Bulletin* No. 68, 1989.
-